Creep Response and Adhesion Dynamics of Glioblastoma Multiforme Cells During Migration in Confined Environment

By

Ishan Kamal Khan

Presented to the Faculty of the Graduate School of

The University of Texas at Arlington in Partial Fulfillment

of the Requirements

for the Degree of

DOCTOR OF PHILOSOPHY

THE UNIVERSITY OF TEXAS AT ARLINGTON

April 2018

Supervising Committee

Cheng-Jen Chuong, Supervising Professor

Young-tae Kim

Kytai Nguyen

Jun Liao

Acknowledgements

I would first like to express my sincere gratitude to my committee chair Dr. Cheng-Jen Chuong, for the motivation and support he provided me throughout this research. His guidance and constructive comments over the years have helped me evolve as a researcher. I would also like to thank all my committee members including Dr. Young-Tae Kim, Dr. Jun Liao and Dr. Kytai Nguyen for the advice and guidance needed to complete this research.

In addition, a very special thanks to Loan Bui, PhD at UTA for fabricating the microchannel devices and providing immunostaining images of the cells. I would also like to thank Qionghua Shen for helping with immunostaining of the cells. A very special thanks to Jamie Wright, PhD at UTA for his input in developing the bleb model and to James Nyagilo, PhD at UT Southwestern for providing the actin and myosin images of blebbing cells.

I would especially like to thank my wife, Mithun for her patience and support throughout this period. I would like to recognize the support and sacrifices of my mother in my life. Everything I have achieved in life, I owe it to her. I would like to thank my entire family especially Tati, Apunia, Chotapu, Phupunia, Phuppa, Abba, Amma, Ushan, Shayor and Shuhita for the unconditional love and inspiration. A very special thanks to all my friends in Arlington (especially Anisha and Ethan) for being like my family far away from home.

Thanks to the University of Texas at Arlington and the department of Bioengineering for all the support.

April 25, 2018

Abstract

Creep Response and Adhesion Dynamics of Glioblastoma Multiforme Cells During Migration in Confined Environment

Ishan Kamal Khan, PhD

The University of Texas at Arlington, 2018

Supervising Professor: Cheng-Jen Chuong

Glioblastoma multiforme (GBM) is the most common and malignant form of primary brain tumor. One of the major challenges facing the treatment of GBM tumors is the detachment and subsequent migration of peripheral cells. Migration of GBM cells take place in mechanically distinct confined microenvironment along the borders of white matter tracts. Studies using microfluidic devices mimicking the in-vivo microenvironment have shown that the migration characteristics are significantly altered with the change in kinematic state of the migrating cell. Several studies on different types of cells have consistently shown that a cancerous cell is more compliant than a normal cell in open 2D environment. However, in the in-vivo microenvironment the migrating pathway of GBM cells are confined and the effect of kinematic states on the compliance of migrating cells are yet to be understood. In this work, we examined the differences in mechanical property of GBM cells when in two different kinematic states. Using a microfluidic platform, we studied the creep response of GBM cells in response to the sudden application of negative pressure (-20, -25, -30, -35, and -40 cm H_2O). Cells studied are either actively migrating in a confined channel of 5 x 5 μm cross section or in a stationary state located at the entrance region to the confined channel from an open surface. Our results showed that, in response to the aspiration pressure load, GBM cells in actively migrating state exhibited higher stiffness than those in stationary state. Through the deformation process, cells in migrating state absorbed more energy elastically with relatively small dissipative energy loss compared with those in the stationary state. At elevated negative pressure loads, there was a linear increase in elastic stiffness and higher distribution in elastic storage than energy loss up to - 30 cm H_2O. For further increase in negative pressure load, the response appeared to reach a plateau. To explore the underlying cause, we carried out immuno-histochemical studies of these cells immediately after creep study. Results showed polarized distribution in actin and myosin at both the front and posterior end of the

cells in migrating state, whereas data from cells in stationary state show the normalized intensity oscillate around unity without specific regional differences.

Cell adhesion plays a major role in migration of a cell and alteration of adhesion mechanism can significantly affect the dynamics of migration of a cell. Studies quantifying adhesion forces have developed our understanding of the migration process on 2D substrate. However, effect of geometric confinement on the adhesion strength between the cell and the extracellular matrix (ECM) have not been investigated. In this study, we quantified the adhesion strength of GBM cells migrating in microchannel of 5 x 5 μm cross section. Using a microfluidic platform, we applied negative pressure to detach migrating GBM cells from its surrounding extracellular matrix. Our results demonstrate detachment force of 685.78±68.65 nN for a total of eight individual experiments. Comparing our results with previous studies we have identified that although a migrating cell prefers adhesion-independent migration in 3D conditions, the overall attachment force is this state is comparable with migration on 2D substrate. Analysis of relative deformation of the cell prior to detachment also revealed that most of the resistance to applied negative pressure is generated by the nuclear region and the posterior end of the cell. Our study underscores the importance of transverse forces applied by the cell on the surrounding ECM for generating traction force during adhesion-independent migration mechanism. During adhesion independent migration, cells have demonstrated that the propelling force is generated partly by hydrostatic pressure. The rise of hydrostatic pressure is signified by the local detachment of plasma membrane from the actin cortex. The detachment of plasma membrane results in spherical protrusions known as blebs. Although it has been suggested in previous studies that the source of hydrostatic pressure is actomyosin contraction in the actin cortex, the mechanism of actomyosin contraction in the intracellular level have not been identified. In this study, we developed a numerical model of a migrating cell in confinement and applied the understanding of actomyosin contraction in muscle tissues in the model. Our study finds, that using the mechanism of muscle contraction, the migrating cell generates intracellular pressure of approximately 3 Pa which is sufficient to generate bleb protrusion comparable to experimentally observed cellular blebs. The findings of this study help broaden our understanding of the changes in mechanical property and adhesion mechanism the GBM cell undergoes while migrating through a confined space in the brain.

Table of contents

List of Illustrations

List of Tables

Chapter 1
Difference in Creep Response of GBM Cells Migrating in Confinement

1.1 Introduction

Glioblastoma Multiforme (GBM), known as the most common and malignant tumor among all adult primary brain tumors, consists of a heterogeneous population of cells within the tumor mass[1]. Differing from other cancer cell types, GBM do not intravasate to the blood stream, but migrate along the myelinated axonal fiber tracts of the white matter or the outer wall of blood vessels[2-4]. This distinctive feature makes the migration dynamics of the GBM cell unique and signifies the role of active migration through narrow extracellular pathways in the metastasis of brain tumor. Several studies indicate that to migrate through confined space of extracellular matrix (ECM), the cells undergo remodeling process, leading to biophysical property changes that facilitate the migration process. Changes in cellular migration phenotype include velocity[5], directionality and persistence[6], among others. In response to the mechanical stimuli, the cell initiates a cascade of biochemical signals, propagates through the cytoplasma, entering at the nucleus, that modulate gene and subsequent protein expressions leading to changes in cell motility through cytoskeleton remodeling [5, 6]. Thus, mechanical interaction of a cell with its microenvironment can play a major role in the development of invasive phenotype of cancer cells. Since the change in mechanical property has been found to have a direct correlation with the change in adhesion, proliferation and migration of cancer cells[7], quantitative assessment of the change in mechanical behavior can provide insight into the biophysical changes in a cancer cell undergoing migration.

Several studies have demonstrated that the ability of a cancer cell to deform under mechanical stress has a direct correlation with its invasiveness[8-11]. These studies conducted on different types of cells have consistently shown that a cancerous cell is more compliant than that at healthy state. Hence, a cell's response to mechanical stimuli can be an important parameter indicating its cancerous progression. In this work, we report the differences in the mechanical properties of GBM cells at two different kinematic states. Specifically, we examined the differences in creep response of the GBM cells in response to the sudden application of negative pressure when they were in two different states: either actively migrating in a confined channel of 5 x 5 μm cross section or in a stationary state stalling at the entrance region to

the confined channel from an open surface. To correlate with the differences in creep responses of GBM cells in two referenced kinematic states, we carried out immuno-histochemical treatments in cells immediately after creep study to examine their respective intracellular distributions of actin and myosin using fluorescence microscopy.

In this study, we chose to use microfluidic platform with the 5 x 5 μm channel, instead of employing the commonly-used micropipette technique. The use of microfluidic platform simplified the experimental procedure[12] and it provides well-controlled consistency in the degree of confinement to a migrating cell, among other advantages, e.g. low cost, imaging compatibility. Understanding the effect of geometric confinement on mechanical properties of a cell during migration is a key factor in identifying the biophysical changes occurring *in-vivo* during metastasis and could provide the platform for future *in-vitro* studies on cancer cell migration.

1.2 Methods

1.2.1 Fabrication of PDMS Device

PDMS (Dow Corning, Sylgard 184) devices with microchannel of 5×5 μm cross section and a length of 530 μm connecting two reservoirs each at 100 μm height were fabricated using photo and soft lithography technique [13]. A silicone elastomer base was mixed with a curing agent at a mixing ratio of 10:1. Reservoirs of 8 and 6 mm diameter were punched at the PDMS block to allow cell seeding and supply of nutrients. To maintain an isolated fluid environment, we plasma-treated the channel surfaces of the PDMS block before completing the device assembly with a like-wise treated glass cover slip. The device was then sterilized and coated with laminin (Sigma-Aldrich) at 10 μg/ml prior to seeding cells.

1.2.2 Cell Culture

CD 133^{+} patient-derived GBM cells, provided by the University of Texas Southwestern Medical Center at Dallas with IRB approval, were used for this study. The cells were maintained in serum-free Dulbecco's Modified Eagle Medium/F-12 medium (DMEM/F-12) with 2% B-27 (Invitrogen), 0.25% insulin-transferin-selenium-X (Invitrogen), gentamicin at 25 μg/ml, and mouse EGF at 20 ng/ml.

1.2.3 Identification of cells in actively migrating and stationary groups

The GBM cells were seeded close to the channel openings to the central (upstream) reservoir (Figure 2) in a density of 500,000 cells/120 µL. Follow the seeding; we monitored the cell motility in the device at least every 6 hours for up to 36 hours. Cells that had reached the channel opening and blocked the opening cross section were identified as part of “stationary state” group. Cells migrated to and subsequently entered channels demonstrated intermittent migration in the channel. Those that had reached at least halfway of the channel length (~ 265 µm) were identified as “actively migrating state” group. Creep test was performed on these two groups of GBM cells and we examined their differences in deformation response parameters.

1.2.4. Experimental setup

For creep test, a prescribed negative pressure was applied at the downstream reservoir and the resulting deformation at the front-end of the cell was measured. Two water columns connected to a three-way valve was used to deliver either the prescribed negative pressure or atmospheric pressure as the baseline value as illustrated in Figure 1, where the enlarged view of the PDMS device illustrates the transmission of negative pressure load from the source through a gauge needle to the cell in the channel. In migrating group, cells had actively migrated half way in the channel; whereas cells in stationary group practically blocked the channel near the channel entrance with large portion of the cell body adhered to the bottom surface of the upstream reservoir.

Prior to the application of negative pressure, the open surface of the downstream reservoir was sealed with a glass cover slip coated with film forming acrylate solution which has been found to be non-cytotoxic[34]. Prescribed negative (suction) pressure was applied to the front-end of the cell instantaneously when we opened the three-way valve to the corresponding water column (Figure 1). A Leica inverted microscope with 20x objective lens was used to record the transient response at a framing rate of 19 fps using software *Leica (*Leica Microsystems*)* and *My Screen Recorder* (Deskshare Inc., Plainview NY). From the moment of negative pressure application, creep response of the cell was recorded in video format for 30 seconds, which was immediately followed by the release of the pressure to zero baseline with the recording continued upto 40 seconds. Deformation at the front-end of the cell was measured from recorded images frame-by-frame using *Image J* (https://imagej.nih.gov/ij/).

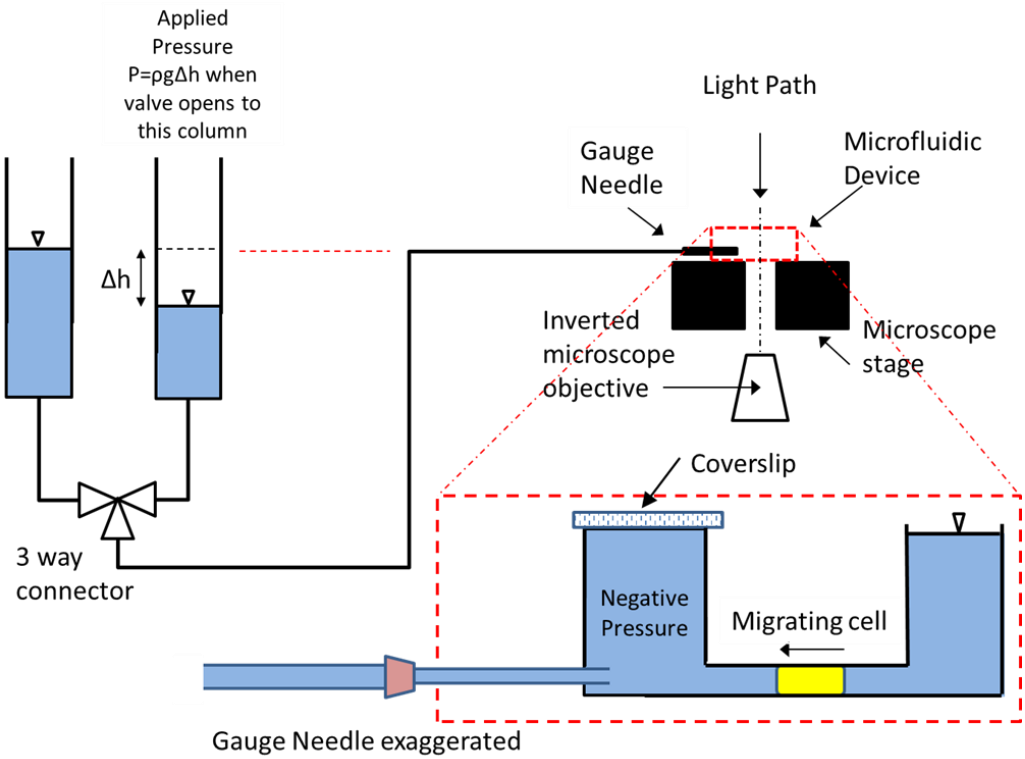

Figure 1: Schematic of the experimental setup for creep experiment. After cell seeding to the bottom surface of the upstream reservoir near the channel, cells migrated into the 5 x 5 µm channel as illustrated. Using a three-way valve, we delivered the prescribed negative pressure to the front-end of the migrating cell through a gauge needed inserted through the wall of the downstream reservoir. The time course of the displacements at the front-end of the cell were measured from recorded video images. Note that, we sealed the pressure at the downstream reservoir right before we activated the negative pressure application using a cover slip

1.2.5. Creep Response- Actively migrating vs stationary

Figure 2 A, B are video images of the GBM cells from stationary and actively migrating groups when under the application of - 20 cm H_2O negative pressure. Figure 2C shows the time course of the pressure application with an instantaneous rise to full value at time = 0 followed by its release at time = 30 sec. Measurements of front-end displacement were taken frame-by-frame from recorded video images for at least 40 seconds that revealed the characteristic differences in creep deformation responses between two groups (Fig 2D).

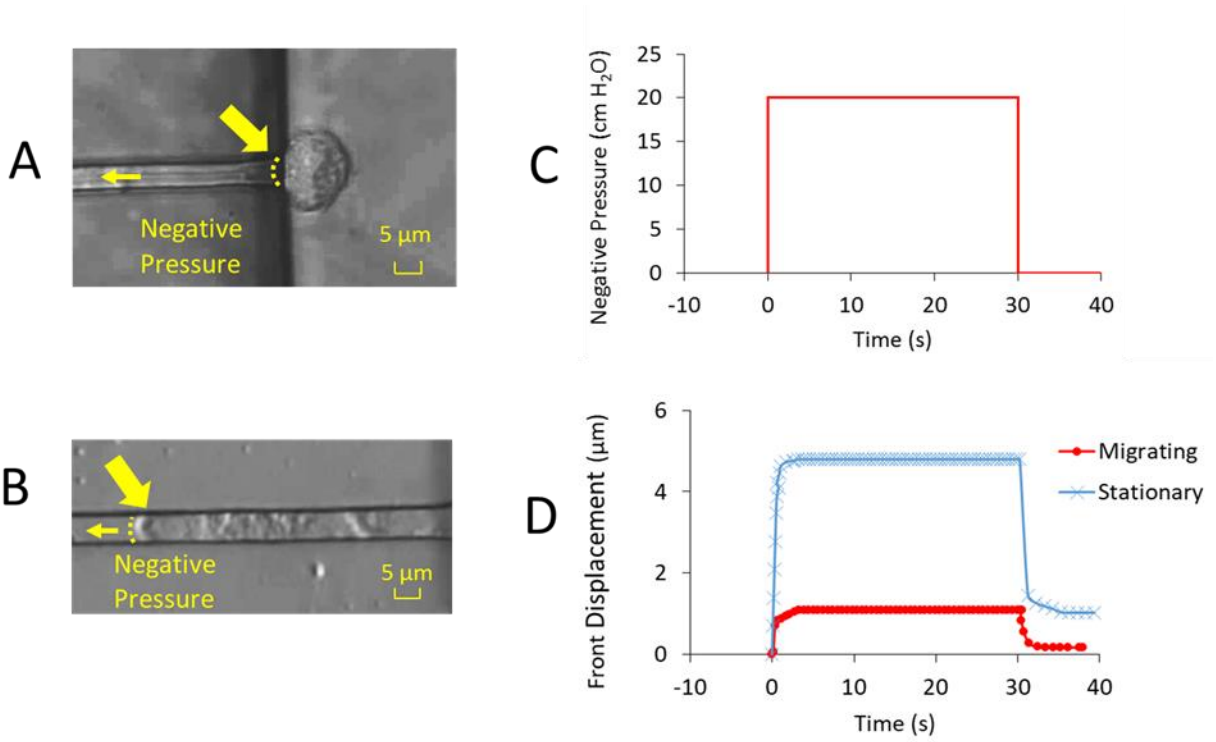

Figure 2 Response of cells in stationary and migrating stage in creep test. Images showing the front-end displacement of a GBM cell in A) stationary and B) actively migrating state under applied negative pressure of – 20 cm H2O at the direction of white arrow head. Yellow arrows highlight the front-end surface of the cell where measurements were taken. C) Prescribed negative pressure was activated, maintained at constant level for 30 seconds before its release to baseline value. D) Representative front-end displacements from the cell in stationary and migrating state through the time course of pressure application

Measurements of the front-end displacement *U(t)* were fitted to a Voigt model that consists of an elastic spring (spring constant *E*) and a viscous damper (damping coefficient *η*) connected in parallel (Fig 3A). From each cell, we fitted displacement measurements to a Voigt model in two separate phases: 1) aspiration phase in response to the instantaneous negative pressure application from 0 to 30 seconds, and 2) retraction phase that after the sudden release of negative pressure from 30 to 40 seconds. Voigt models for these two phases are written as:

Aspiration: $$U(t) = U_{peak} * \left(1 - \exp^{-\frac{t}{\left(\frac{h}{E}\right)}}\right) \qquad for\ 0 \le t \le 30\,\text{sec}$$

Retraction: $$U(t - 30) = U_{peak} - \left(U_{peak} - U_{residual}\right) * \left(1 - \exp^{-\frac{t-30}{\left(\frac{h}{E}\right)}}\right) \qquad for\ t > 30\,\text{sec}$$

The fitting to the model was done by finding η/E and U_{peak} (*or* $U_{residual}$ for retraction phase) that minimize the objective function *E*, defined as the sum of the normalized difference between fitted Voigt model displacement and experimental measurements written as:

$$E = \left(\frac{1}{N}\right) \sum_{n=1}^{N} \left[\frac{U_{\exp t}(t_n) - U_{Voigt}(t_n)}{U_{\exp t}(t_n)}\right]$$

where *N* denote the total number of data points. Using generalized reduced gradient regression method **GRG2** (*Microsoft Excel & Frontline Systems Inc., NV*), fitted model parameters η/E and U_{peak} (*or* $U_{residual}$ for retraction phase) were calculated as the pair that minimized the objective function *E* with a tolerance for convergence set at < 0.001. For data from each cell, regression was carried out separately for aspiration and retraction phase. The division of creep response in two phases and their respective model parameters η/E and U_{peak}, $U_{residual}$ are illustrated in Fig 3B.

At each pressure level, we compared the creep response parameters U_{peak} (or $U_{residual}$) and η/E between the actively migrating group and stationary group for the aspiration phase as well as the retraction phase. To examine any nonlinear effect at elevated levels of negative pressure, we repeated the experiment for a range of pressure levels: -20, -25, -30, -35, and -40 cm H_2O.

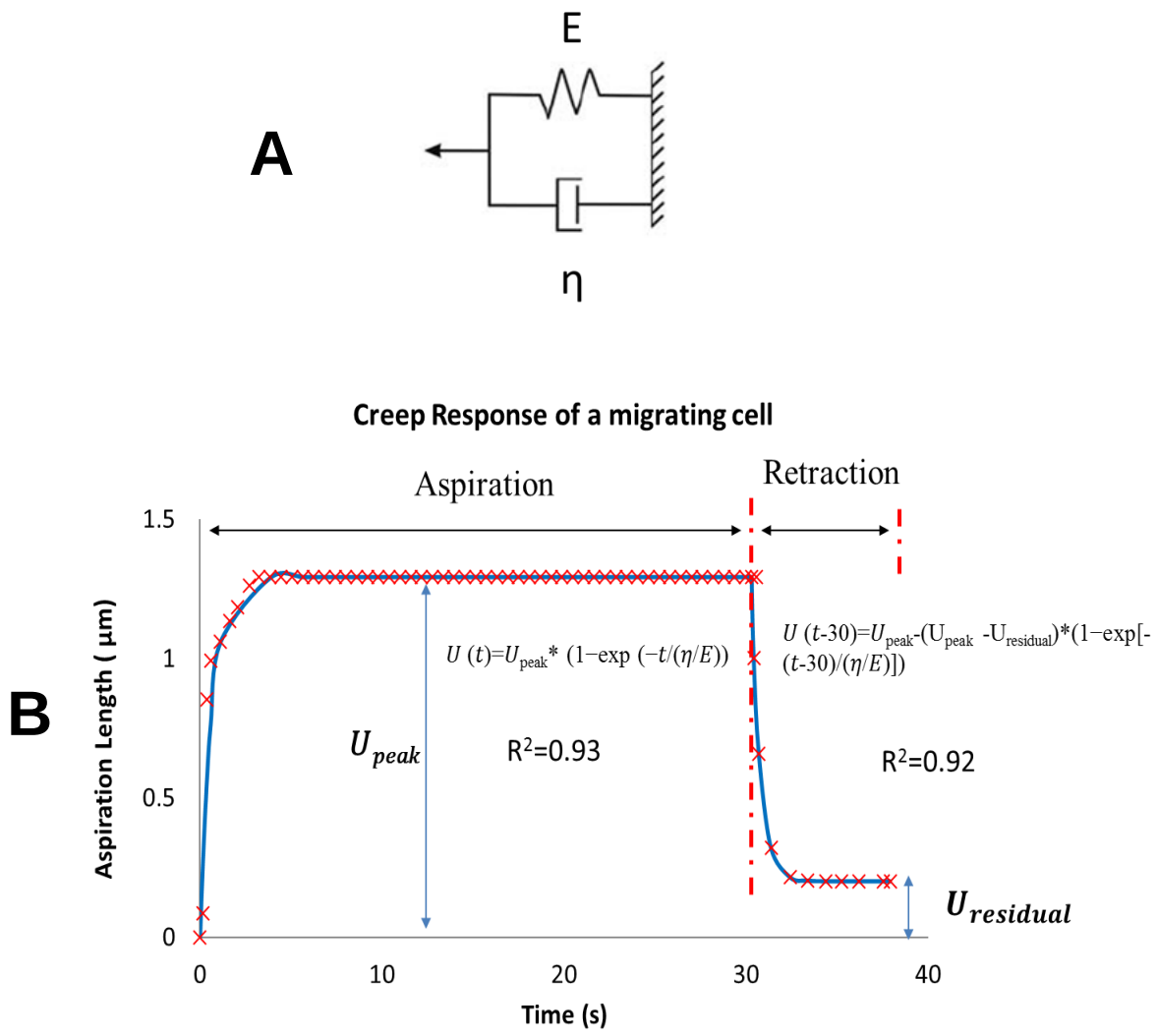

Figure 3 Curve fitting creep response with a Voigt Model. A) A Voigt model representation that consists of an elastic spring (spring constant *E*) and a dashpot (damping coefficient *η*) connected in parallel. B) Measurements of recorded front-end displacements was divided into two phases: aspiration from 0-30 seconds and retraction phases from 30-40 seconds. Each phase was curve fitted to a Voigt model representation as shown.

1.2.6. Any rigid body sliding movement of the cell?

To ensure that the recorded cellular front-end displacements are the intrinsic cellular response in deformation to the negative pressure application, excluding any rigid body sliding movement due to cell

dislodgment from channel walls, displacement at the corresponding posterior-end of the same cell was measured as well to allow assessment of any such sliding movement.

1.2.7. Immunohistochemistry of filamentous Actin and Myosin

To observe the differences in actin and myosin distributions between actively migrating and stationary groups, we immuno-stained filamentous actin, myosin, and nucleus of the GBM cells to aid visualization. Immediately after the creep study, we removed cell culture media from the device and fixed the cells with 4% paraformaldehyde in 1×PBS at 4°C for 10 minutes. Following the removal of paraformaldehyde, the devices were washed with 1×PBS for three times. For visualization of cell nucleus, 7 µL of 4′,6-diamidino-2-phenylindole (DAPI) dissolved in 10 mL of solution (0.5% triton in 1×PBS) was introduced into the samples. For visualization of myosin filaments, the samples were blocked in goat serum for one hour followed by staining with Rabbit Anti-Myosin IIa (#3403, 1:50, Cell Signaling Technology) overnight in 4°C. The next day, we washed the samples with 1xPBS three times and incubated them with Alexa Fluor® 594 AffiniPure Goat Anti-Rabbit IgG (1:200, Jackson Immuno Research Laboratories) at room temperature for 2 hrs. For visualization of actin filaments, the samples were stained with Actin-stain™ 488 (3:500, #PHDG1, Cytoskeleton) at room temperature for 2 hrs. Expression of actin filament and myosin IIa were visualized using fluorescence microscopy (Zeiss Observer Z1) with images captured using 20 X objective.

1.2.8 Statistical Treatment

A non-parametric two-tailed *t*-test (Excel, Microsoft) was used to compare aspiration lengths U_{peak} (or residual lengths $U_{residual}$) and E/η ratios between the actively migrating and the stationary groups for data from both the aspiration and the retraction phases. We considered the differences in these creep response parameters to be significant if $p < 0.05$.

1.3 Results

1.3.1 Different creep responses between actively migrating and stationary GBM cells at different levels of aspiration pressure

Aspiration phase (Figure 4)

Comparison of creep response parameters U_{peak} and η/E ratio at different levels of negative pressure application from the aspiration phase are presented in Figure 4A, B. For all pressure levels, the stationary group is seen to have much higher U_{peak}, indicating their higher compliance than the cells in the migrating group. For all pressure levels, the migrating group was found to have a much lower η/E ratio, being less than 1, indicating the relative dominance of the elastic response over the damping or energy dissipation in the deformation response. The table in Figure 4C summarizes the numbers of cells used in the study.

From both groups, our results show increasing levels of displacement at increasing negative pressure load up to -30 cm H_2O, with the response reaching a plateau at higher negative pressure levels (Fig 4A). That is, the elastic response is approximately linear through -30 cm H_2O. The cells became much stiffer at higher negative pressure load with little increase in aspiration length for further increase in negative pressure load. Results also show decreasing η/E ratio when negative pressure load increased up to -30 cm H_2O. It became flatten out at further increase in negative pressure load. Reducing damping-to-elastic ratios is indicative of the progressively higher contribution from elastic response and lower fluid-like energy dissipation behavior through -30 cm H_2O. Above which, the distribution between elastic and viscous responses appear to remain the same at further increase in negative pressure load (Fig. 4B).

A

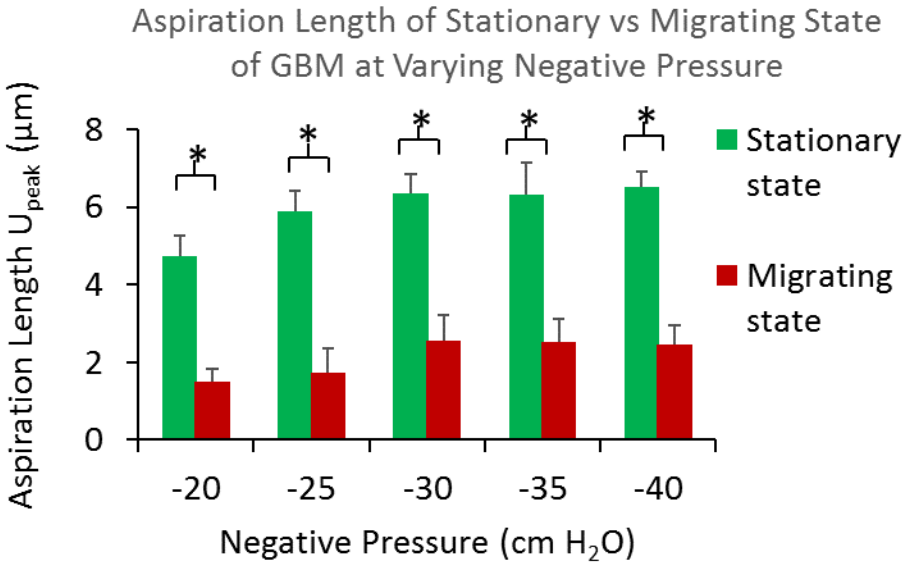

B

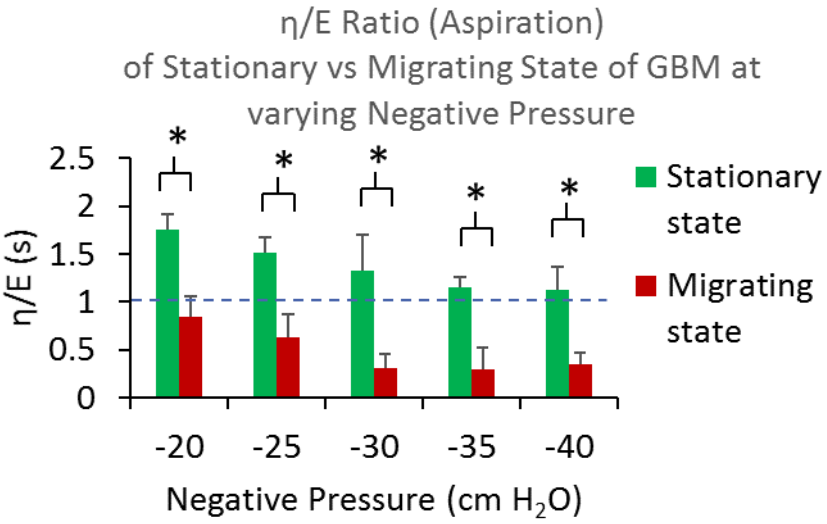

C

Sample Size, n					
Cell Group	Applied Negative Pressure (cm H_2O)				
	20	25	30	35	40
Stationary	6	4	3	3	3
Migrating	7	7	4	4	4

Figure 4 Results of creep test in the aspiration phase. A) Aspiration lengths of cells in migrating group were found to be much lower than that in stationary groups for all negative pressure load from -20 to -40 cm H_2O. B) *η/E* ratios of cells in migrating group were found to be less than 1 and much lower than that in stationary groups for all negative pressure load from -20 to -40 cm H_2O.

C) A table summarizing sample sizes from stationary and migrating groups at different pressure levels.

Retraction Phase (Figure 5)

Responses from retraction phase show how cells respond to the release of applied negative pressure load before their full recovery. Residual length ($U_{residual}$) accounts for the residual displacement at the front end of the cell after the recoil of the cell has conceded. The magnitudes of η/E ratio is indicative of the rate of immediate recoil from the deformed state after the release of aspired negative pressure.

For all pressure levels, we found much smaller residual lengths from cells in the migrating group compared to stationary group, indicating their favored elastic response in the recovery from deformed state at the release of aspired negative pressure. Higher residual lengths were found from the stationary group. They exhibited lower residual lengths as the pressure load is below -25 cm H_2O. For higher pressure loads a plateau is reached in residual lengths. Residual lengths from migrating groups, although with significantly lower residual lengths from all pressure levels, we were not able to see a clear trend or pattern in relation to the levels of pressure load. Lower η/E ratios of the migrating group (being less than 1) indicate the higher contribution in elastic recovery over that of energy dissipation or frictional loss.

A comparison of η/E ratios between the stationary and actively migrating group revealed the dominance of viscous over elastic response of the cell in the stationary groups. In contrast, the migrating cells demonstrated much less than unity value in the ratio across all levels of negative pressure applied, indicating their higher stiffness and diminished viscous behavior in actively migrating state.

A

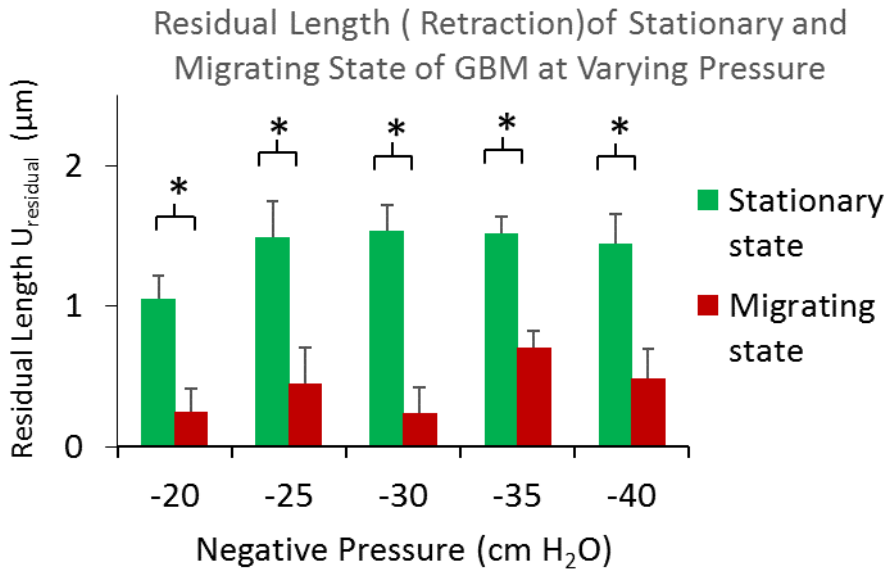

B

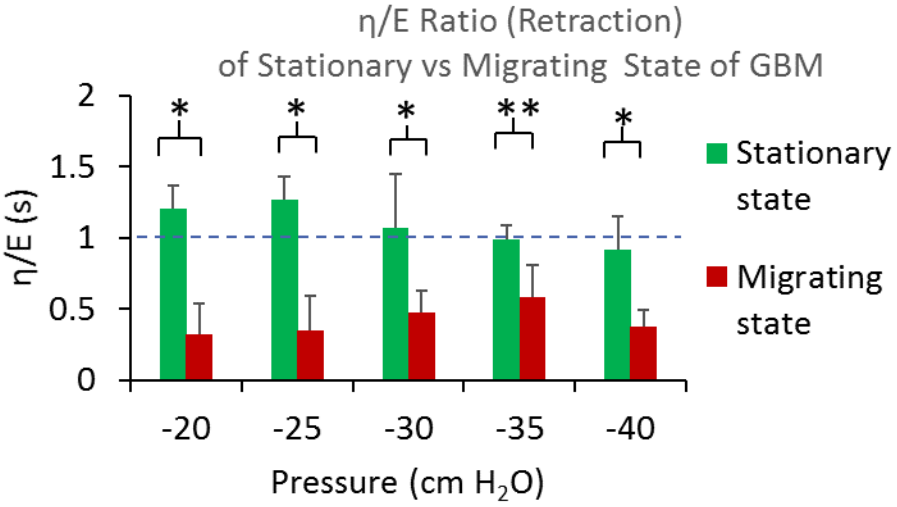

C

Sample Size, n					
Cell Group	Applied Negative Pressure (cm H_2O)				
	20	25	30	35	40
Stationary	6	4	3	3	3
Migrating	7	7	4	4	4

Figure 5 Results of creep test in the retraction phase. A) Residual lengths (from retraction phase) of cells in migrating group were found to be much lower than that in stationary groups for all negative pressure load from -20 to -40 cm H_2O. B) *η/E* ratios of cells in migrating group were found to be less than 1 and all

much lower than that in stationary groups for all negative pressure load from -20 to -40 cm H_2O. C) A table summarizing sample sizes from stationary and migrating group at different pressure levels.

1.3.2 Any rigid body sliding movement of the cells?

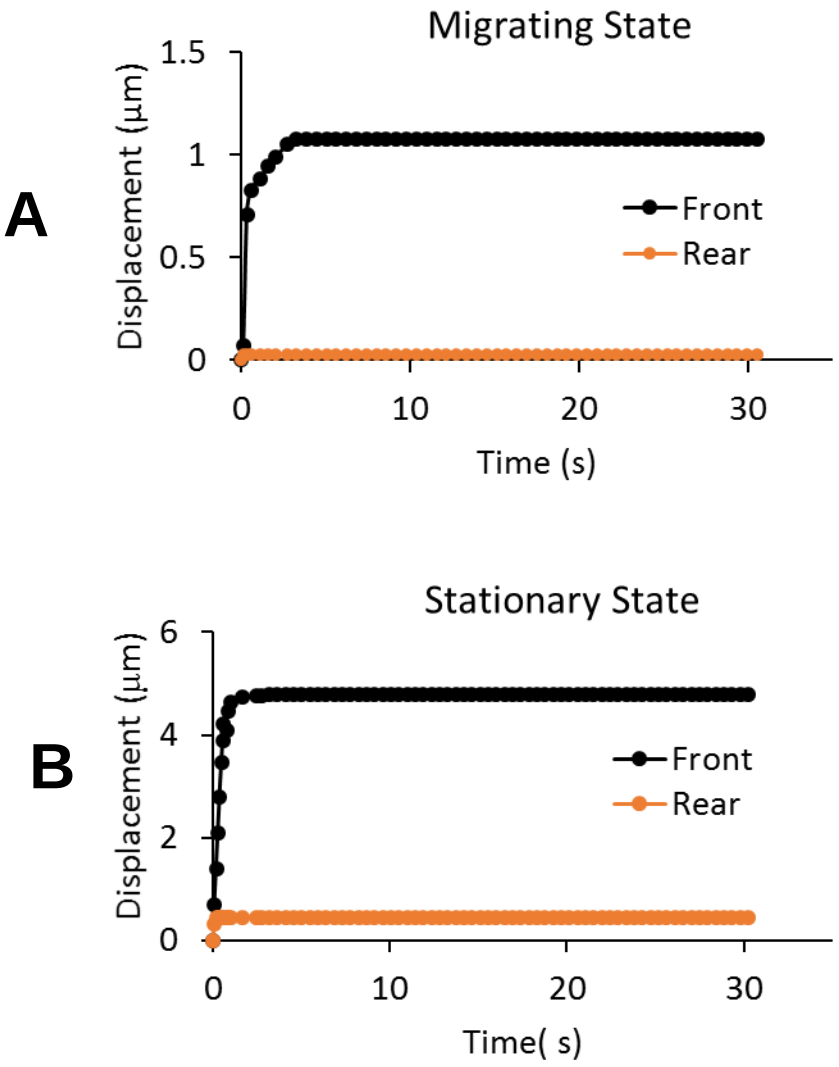

Figure 6 Identifying rigid body motion in stationary and migrating state. A) Simultaneous recording of the front and posterior-end displacements of GBM cell in actively migrating state show near-zero displacement at the rear-end, indicating the recorded front-end displacement are due to the cell deformation in response to the negative pressure load, excluding any likely sliding movement of the cell in

the channel. B) Cells from stationary group showed a rear-end displacement at ~ 8 % compared to that at the front-end

Results from simultaneous recording of the front and posterior-end displacements of actively migrating cells show near-zero displacement at the posterior end, indicating that recorded front-end displacements are due to the deformation of the cell in response to the negative pressure load, excluding any likely sliding movement of the cell in the channel (Figure 6A). From stationary group, we did observe a posterior-end displacement at ~8 % of that from the front-end (Figure 6B). Note that cells in stationary group are in a stalling state with a small portion of cytoplasma blocking the entrance to the 5 x 5 μm channel and the rest adheres to the surfaces of the upstream reservoir. Unlike cells in migrating group, these cells are not in a confined state. We attributed the measurement from the posterior-end to the movement of the cell body on the surfaces of the reservoir outside of the channel.

1.3.3 Correlation with Actin and Myosin Distribution

Immuno-histochemical examination of intracellular actin and myosin distributions showed a significantly higher level of polarized actin and myosin-II filaments at both the front and posterior ends of cells in migrating group (Figure 7A). On the other hand, intracellular actin and myosin distributions from stationary group showed low level of expression without any regional preference. To compare the differences in two groups and to allow assessment of regional differences in the degree of polarization, we expressed the light intensity along the axial length of the cell as a factor normalized with respect to the mean values of light intensity averaged over the entire cell length (Figure 7 B, C). Normalized intensity higher than unity indicates a high degree of polarization of actin and myosin at the front and posterior ends of cells in migrating group (Figure 7B). On the other hand, data from cells in stationary group, show the normalized intensity oscillates around unity without specific regional differences (Figure 7C).

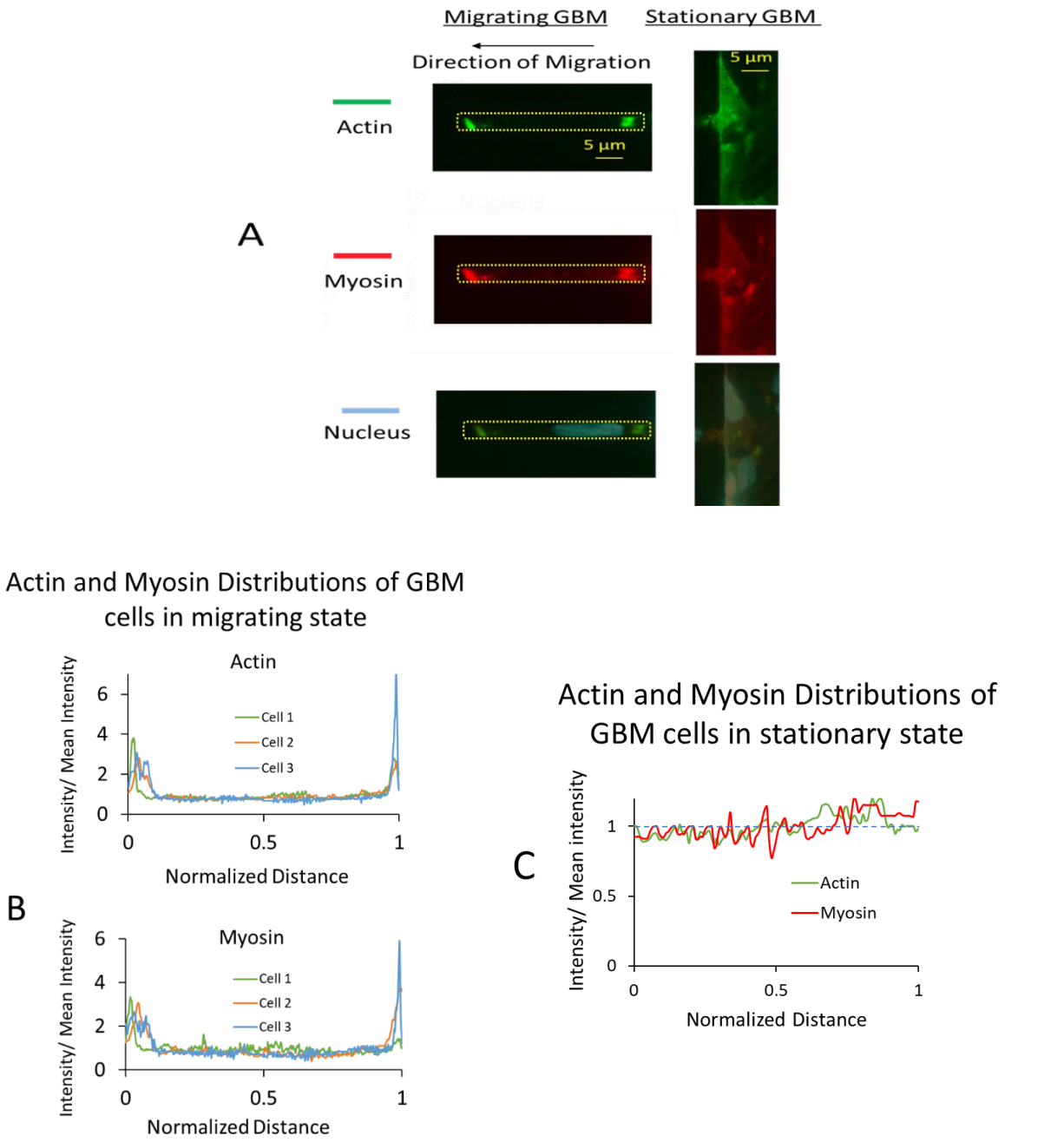

Figure 7 Actin and myosin distribution in stationary and migrating state. A) Immuno-histological examination showed a significantly higher level of polarized actin and myosin-II filaments at both the front and posterior ends of cells in migrating group. B) Polarized distributions in actin and myosin were found from GBM cells in migrating group. C) From GBM cells in stationary group, their normalized intensities in both actin and myosin oscillate around 1.

Chapter 2
Characterization of Adhesion Strength of GBM cells migrating in confinement

2.1 Introduction

Glioblastoma Multiforme (GBM), is one of the most malignant and anaplastic primary brain tumors [1, 15]. A unique feature of GBM cells is that they do not intravasate to the blood stream, but prefer to migrate using the outer boundary of blood vessels or along the axonal fibers of the white matter[2-4]. The ability of a primary tumor cell to metastasize to a different location and form a secondary tumor is partly dependent on the physical interaction with its microenvironment [16]. Therefore, understanding the interaction between a migrating GBM cell and its surrounding extracellular matrix (ECM) is essential for fully comprehending the migration process in confined 3D environment. Despite of our detailed understanding of signaling pathways and biomolecules involved in cell adhesion on open 2D substrates, studies are yet to be conducted on the mechanical aspects of cell-ECM adhesion in 3D environment and its impact on the migration behavior of invasive cells.

Several studies have identified two mechanisms used by the cell during migration: one is driven by actin polymerization (a.k.a. mesenchymal) and another is governed by hydrostatic pressure generated because of actomyosin contraction. The mesenchymal migration technique It has also been observed that a migrating cell can spontaneously switch between these two mechanism and the switching can be induces by the change in altering geometry of extracellular matrix[17]. Another study has also demonstrated that migration behavior in 3D environment is significantly different than migration along open substrates and that migration in 3D can be achieved with or without any involvement of cell adhesion[17, 18]. In contrast to migration on a 2D substrate, cells migrating in confined 3D space do not exclusively rely on adhesion-dependent migration techniques.

Therefore, investigation of the mechanical aspect of cell adhesion is essential for obtaining a deeper insight into the mechanisms involved in altering migration behavior. Any alteration of adhesion dynamics is expected to alter the strength of the cell-ECM attachment and therefore the adhesion strength can be a key indicator of the interaction between a migrating cell and its micro-environment. Different techniques have been used to measure the adhesion force between cell and its two-dimensional substrates among them hydrodynamic techniques are the most commonly used method [19-21]. This

method is used to apply shear force on a population of adherent cells and analytically calculate the summation of shear force applied by fluid on the cell surface at the point of detachment. In the recent decades, several studies have also focused on quantifying the adhesion strength between single cells and substrates using single-cell force spectrometry (SCFS)[22]. These studies encompass a wide variety of techniques including micropipettes[23], optical tweezers[24, 25], magnetic twisting[26] and atomic force microscopy[27-29]. Although these studies have broadened our understanding of cell-ECM interaction, they have been focused primarily on the cells attached to a flat 2D substrate. To fully comprehend the migration dynamics of cells in physiological conditions it is essential to understand the cell-ECM interaction in confined 3D spaces.

In this study, we aim to quantify the mechanical force required to detach an actively migrating GBM cell from its confined ECM of 5×5 μm cross-section. By quantifying the mechanical force involved in the cell-ECM attachment in confined conditions, we aim to enhance our understanding of the role of cell adhesion in facilitation migration of cancer cells in 3D extracellular matrices.

2.2 Methods

2.2.1 Fabrication of PDMS Device

Using soft and photo lithography techniques, PDMS (Dow Corning, Sylgard 184) devices with a channel of 5x5 μm rectangular cross-section and 530 μm length connecting two reservoirs (each of 100 μm height) were fabricated [30]. A curing agent was mixed with a silicone elastomer base maintaining a ratio of 1:10. Once the PDMS blocks were formed on the silicon wafers, reservoirs of 8 and 6 mm diameters were punched to allow cell seeding and maintain nutrient supply. The bottom surface of the device was plasma treated and assembled with a glass cover slip followed by sterilization and laminin (Sigma-Aldrich) coating at 10 μg/ml.

2.2.2 Cell Culture

For this study, CD 133^+ patient-derived GBM cells provided by the University of Texas Southwestern Medical Center at Dallas were used with IRB approval. The cells were maintained in serum-free Dulbecco's Modified Eagle Medium/F-12 medium (DMEM/F-12) with 2% B-27 (Invitrogen), 0.25% insulin-transferin-selenium-X (Invitrogen), gentamicin at 25 μg/ml, and mouse EGF at 20 ng/ml.

2.2.3 Experimental Setup

The downstream well of the device was sealed with a coverslip while the upstream well was kept open to the atmosphere (Figure 8). Negative pressure was applied at the downstream end of the migrating cell by pulling the plunger of a syringe which was connected to the PDMS device. A manometer was connected to the syringe to record the applied pressure in the device. Upon detachment of the cell, the dislodging pressure was recorded by the manometer Benetech GM520 (Shenzhen Jumaouyan Science and Technology Co. Ltd, Shenzhen, China). A Leica inverted microscope with 20x objective lens was used to observe the deformation and subsequent detachment of the cell. The transient response of the cell to applied negative pressure were recorded at a framing rate of 18 fps by Leica (Leica Microsystems) and My Screen Recorder (Deskshare Inc., Plainview NY) softwares. Deformation at the different locations of the cell was measured from recorded images using ImageJ(https://imagej.nih.gov/ij/). Displacement of the posterior end of the cell is tracked by Matlab (Mathworks Inc.). The movement of the posterior end of the cell was tracked by tracking a changing spatial co-ordinate of a group of pixels representing the posterior end of the cell.

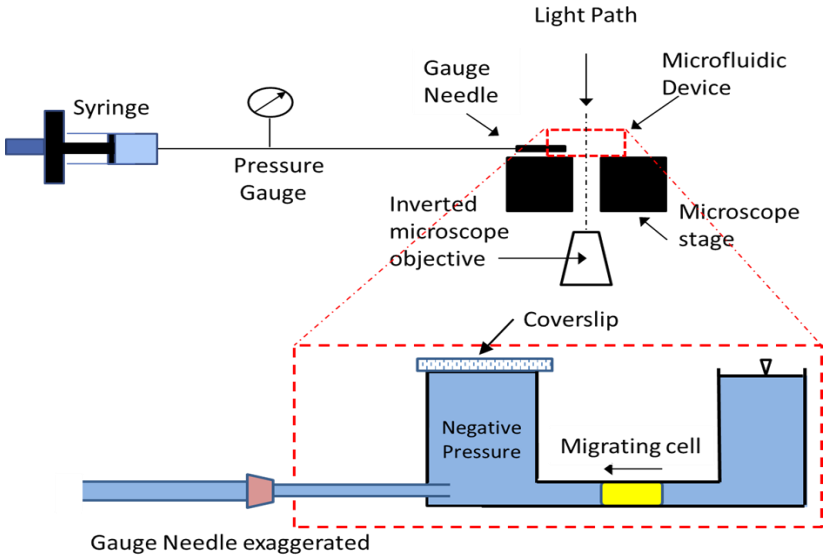

Figure 8: Experimental setup for quantifying dislodging pressure of migrating cell. The downstream well was sealed with glass coverslip and the upstream well was open to the atmosphere. Negative pressure was applied using the syringe and the dislodging pressure was recorded using a manometer.

2.3 Results

2.3.1 Force required to detach migrating cell from confined ECM

The calculated adhesion force between migrating GBM cells and its confined microenvironment presented in Table 1 is comparable to the results obtained from studies on adhesion strength on 2D substrates. Although the driving forces and mechanism for migration in 3D is different, the results are indicative of the amount of force generated by cell to propel itself forward is comparable in the two migratory circumstances.

Number of single cell experiments	Detachment Pressure (cm H_2O)	Detachment Force (nN)	Length of the cell (µm)	Shear Stress (kPa)
8	279.71±28	685.78±68.65	27.76±4.5	1.24±0.76

Table 1 Summary of detachment experiments

The results obtained in **Fig 5** demonstrate the relative resistance of the different compartments of the cell under applied negative pressure. The hydrostatic pressure forces, which is dominant during migration in 3D is apparently more prominent in the posterior end of the cell which holds the cell to its original location until the applied force overcame the total transverse forces exerted on the wall.

2.3.2 Deformation of a cell prior to detachment

The deformation of the different locations of the GBM cells were tracked using ImageJ and represented in Figure 9. Individual tracking of front, middle (nuclear) and posterior ends of a cell demonstrated that the posterior and nuclear region of a cell exhibits highest resistance to deformation. Upon application of very high level of negative pressure, the front of the cell deforms most significantly and the posterior end of the cell demonstrates the highest resistance to deformation.

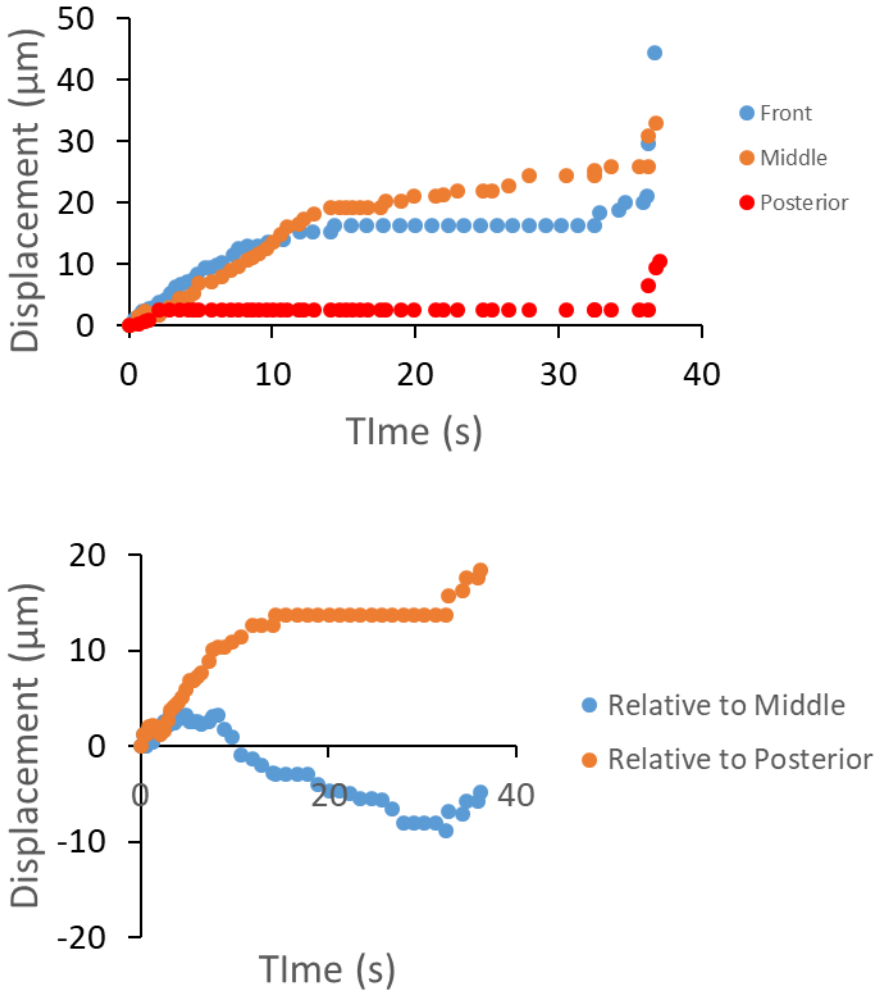

Figure 9 Comparative deformation of different ends of a cell prior to detachment. Displacement of the front, middle and posterior ends of the cell (top) and relative deformation of the front of the cell with respect to the middle and posterior before detachment

Tracking the velocity and acceleration of the cell at the point of detachment (Figure 10), the resulting velocity was found to be ranging from 2000-4000 µm/s. This signifies the high level of energy required to detach the cell from its surrounding environment as well as the amount of resistance offered by the cell and its kinematic state.

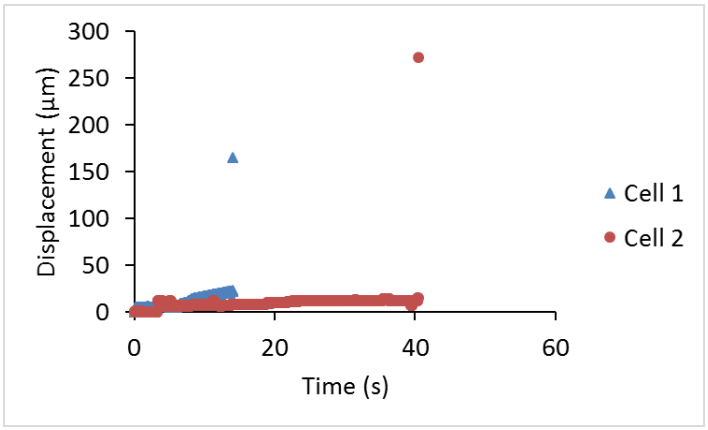

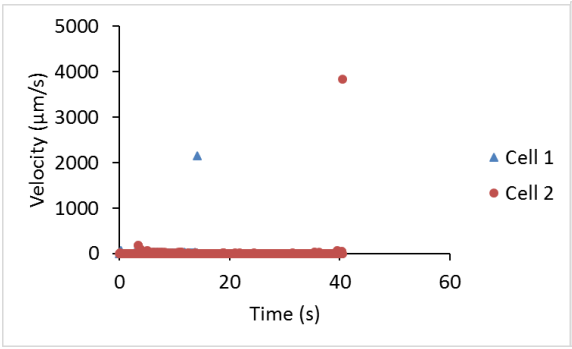

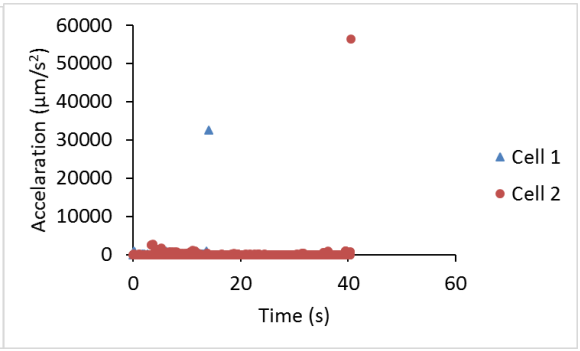

Figure 10 Displacement tracking of posterior end for calculating detachment velocity and acceleration

Chapter 3
Generation of Hydrostatic pressure in Confinement

3.1 Introduction

Blebs are pressure driven plasma membrane protrusions that occur when part of the cell membrane is detached from the actin cortex of the cell and are commonly observed during migration, apoptosis and cytokinesis[33-35]. Recent evidences suggest that blebs play an essential role during cell migration especially during embryonic development and tumor cell propagation[34, 36]. During migration, blebs have been observed as leading-edge protrusions in 2D substrates [37-39] as well as in confined three-dimensional spaces[40-42]. The mechanism of bleb protrusion is significantly different from actin cortex driven protrusions, such as lamellipodia, and during migration in confined 3D space, tumor cells have demonstrated a switch between these two migration mechanisms and studies have also suggested that these two mechanisms complement each other in directional migration [35, 41, 43].

Blebs can expand up to 4 μm from the original position of the plasma membrane and demonstrates a dynamic life cycle that lasts approximately 2 minutes [35]. Under different experimental conditions, blebs formed by various types of cells follow a remarkably similar pattern exhibiting a rapid expansion phase (5-20 s), a brief static phase(10-30 s) and a relatively slow retraction phase (1-2 min) that returns the cell membrane back to its original position[44]. Unlike other protrusions such as lamellipodial and philopodial protrusions which are driven by actin polymerization, the mechanism of bleb protrusion and retraction is a result of the interplay between the rheology of the cytoplasm, membrane tension and reformation of the cortex underneath the plasma membrane [33, 35, 45].

Since blebbing occurs on small spatiotemporal scales, it is difficult to experimentally observe the interplay of the bio-mechanical processes in a bleb cycle. Thus, numerical modeling has been used as an alternative to investigate intracellular pressure and blebbing dynamics. Several numerical modeling frameworks have proposed to model various aspects of cellular blebbing. *Tinevez et al.* [45] proposed a model of bleb expansion driven by hydrostatic pressure and membrane tension. By comparing theoretical and experimental results they predicted a minimum value of membrane tension for blebs to expand. *Strychalski & Guy* [46] modeled the interaction between elastic membrane, actin cortex and intracellular fluid which demonstrated multiple timescales in intracellular pressure dynamics. *Young & Mitran* [47]

developed a volume conserving approach where the retraction phase is governed by myosin and actin monomer concentration. *Spangler et al.* [48] used spring attachments to model the interaction between cortex and the membrane and predicted that blebbing is favourable when membrane area is higher than the area of the cortex. *Tozluoğlu et al.* [49] modeled the cell cytoskeleton as viscoelastic material connected to bio-molecular agents and aimed to predict the efficient strategy for rapid migration in different matrix geometries. These numerical models investigated individual aspects of cellular blebbing without fully addressing the interplay of the mechanical processes and acto-myosin kinetics during both expansion and retraction phase of a bleb cycle.

Although, the exact mechanism of acto-myosin contraction in the cellular level have been difficult to observe and validate experimentally, the contractile mechanism has been extensively studied in skeletal muscles[50]. The shortening of contractile unit or sarcomeres have been described by cross bridge model[51] and the forces involved in muscle contraction has been defined by power stroke model[50].

In our study, we are applying the theoretical models of muscle contraction to describe the acto-myosin contraction in migrating cells. We are assuming that the contractile mechanisms in migrating GBM cells and striated muscle cells are similar. In this article, we used finite element method to systematically investigate the different roles of key cytoskeletal material parameters in the expansion and subsequent retraction of a cellular bleb under the conditions of confined migration. We modeled a part of the blebbing cell with a poroelastic cell body, an elastic membrane and an intermediate fluid filled domain. Actomyosin contraction has been introduced as the driving force of bleb formation and in combination with our experimental observations, we also aim to identify the optimal rate of myosin attachment to actin fibers which generates the pulling force on the plasma membrane during bleb retraction.

3.2 Methodology

3.2.1 Description of the three-dimensional model

A three-dimensional domain (5μm × 5μm × 2.5μm) represents the poro-elastic cytoskeleton of a cell with elastic cell membrane of 50 nm thickness. Bleb formation is characterized by detachment between the cell cytoskeleton and a portion of the cell membrane followed by fluid flow into the detached membrane resulting in membrane protrusion. To incorporate the effect of fluid flow in bleb formation, a narrow rectangular fluid domain of 50 nm thickness is created between the poro-elastic cytoskeleton and elastic cell membrane (Fig 11). The cell membrane domain is divided into two parts where the central part of 3μm diameter height is subjected to detachment from the actin cortex after a critical pressure level was reached. Remaining part of the membrane segment was constantly attached to the actin cortex with spring elements (Fig 13).

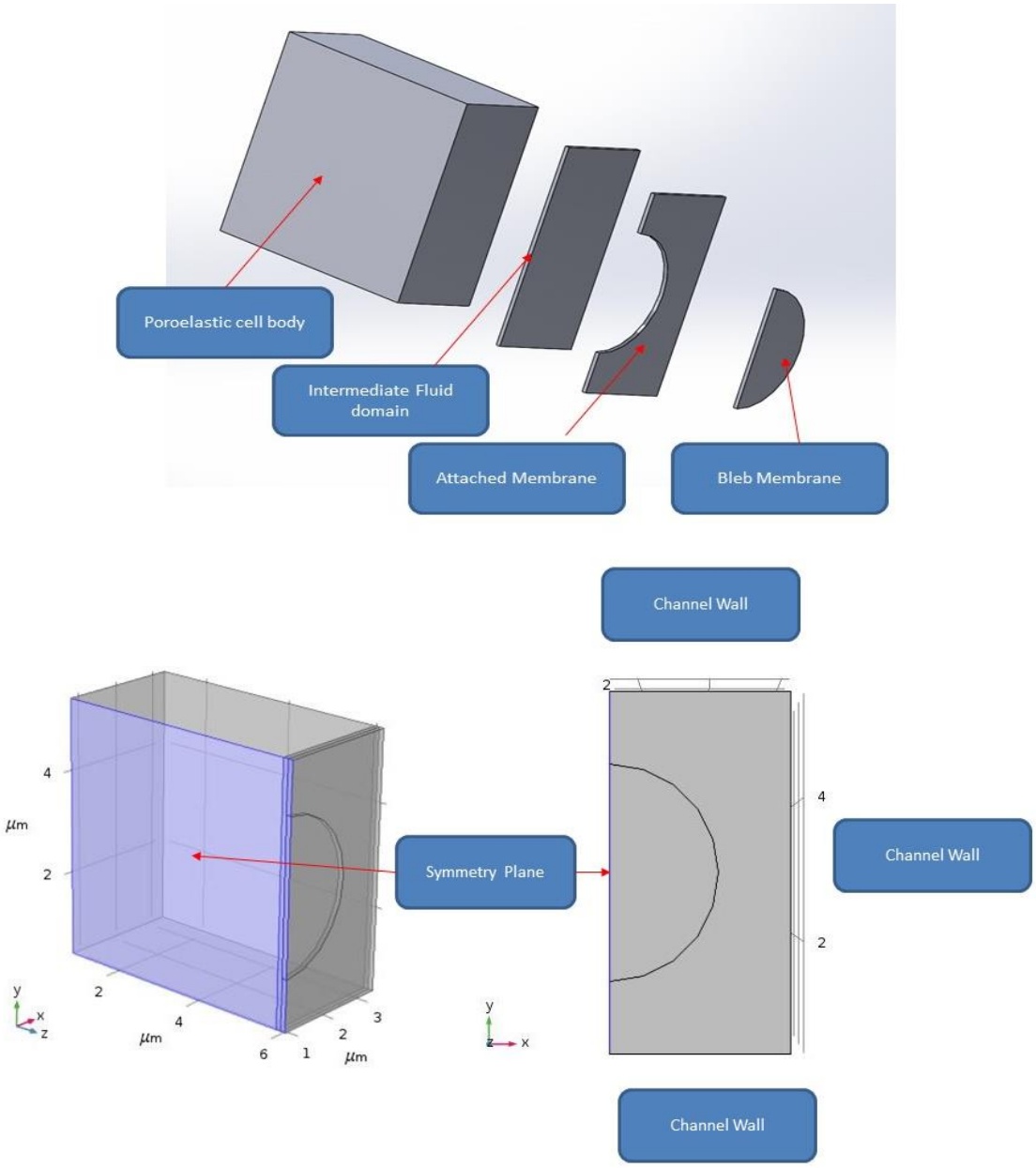

Figure 11 Description of the model Geometry.The model consists of an assembly of a poroelastic cell body, an intermediate fluid domain and membrane divided into two segments.

3.2.3 Formulation of Governing Equations

Property	Symbol
Stress in solid	σ_s
Displacement in solid	x
Fluid Pressure (poroelastic domain)	P_f
Density of fluid	ρ
Dynamic Viscosity	μ
Fluid Velocity	u
Fluid Pressure	p
Fluid Volume Fraction	ϕ_f
Permeability	κ
Actin Contractility Factor	F_{Actin}

Table 2 Symbols used in the governing equations

The actomyosin attachment kinetics is governed by the following equation

$$\frac{\delta C}{\delta t} + \nabla.(-D\,\nabla C) + u.\nabla C = \mathrm{R}$$

The concentration of the actomyosin complex governs contractile force in the poroelastic cell body as well as the pulling force during retraction. The poroelastic domain is governed by the following two equations

$$\phi_f\left(u - \frac{\delta x}{\delta t}\right) = -\frac{\kappa}{\mu}\nabla P_f$$

$$\sigma = \sigma_s - P_f I$$

The resulting fluid pressure of the poroelastic domain is coupled with the fluid pressure of the purely fluid domain at the interface:

$$P_f = p$$

The fluid domain is governed by stokes equation and the fluid-membrane interface the displacement of the membrane is governed by the following equation:

$$\nabla.[pI - \mu(\nabla u + (\nabla u)^T)] = \nabla.\sigma_{Cortex} + \nabla.\sigma_{elastic} - \nabla.\sigma_{pulling}$$

The term σ_{Cortex} is dependent on the spring elements attaching the bleb membrane and the cortex are defined as following

$$K_{cortex} = K_1 - K_1 * f(P)$$

The function f(p) dictates the state of membrane-cortex attachment and the value is zero when the generated pressure reaches above a critical pressure level.

$$f(P) = 0; \qquad 0 \leq P < P_{critical}$$

$$f(P) = 1; \qquad P_{critical} \leq P$$

3.2.4 Active forces involved in local acto-myosin Contraction

Based on the cross-bridge model, which describes the attachment of myosin motor to actin to form the actomyosin complex we are defining the attachment as a second order kinetic reaction

$$Actin\ Fiber + Myosin\ II \rightarrow ActoMyosin\ Complex$$

$$\frac{d[Myosin\ ]}{dt} = -k[Actin] * [Myosin]$$

$$\frac{d[ActoMyosin]}{dt} = k[Actin] * [Myosin]$$

Here, k is the reaction constant of the second order reaction.

The interplay of the forces during acto-myosin contraction has been defined by the power stroke model[50]. There are two major forces that are involved during the localized contraction of acto-myosin

complex. The contractile force $F_{contraction}$ is generated by myosin motor, the elastic drag force $F_{elastic\ drag}$ is generated by actin helix which compresses the myosin motor before detachment from actin.

$$F_{contraction} = \frac{k_m}{2 \times \Delta}\delta$$

$$F_{elastic\ drag} = \frac{k_m}{2 \times \Delta}(v \times t_r)^2$$

Assuming the behavior of myosin motor as a linear spring in a power stroke model,

δ = Myosin stroke distance = 5 nm [50]

k_m= spring constant of myosin =5 pN/ nm [50]

Δ = Pitch of actin Helix = 36 nm[50, 52]

v = sliding velocity

t_r = release time = 0.6 ms[50]

$d_s = t_r \times v = sliding\ distance$

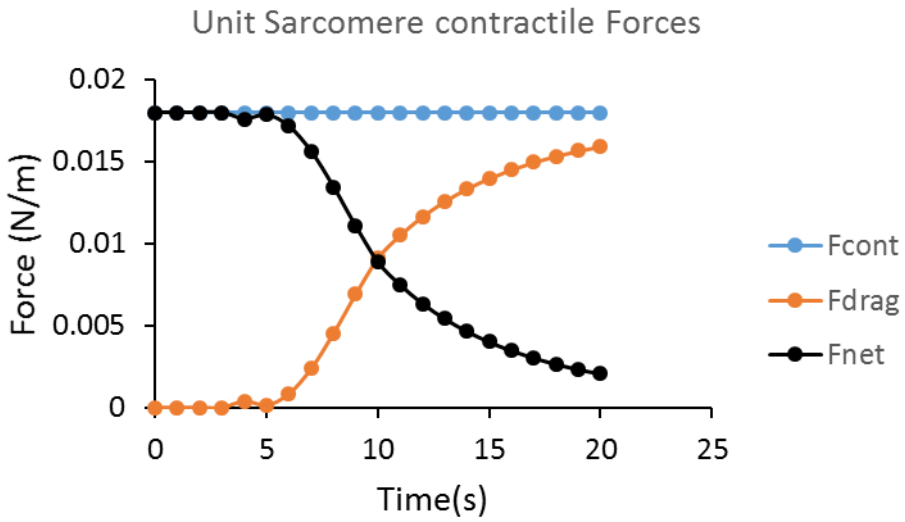

Figure 12 Unit contractile force of the poroelastic cell body during the bleb expansion phase.

The calculated contractile and drag forces therefore yield the following

$$F_{contraction} = 18\ pN/nm;\ F_{elastic\ drag} = \ 0.0689\ d_s^2\ pN/nm$$

The net forces in every unit of actomyosin contraction is defined by the following

$$F_{net} = \left(F_{contraction} - F_{elastic\ drag}\right)$$

Transient change of drag force is illustrated in Figure 12. When a unit of poroelastic cortex is subjected to larger displacement, the opposing elastic drag force also rises over time. The net contractile force reaches a steady state value when the drag force has reached a threshold value. The total force at a time step depends on the amount of bound actomyosin complex and is determined by the following

$$\text{Total force} = F_{net} * [Actomyosin] * Unit\ Contractile\ force\ per\ molar\ volume$$

3.2.5 Initial and Boundary Conditions for Actomyosin Reaction

The initial actin concentration was set at 0.10 x10^{-6} mol/m^3 [53, 54] which is the saturated concentration of filamentous actin and the myosin concentration level was set at 0.6x10^{-6} mol/m^3 [53, 55].. To prevent the concentration of myosin-II and acting from dropping significantly, the concentrations at the far end of the poroelastic domain have been kept constant at the same level of initial concentration.

Parameter	Value	Reference
Young's Modulus of cell, Ec	500 Pa	[56]
Porosity ϕ_f	0.5	[56]
Poisson Ratio, ν	0.3	[57]
Density ρ	1000 kg/m^3	[56]
Dynamic Viscosity μ	0.001 Pa-s	[56]
Permeability κ	4×10^{-12} m^2	[56]
Actin Diffusivity in cell body, D	5×10^{-12} m^2s^{-1}	[54]
Actin molar Contractility factor, F_{Actin}	500 pN/ μm^{-3}	[45]

Table 3 Material properties and parameters used in the computational model

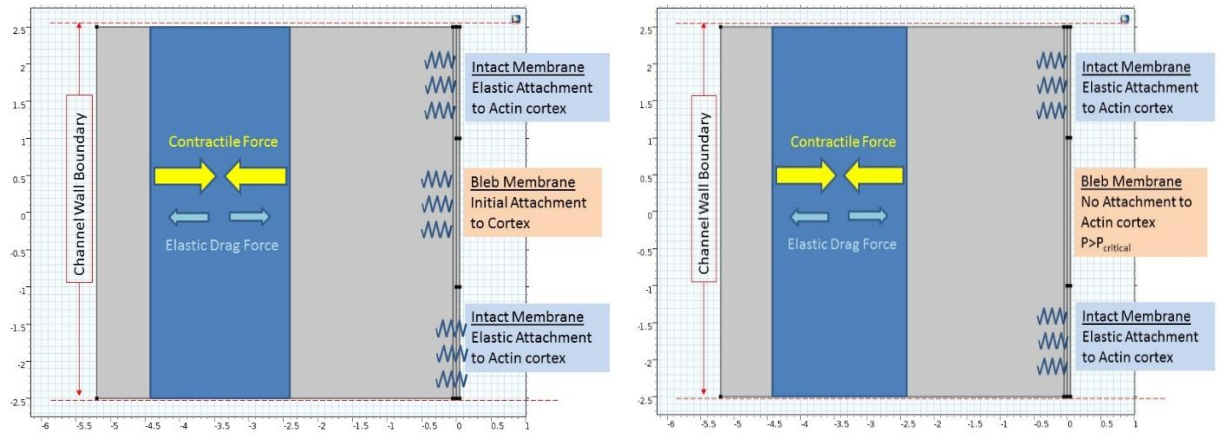

Figure 13 Initial and boundary conditions(left) of the bleb membrane. When a critical pressure level is reached, spring elements attaching the membrane to the cortex are turned off (right)

3.2.6 Retraction of plasma membrane by active pulling of Actomyosin complex

Expansion of plasma membrane results in the influx of fluid in the bleb region and creates a gradient of actin and myosin concentration. The gradient generates an outflow of actin and myosin molecules from the cortex to the newly formed bleb.

$$Actin + Myosin \rightarrow ActoMyosin$$

$$\frac{d[ActoMyosin]}{dt} = k_2[Actin] * [Myosin]$$

The force generated by actomyosin assembly pulls the membrane inward towards the actin cortex. The pulling force is governed by following equation

$$F = [ActoMyosin] * f_{retract}(t) * F_{unit}$$

The value of $f_{retract}(t)$ switches from 0 to 1 at the end of the expansion phase (t=20).

3.2.7 Actomyosin pulling rate of bleb membrane of a cell migrating in-vitro

Human glioblastoma multiforme (GBM) cells transfected with pEGFP-C1 F-tractin- EGFP was seeded in front of a PDMS channel of 5 ×5 µm cross-section. Once the cell has migrated completely inside the

channel, filamentous actin and myosin-II activity was measured using live imaging(fpm=4). Multiple front and rear blebs were identified, and the area of each bleb was measured over time using ImageJ (Fig 15).

The change of bleb area was compared to the result of a parametric study of bleb retraction with actomyosin reaction rates (1,2,3 m^3/mol-s) and the actomyosin reaction rate was estimated for the cell migrating in-vitro.

3.2.8 Calculating Work done by actomyosin contraction

$$\text{Work Done } W = P\,\Delta V,$$

where, P= fluid pressure generated underneath the blebbing membrane

ΔV= Change of volume of the fluid domain underneath the blebbing membrane

A part of the energy applied will expand the membrane bleb with the increase in fluid volume, while a small portion of the energy will be stored in the elastic membrane under deformation. The recoverable elastic energy is known as elastic strain energy and the strain energy density is defined as

$$W_s = \frac{1}{2}(\sigma_x \epsilon_x + \sigma_y\, \epsilon_y + 2\, \sigma_{xy} \epsilon_{xy})$$

Strain energy is the product of Strain energy density and the volume of the elastic blebbing membrane.

$$Membrane\ Volume\ V_{membrane} = \frac{4}{6}\pi\,((R+t)^3 - R^3)$$

$$Strain\ Energy = W_s\ \times V_{membrane}$$

Where *R* is the inner Radius of the Bleb and *t* is the thickness of the membrane

3.3 Results

3.3.1 Regional Hydrostatic Pressure generated by actomyosin contraction

The contractile forces generate regional displacement in the poroelastic cell body which results in the relative velocity of the fluid. Due to the confined geometry of the surrounding ECM, the relative velocity

results in the rise in static pressure in the cell body which triggers the rupture of the cortex-membrane attachment. *Maugis et. al* [38] estimated that the driving pressure value for generating membrane detachment for cortex ranges between 1 to 10 Pa. Our model demonstrates a developed hydrostatic pressure of over 3Pa (Fig 14) due to actomyosin contraction in the poroelastic cortex. The generated pressure leads to rupture of cortex-membrane assembly and leads to bleb protrusion.

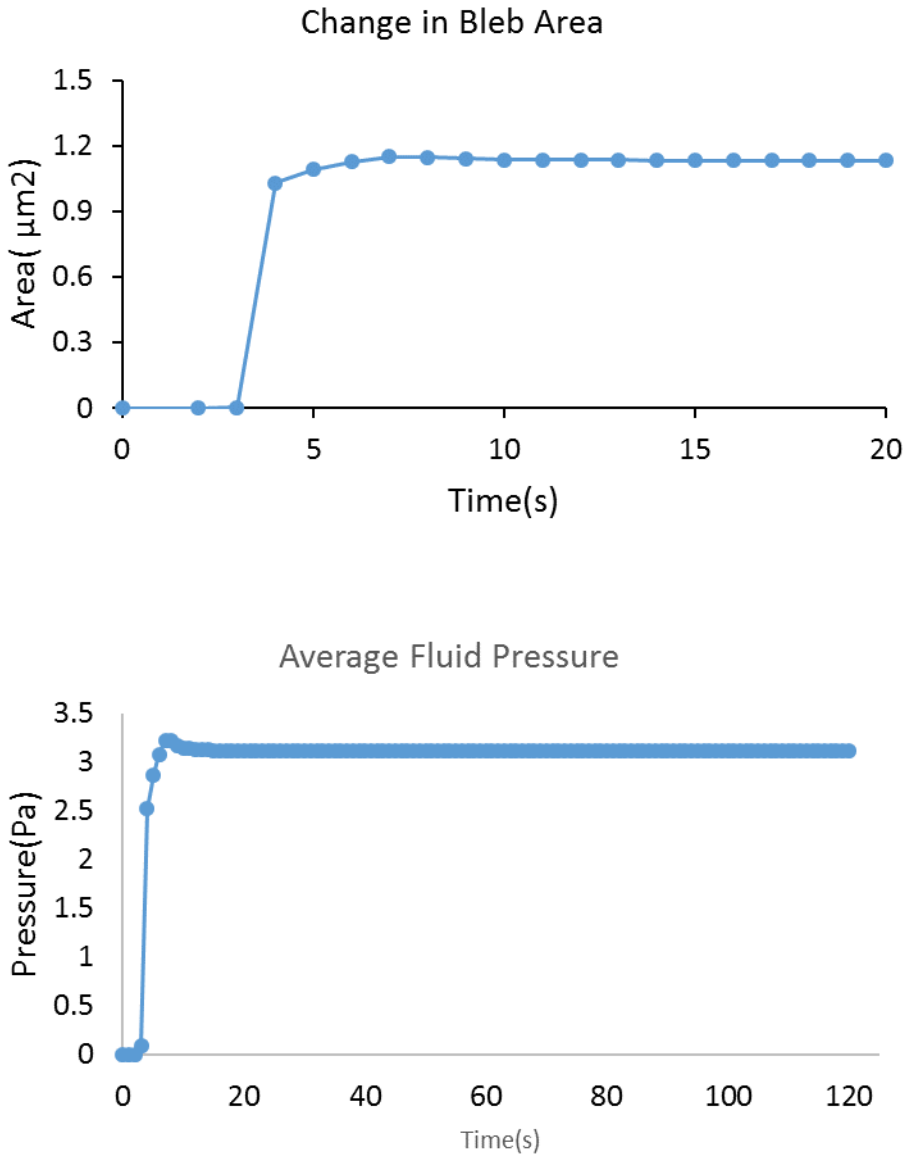

Figure 14 Change in Bleb area and average pressure during bleb formation.

3.3.2 Comparison between the numerical results and experimental observation

Live imaging of actin revealed that both front and rear population have cross sectional area around approximately $2\mu m^2$(Fig 14). Our numerical results demonstrate bleb area of over $1\mu m^2$ but the value is within the margin of distribution as illustrated in Fig 15. It is possible that the amount of actomyosin contraction is higher for cells in pressure driven migration in confined ECM and that a larger portion of plasma membrane at the front and leading edges is detached.

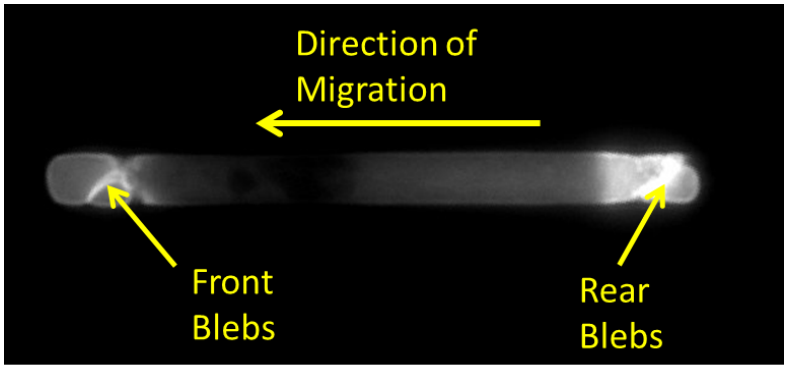

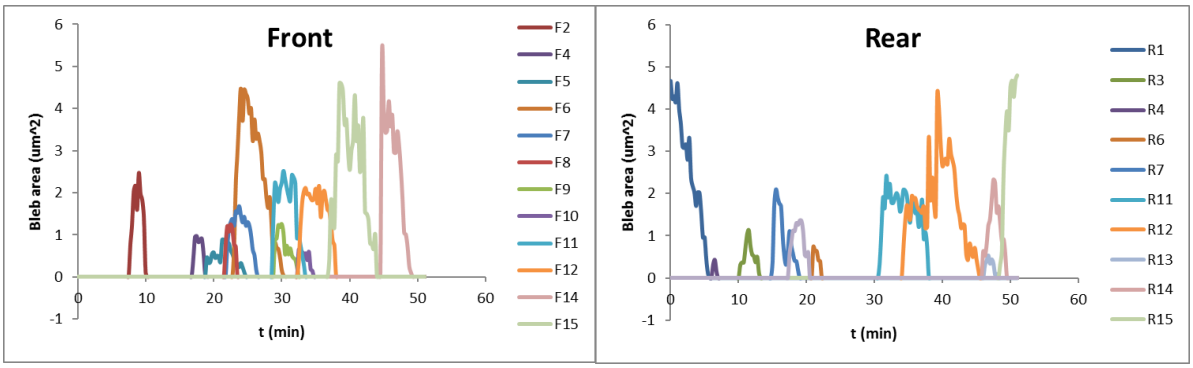

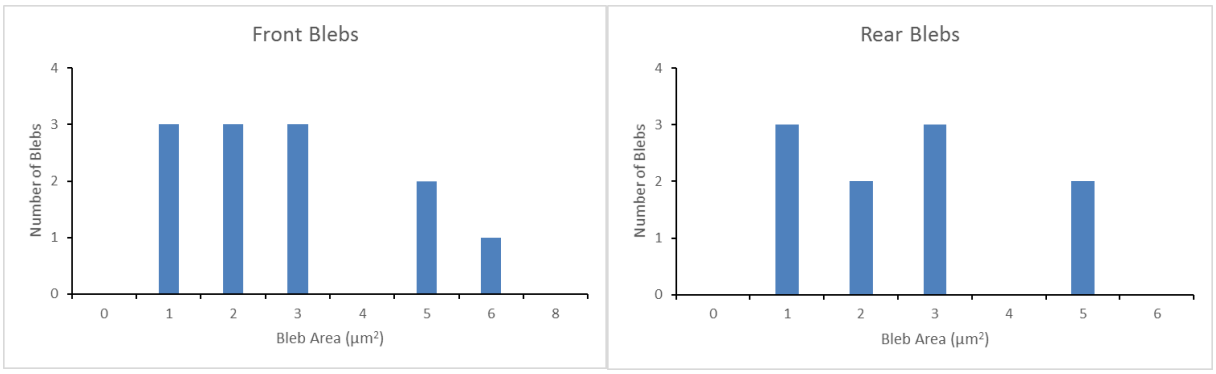

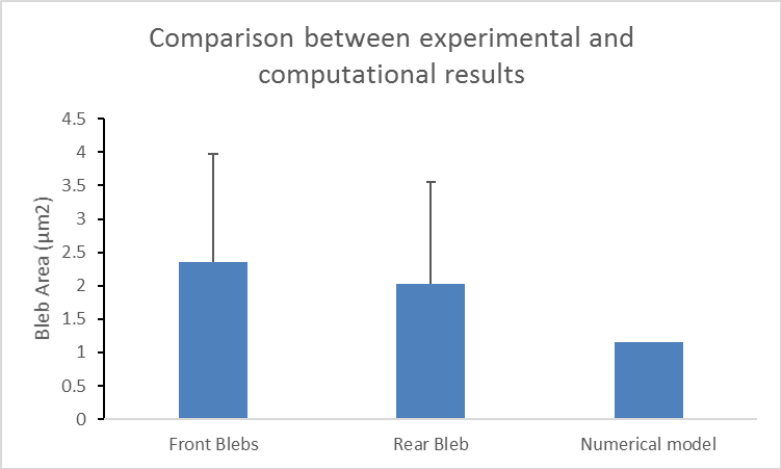

Figure 15 Histogram plot of front and rear bleb area distribution. The mean area for front and rear bleb are (2.35±1.61) µm^2 and (2.02±1.53) µm^2 respectively.

3.3.3 Estimating the optimal reaction constant of Blebs in a migrating cell

Using the obtained relationship between pulling rate and time required for retraction, actomyosin retraction rate for individual blebs observed during the experiment were calculated using the empirical relationship, $k_2 = 72.651(T_R)^{-0.759}$. (Fig 16). The relationship obtained from the numerical model was used to estimate the reaction rate multiplier k_2 for the front and rear blebs which are illustrated in Fig 17**.** The rate of actomyosin pulling is within the similar range of values and no statistical difference has been observed in the retraction parameter of the front and rear blebs.

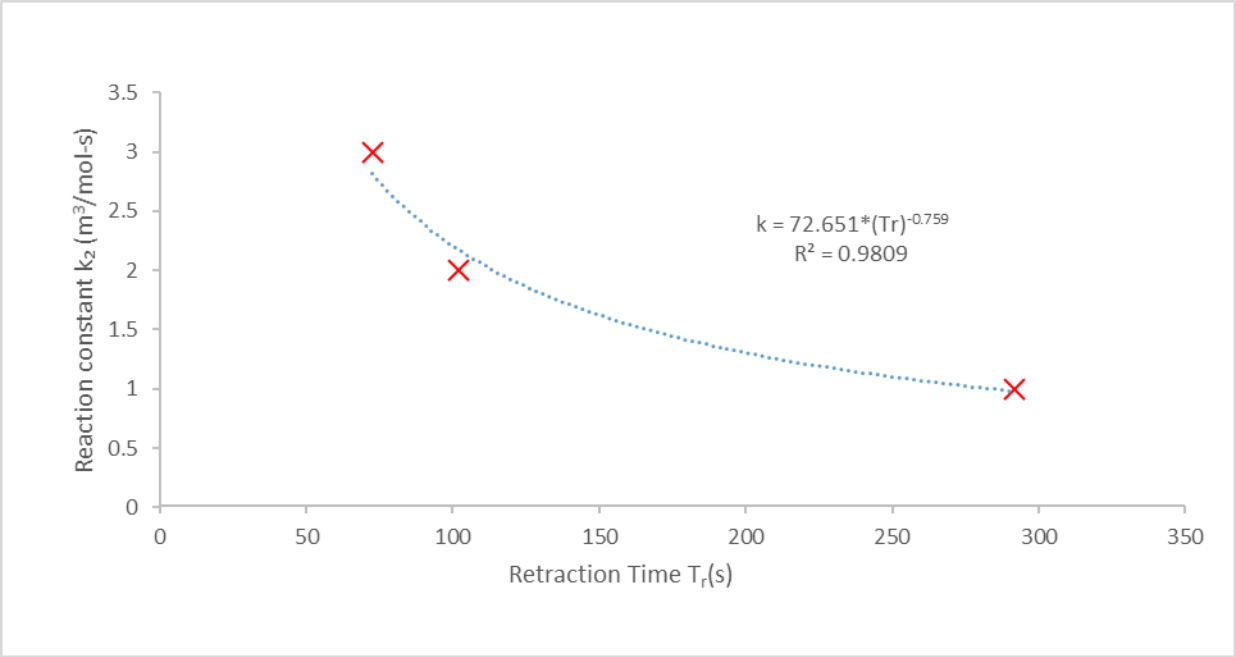

Figure 16 Relationship between retraction time and Actomyosin pulling rate obtained from the parametric study of reaction rate k_2.

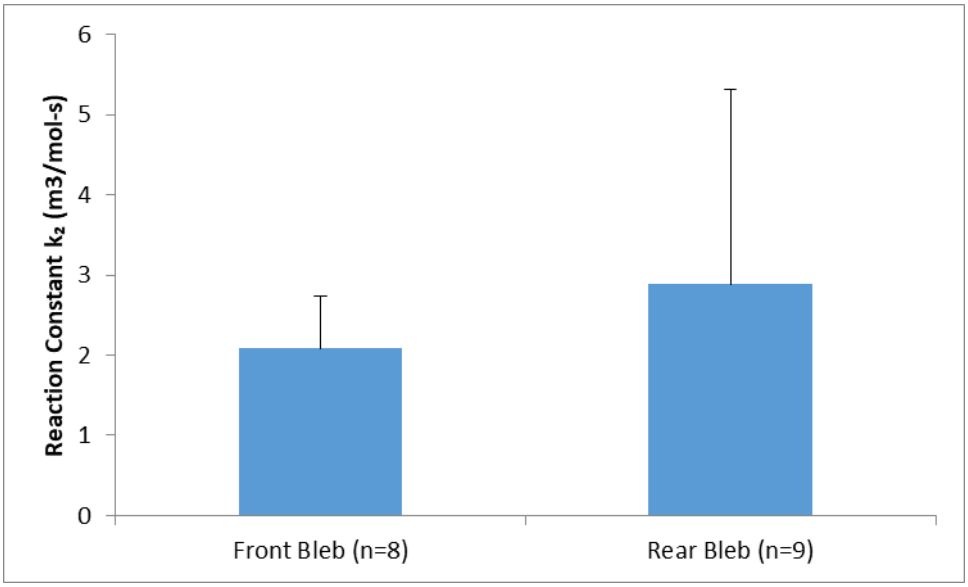

Figure 17 *Estimated* reaction constant k_2 of the front and rear blebs of the migrating cell.

3.3.4 Effective sarcomere units for Bleb generation

For a single muscle contraction, the total work done by average sarcomere unit is 4 kT= 8.22× 10^{-21} J[58]. Using our calculation of work done during bleb formation, the maximum work done at the peak of bleb expansion is 3.6× 10^{-18} J (Fig 18). Based on the results we estimated that the number of effective sarcomere-like units in a migrating GBM cell is approximately 437.

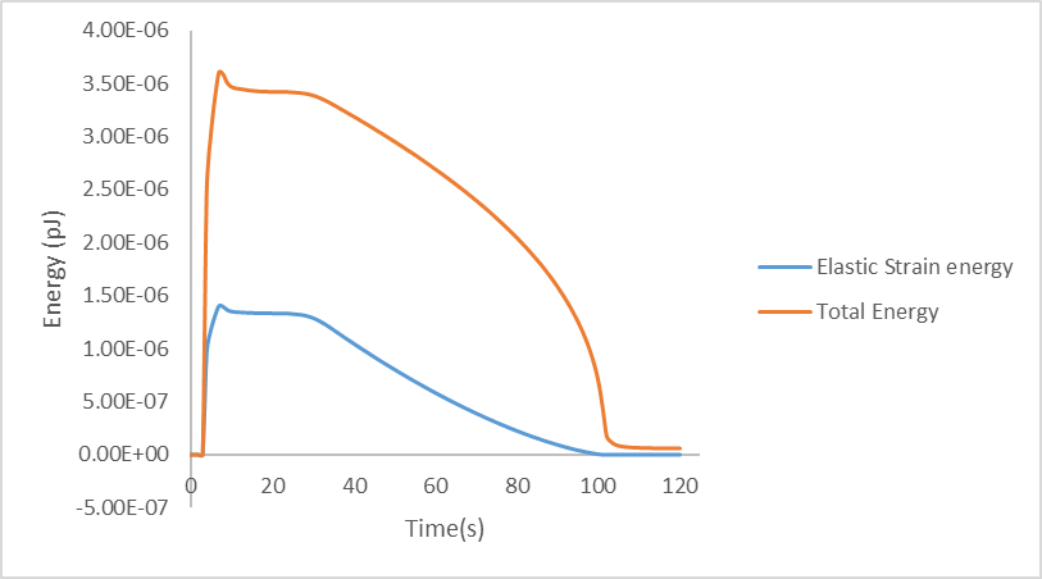

Figure 18 Comparison of the work done by actomyosin contraction and the elastic strain energy of the membrane.

Chapter 4
Discussion

4.1 Difference in creep responses and the intracellular actin/myosin distribution

Our results revealed that, in response to aspiration pressure load, actively migrating GBM cells exhibit higher stiffness than those in stationary state. Through the deformation process, cells in migrating group could absorb more energy elastically with relatively small dissipative energy loss compared with those in the stationary group. At elevated negative pressure loads, there is a linear increase in elastic deformation and higher distribution in elastic storage than energy loss up to - 30 cm H_2O. For further increase in negative pressure load, cells respond with higher stiffness and the deformation appears to reach a plateau. Results from retraction phase also exhibit similar difference between the two cell groups.

To explore the underlying causes in creep responses between the two groups at different kinematic states, we examined their respective intracellular distributions of actin and myosin. Results from migrating group show high level of polarized distributions of actin and myosin at both the front and posterior ends of the cells. Actomyosin contraction generates forces leading to regional build up in intracellular pressure and elevated mechanical stiffness. It also affects the corresponding distribution in the response of the cell between elastic and viscous components to the negative pressure load applied. We hypothesize that the elevated front-end stiffness facilitates the migrating cells to overcome the resistance arising from confinement for forward movement. In terms of Voigt model representation (Fig 3A) migrating cells have a spring with high stiffness and a damper with lower frictional coefficient. On the other hand, cells at the stationary state have a spring with low stiffness (more compliant) and a damper with higher frictional coefficient.

Results from immune-histochemical study also showed polarized distribution in actin and myosin at the posterior-end of the migrating cells. We hypothesize that they serve the anchoring effect and help pushing the forward movement of the nucleus, as suggested by *Lämmermann et al*.[59], noting that the diameter of the nucleus are comparable to that of channel cross-section at 5 x 5 μm.

4.2 Mechanical properties of cancer cells

Various studies have demonstrated that the metastatic potential of a cancer cell is directly correlated with its capability to deform under mechanical stress and that the phenotype of cancerous cells is relatively more compliant than healthy cells [7, 8, 60, 61]. This observation have been found to be consistent in studies of fibroblasts[62], ovarian cells[8], lung carcinoma cells[10], melanoma cells[11] and hepatoma cells in mouse; and in epithelial cells[60, 61], kidney cells[63], breast cancer cells[64, 65], colon cancer cells[66], leukemia cells [67], pancreas[68] and prostate cancer cells[69] in humans. Results from these studies suggested that the change in cytoskeletal structure is associated with tumorigenesis and reduction in cellular stiffness is directly associated with the degree of malignancy of a cancerous cell. Studies on various cell lines have also confirmed that the metastatic potential of cancer cells increases with the increase of cellular compliance or fluidity of the cells and that the mechanical stiffness of a cell is an essential indicator of the cell's invasiveness[70-72].

The rise in cellular compliance could aid the cell to migrate through deformation and flow, allowing the cell to migrate from an open environment to a confined environment with less energy cost. During the transition, it is likely that modulated mechanical properties could effectively facilitate cancer cell migration leading to enhanced invasiveness. Many of these studies have been conducted with cells on 2D substrate and have not addressed the effect of kinematic states. Our results show that the mechanical properties of cancer cells could depend on their kinematic states.

4.3 Redistribution of Actin and Myosin during migration

Distributions of cytoskeletal components, their architecture, and relative biochemical process could modulate regional compliance of a cell to engage in cellular function and activity. Yanai et al.[73] reported regional differences in stiffness and viscosity of migrating neutrophils on 2D substrate with much lower stiffness and viscosity at the leading edge than the body and trailing edge. The finding supports the commonly described mesenchymal mode of cell migration on 2D substrate that consist of protrusion, adhesion, at the leading edge, followed by contraction and release phases at the trailing side[74].

Cell migration on 2D environment is governed by the interplay of three types of forces: cell-ECM adhesion, actin polymerization and actomyosin contraction[75] . In a confined 3D environment, the interplay of these forces can alter significantly [40, 75, 76]. Studies have confirmed that in confined conditions a cell can migrate in the absence of cell-ECM attachment and actin polymerization[40, 76, 77]. These studies suggest that in 3D confinement the cell is propelled by intracellular hydrostatic pressure generated by actomyosin contraction.

The mechanism and effect of actomyosin contraction have been broadly studied in muscle tissues. Studies conducted on contractile muscle tissues have demonstrated that the degree of voluntary muscle contraction is directly correlated to the overall stiffness of muscular tissues[78-81]. *Buillard et al.* [78] showed the shear modulus of the muscle tissues increase from 20 to 150 kPa in proportion to the higher level of voluntary muscle contraction. Studies derived from human biceps (brachialis) by *Gennisson et al*.[79] and *Yoshitake et al.* [80] have confirmed a rise in shear modulus under higher loading intensities. Real time ultrasound mapping of local stiffness of muscle tissues by *Shinohara et al.* [81] showed a significant rise in Young's modulus from ~40 kPa at resting state to ~258 kPa at contractile state. These findings suggest that during muscle contraction, the shortening of sarcomeres results in the increase in regional tissue stiffness.

Studies on isolated cells have also demonstrated that increased actomyosin contractility reduces cellular compliance [82, 83]. Using magnetic tweezer *Kollmannsberger et al.*[82] analyzed the elastic behavior of the cytoskeleton in mouse fibroblasts. They reported that the non-linearity of the stiffness of the cell is caused by the changing internal tension of the cytoskeleton which is governed by the activity of actomyosin contractile apparatus. Similar conclusions have been drawn by *Steven et al.* [83] that demonstrated reduction in localized compliance of a cell when under the presence of a contractile agonist serotonin.

Although these prior studies were mostly focused on muscle tissues and isolated muscle cells, the results indicate that contraction of actin-myosin filaments can result in localized stiffness increase which can also occur in non-muscle cells. Concentrations of intracellular actin and myosin filaments in certain regions can thus be indicators of contractile site formation and subsequent increase in localized stiffness due to

actomyosin contraction. In our study, from migrating GBM cells, we observed significantly higher amount of actin and myosin localized at the front and posterior ends of migrating GBM cells (Fig 7). It suggests increased level of regional actomyosin contraction, higher intracellular pressure, and hence regional mechanical stiffness and the partition of energy between elastic storage and frictional loss.

4.4 Cell-ECM interaction in confined conditions

The ability of a cell in sensing its surrounding physical environment plays an essential role in cellular processes such as proliferation, differentiation and migration[22, 84]. In a migrating cell, the force generating mechanisms are triggered and regulated by the geometry of the surrounding matrix which also governs the preferred migration mode (between mesenchymal and amoeboidal) of the cell[75]. Studies carried out extensively on cells migrating in open 2D substrates have underscored the importance of adhesion receptors in transmitting the intracellular forces from the cytoskeleton to the substrate[17, 18]. These adhesion receptors, (known as integrins) bind with ECM proteins and form focal adhesion complex (FAC) that link the cytoskeleton to the ECM.

However, studies indicate that during migration in a confined 3D environment, cells can achieve migration without forming focal adhesions or any other form of cell-ECM attachments[18, 59, 85, 86]. It is therefore likely that during migration in a confined environment, GBM cells do not prefer to use adhesion based attachments even in the presence of ECM proteins like fibronectin or laminin. In contrast, the cells have been found to generate normal stress on the surrounding surfaces on all sides to provide anchorage to the substrate and generate shear force to propel the cytoskeleton in forward motion[40]. The normal stresses on the surrounding walls are exerted by hydrostatic pressure forces generated by actomyosin contraction in the random locations of the cytoskeleton[33, 35, 40, 41]. Generation of hydrostatic pressure inside the cell is often indicated by plasma membrane protrusions (a.k.a. Blebs) and the pressurized condition of the cell allows the cell to anchor to the surroundings and protrude forward in a “chimneying” mode of amoeboid migration[40]. *Lämmermann and Sixt* [75] also argued that migration in confinement has very little role of cell adhesion and the propelling force is likely a result of myosin II driven contractile force coupled with significant amount of hydrostatic forces.

4.5 Comparison of Detachment force

Several quantitative and qualitative assays have been developed to study cell adhesion in 2D substrates. Quantification of the adhesion forces are measured by the forces required to detach the cells from the substrate and the quantified results provide an insight in the mechanical strength of cell-ECM attachment under different conditions. Some of these studies have focused on detachment of a statistically significant fraction of cell population while some of the studies have focused on detachment of cells. In our study, we have focused on the quantifying the detachment forces of individual cells in confined conditions to understand the difference of cell-ECM attachment forces between 2D and 3D matrices.

Our results suggest that the detachment force of GBM cells in confined microchannel are comparable to the detachment forces of various cell populations summarized in Table A-8. Compared to healthy brain cells, GBM cells have been found to express certain $\alpha\beta$ family integrins in larger quantity [15] and tumor cell expression of β family integrins have been correlated with metastatic progression of various types of cancer cells[87]. Surprisingly, glioma cells demonstrate a higher degree of invasiveness in narrower pathways,[5] although in these confined conditions the cells utilize no or little integrin receptors for migration. This suggests that when cell switches its migration mode from mesenchymal to adhesion-independent amoeboidal, the lost traction from integrin-ECM attachments is compensated by generating sufficient perpendicular forces to maintain its invasiveness. Therefore, quantification of detachment force has provided a better understanding of the physical interaction between the cell and its surrounding ECM.

4.6 Bleb formation due to rise in hydrostatic pressure

Yip et al. [40] has demonstrated that in the absence of ECM proteins human promyelocytic leukemia cells can migrate using bleb protrusions when the cells are confined by two pieces of gel. The frequency of bleb nucleation rises as the space between the confinement is reduced. *Charras and Sahai* [88] also demonstrated that change in geometry of confinement results in change of cell migration mechanism and showed that migrating cells exhibit reduced presence of lamellipodia in confined geometry. The suppression of cell-ECM adhesion in confined environment gives rise to higher levels of intracellular

hydrostatic pressure generated by high level of acto-myosin contractility[59, 75]. Higher intracellular pressure results in expansion of membrane segments that are detached from the actin cortex resulting in nucleation of bleb. Therefore, understating the dynamics of cellular blebbing is essential to understand the migration of cell in confined ECM.

In our study, the governing equations are formulated to represent the physical events leading to the formation of bleb. To accurately reproduce experimental observations, springs were added to the undetached membrane to withstand the effect of hydrostatic pressure and the membrane portion detached from the actin cortex could expand forward as the intracellular pressure propagated from poroelastic cell body to the membrane region. Although the folded structure of the lipid bilayer was not considered in the model, the parametric study on membrane elasticity demonstrated that when the Young's modulus of the membrane is reduced to 500 Pa the maximum area of the bleb would go up to almost 1 μm^2 (Fig 14). The variation of effective stiffness of the membrane governed by degree of unfolding of the bleb membrane could therefore explain the variability in bleb size.

The cortex is normally attached to plasma membrane with linker proteins such as ezrin, radixin and myosin[46]. Following the rapid bleb expansion, the relatively slower bleb retraction is initiated by actin cortex re-assembly which is characterized by recruitment of G-Actin to plasma membrane region followed by recruitment of myosin II to continuous rim-like formation of F-Actin and membrane linker proteins[41]. The membrane is retracted by an acto-myosin driven contraction mechanism which is a much slower process (60- 120s) than the expansion phase. The optimal rate for front and rear blebs ranges between 1-2 m^3 /mol-s (Fig 17). There is no experimental evidence of reduction of hydrostatic pressure when the bleb is retracting, therefore it is possible that the pressure force working opposite to the retraction force plays a role in the elongating the period of bleb retraction.

Studies conducted on *C.Elegan* cells have exhibited upto 10 sarcomere units in mature wild type cells[89]. Our results demonstrate, that in migrating GBM cells the effective number of sarcomere-like units required to generate the energy for expanding a single bleb is 437 which is significantly higher than observed in contraction generating elegan cells. Based on our results, to generate the pressurized condition and maintain the constant pressurized state during migration in confinement, the cell requires

significant upregulation of actin and myosin II molecules. When the cell is migrating in amoeboidal migration mechanism the presence of actin polymerization and receptor-ECM attachment is diminished. The major source of force generation therefore relies completely on acto-myosin contraction and hence it is possible that the number of actin and myosin molecular units are increased under such migratory conditions.

Appendix

Raw data of Creep Experiment

Aspiration Data: Migrating state

Applied Pressure (cm H_2O)		U∞	η/E
20	Cell 1	1.292004	0.550116
	Cell 2	1.641879	0.947401
	Cell 3	1.624699	1.019599
	Cell 4	1.092986	1.213127
	Cell 5	1.674998	0.807479
	Cell 6	1.367952	0.879094
	Cell 7	1.973	0.717629
25	Cell 1	1.423999	0.414371
	Cell 2	1.916	0.443782
	Cell 3	2.753878	1.019599
	Cell 4	1.464093	0.824776
	Cell 5	1.909	0.527346
	Cell 6	0.99	0.533209
	Cell 7	0.994212	3.167719
30	Cell 1	1.819	0.183786
	Cell 2	3.259889	0.465064
	Cell 3	3.384999	0.142244
	Cell 4	2.205	0.465508
	Cell 1	2.032	0.604478
	Cell 2	1.935991	0.169028

35	Cell 3	2.64239	0.369942
	Cell 4	2.605	0.359581
40	Cell 1	2.198001	0.399303
	Cell 2	1.882539	0.479264
	Cell 3	2.842999	0.201
	Cell 4	2.899001	0.318353

Table A 1: Summary creep data (aspiration) in migrating state

Aspiration Data: Stationary state

Applied Pressure (cm H_2O)		U∞	η/E
20	Cell 1	4.533597	1.496714
	Cell 2	4.802933	1.09203
	Cell 3	4.682537	1.830472
	Cell 4	4.63487	1.810732
	Cell 5	4.042847	1.817882
	Cell 6	5.608691	2.739888
25	Cell 1	6.623865	1.718844
	Cell 2	5.534632	1.294483
	Cell 3	5.901325	1.61284
	Cell 4	5.464954	1.440231
30	Cell 1	6.376859	1.324132
	Cell 2	6.983204	1.203846
	Cell 3	6.239451	1.233734
	Cell 1	5.368384	1.003561

35	Cell 2	6.65204	1.203846
	Cell 3	6.952057	1.233734
40	Cell 1	6.376859	0.832522
	Cell 2	6.983204	1.203846
	Cell 3	6.239451	1.354734

Table A 2: Summary creep data (aspiration) in stationary state

Retraction Data: Migrating state

Applied Pressure (cm H_2O)		U_∞	η/E	U_{res}
20	Cell 1	0.895534831	0.150014	0.356093
	Cell 2	1.326001086	0.419913	0.089258
	Cell 3	1.642042121	0.199727	0.475997
	Cell 4	1.040995836	0.163257	0.683214
	Cell 5	1.09299895	0.57856	0.084229
	Cell 6	1.251405889	0.304895	0.263285
	Cell 7	1.55999998	0.419913	0.323257
25	Cell 1	1.515387	0.590942	0.356093
	Cell 2	2.718959	0.164044	0.789
	Cell 3	1.915997	0.201119	0.483922
	Cell 4	1.42402	0.417148	0.282837
	Cell 5	1.326001	0.419913	0.089258
	Cell 6	1.675141	0.304895	0.687019
	Cell 7	1.43402	0.448379	0.301537
	Cell 1	1.419	0.417148	0.277818
	Cell 2	1.297408	0.172496	0.078

30	Cell 3	3.384979	0.164155	0.441
	Cell 4	1.805029	0.523312	0.373
35	Cell 1	1.936	0.472496	0.716592
	Cell 2	2.841779	0.511834	0.524
	Cell 3	2.605002	0.638856	0.81394
	Cell 4	3.036926	0.70018	0.754796
40	Cell 1	2.715824	0.615762	0.494137
	Cell 2	1.923851	0.25276	0.778174
	Cell 3	2.796197	0.111834	0.363
	Cell 4	1.899	0.506719	0.301637

Table A 3: Summary creep data (retraction) in migrating state

Retraction Data: Stationary state

Applied Pressure (cm H_2O)		U_∞	η/E	U_{res}
20	Cell 1	4.533597	0.998325	0.821098
	Cell 2	4.802933	1.09203	1.157134
	Cell 3	4.682537	1.120304	0.571506
	Cell 4	6.487852	1.211085	1.110967
	Cell 5	4.042847	1.217882	1.159294
	Cell 6	5.608691	0.939888	1.141182
25	Cell 1	6.623865	1.318844	2.121098
	Cell 2	5.534632	1.294483	1.157134
	Cell 3	5.901325	1.01284	1.571506
	Cell 4	5.464954	1.440231	1.110967
	Cell 1	6.376859	1.124132	1.798773

30	Cell 2	6.983204	0.903846	1.223945
	Cell 3	6.239451	1.233734	1.323668
35	Cell 1	5.368384	1.113561	1.798773
	Cell 2	6.65204	0.703846	1.423945
	Cell 3	6.952057	1.133734	1.323668
40	Cell 1	6.376859	0.732522	1.798773
	Cell 2	6.983204	1.203846	1.223945
	Cell 3	6.239451	0.815473	1.323668

Table A 4: Summary creep data (retraction) in stationary state

Immunostaining measurement data of Actin and Myosin intensity

Cell 1

Norm Dist	Actin	Myosin
0	1.545151	1.2884098
0.001792339	1.593336	1.4178328
0.003584678	1.707129	1.7486396
0.005375965	2.027377	2.1299811
0.007168304	2.339791	2.4061085
0.008960643	2.792783	2.509789
0.010752982	3.231274	2.5429153
0.012545322	3.520024	2.7067589
0.014336608	3.718553	2.9924994
0.016128947	3.601523	3.2165584
0.017921287	3.801102	3.3533951
0.019713626	3.813989	3.2514053
0.021504912	3.706037	3.2015363
0.023297252	3.545001	3.1172168
0.025089591	2.834402	2.5675805
0.02688193	2.26173	2.1619852
0.028674269	2.023159	2.1504269
0.030465556	1.587156	2.047876
0.032257895	1.295006	1.9059521
0.034050234	1.212125	1.7630332

0.035842573	1.139587	1.5505401
0.037634912	1.141874	1.3371118
0.039426199	1.212403	1.2097012
0.041218538	1.158863	1.1630491
0.043010877	1.158863	1.1267208
0.044803216	1.158863	1.0779216
0.046594503	1.158863	1.0811385
0.048386842	1.135601	1.0957416
0.050179181	1.07089	1.1221648
0.05197152	1.049204	1.1315387
0.05376386	1.02955	1.0890535
0.055555146	0.978598	0.9476084
0.057347485	0.98192	0.9572365
0.059139825	0.968153	0.9725429
0.060932164	0.922471	0.9725429
0.062724503	0.895739	0.9542516
0.06451579	0.849833	0.9040085
0.066308129	0.829174	0.8977319
0.068100468	0.796595	0.8977319
0.069892807	0.849833	0.8977319
0.071684094	0.849833	0.9179458
0.073476433	0.849833	0.9653012
0.075268772	0.849833	0.9468228
0.077061111	0.832033	0.9114073
0.07885345	0.79002	0.9308881
0.080644737	0.78754	0.9725429
0.082437076	0.772575	0.9582091
0.084229415	0.772575	0.9242748
0.086021754	0.772575	0.9274917
0.087814093	0.781931	0.930716
0.08960538	0.820869	0.9345913
0.091397719	0.849833	0.933125
0.093190058	0.849833	0.9299081
0.094982398	0.849833	0.9266912
0.096774737	0.842687	0.9498527
0.098566023	0.826571	1.0108386
0.100358363	0.835208	0.9526132
0.102150702	0.849833	0.8977319
0.103943041	0.849833	0.8943355
0.105734328	0.849833	0.8906174
0.107526667	0.849833	0.8977319

0.109319006	0.849833	0.8977319
0.111111345	0.849833	0.9171304
0.112903684	0.853155	0.9757597
0.114694971	0.856477	0.9789766
0.11648731	0.859799	0.9797247
0.118279649	0.859745	0.9725429
0.120071988	0.849833	0.9725429
0.121864327	0.849833	0.9774131
0.123655614	0.849833	0.9950685
0.125447953	0.856469	1.0169656
0.127240292	0.879739	1.0763132
0.129032632	0.883061	1.0795301
0.130823918	0.896404	1.0827469
0.132616257	0.927091	1.0859638
0.134408596	0.927091	1.0972229
0.136200936	0.927091	1.1221648
0.137993275	0.927091	1.1338129
0.139784561	0.939861	1.1792531
0.141576901	0.983581	1.1969758
0.14336924	0.986903	1.1791858
0.145161579	0.990225	1.118933
0.146953918	0.977911	1.1141676
0.148745205	0.927091	1.1221648
0.150537544	0.927091	1.1395958
0.152329883	0.927091	1.1971629
0.154122222	0.927091	1.1765674
0.155913509	0.927091	1.1265039
0.157705848	0.927091	1.1221648
0.159498187	0.927091	1.1051828
0.161290526	0.927091	1.0473539
0.163082865	0.927091	1.0305513
0.164874152	0.909831	0.9725429
0.166666491	0.849833	0.9669994
0.16845883	0.866907	0.967149
0.17025117	0.927091	1.0473539
0.172043509	0.927091	1.0310002
0.173834795	0.918778	0.956279
0.175627135	0.883038	0.8977319
0.177419474	0.849833	0.8977319
0.179211813	0.839349	0.8977319
0.181004152	0.792199	0.9028639

0.182795439	0.805248	0.9300427
0.184587778	0.910843	0.9725429
0.186380117	0.836807	0.9725429
0.188172456	0.797846	0.9725429
0.189963743	0.849833	0.9587402
0.191756082	0.864682	0.9025572
0.193548421	0.909986	0.8993403
0.19534076	0.833802	0.8974027
0.197133099	0.784195	0.9089835
0.198924386	0.849833	0.9725429
0.200716725	0.849833	0.9725429
0.202509064	0.849833	0.9696701
0.204301403	0.849833	0.9435835
0.206093743	0.849833	0.8977319
0.207885029	0.849833	0.8977319
0.209677368	0.849833	0.8977319
0.211469708	0.864697	0.8977319
0.213262047	0.927091	0.8977319
0.215053333	0.927091	0.8835178
0.216845673	0.912504	0.8229209
0.218638012	0.849833	0.8229209
0.220430351	0.849833	0.8229209
0.22222269	0.840292	0.8275367
0.224013977	0.790878	0.8544088
0.225806316	0.814944	0.8977319
0.227598655	1.004348	0.9221277
0.229390994	0.990411	0.9991531
0.231183333	0.927091	0.8569973
0.23297462	0.913339	0.9848568
0.234766959	0.836174	1.0189107
0.236559298	0.760129	0.9375313
0.238351637	0.70778	1.0901233
0.240143977	0.750124	0.9877295
0.241935263	0.896551	1.0049136
0.243727602	0.901256	0.9370825
0.245519941	0.899494	0.9104273
0.247312281	0.846333	0.9851485
0.249103567	0.816852	1.0598697
0.250895906	0.777126	1.1141526
0.252688246	0.800713	1.0746
0.254480585	0.810548	1.0635878

0.256272924	0.844348	1.0190603
0.258064211	0.753145	1.0480047
0.25985655	0.707687	1.0458352
0.261648889	0.789603	0.9821486
0.263441228	0.884406	0.9508626
0.265233567	0.919813	0.9842508
0.267024854	0.886832	1.058972
0.268817193	0.877514	1.1155964
0.270609532	0.731683	1.0616577
0.272401871	0.792755	0.9804953
0.274193158	0.849833	0.9115719
0.275985497	0.838793	0.9297285
0.277777836	0.772575	1.0805999
0.279570175	0.783932	1.3148181
0.281362515	0.871388	1.5799707
0.283153801	0.962312	1.6284333
0.28494614	0.772575	1.220272
0.28673848	0.772575	1.3626897
0.288530819	0.772575	1.3342615
0.290323158	0.772575	1.1237733
0.292114444	0.772575	1.0086541
0.293906784	0.772575	1.0723332
0.295699123	0.772575	1.0371646
0.297491462	0.772575	0.9422444
0.299282749	0.772575	0.7681293
0.301075088	0.772575	0.9175718
0.302867427	0.772575	1.0473539
0.304659766	0.772575	1.0376135
0.306452105	0.772575	0.9725429
0.308243392	0.772575	0.9725429
0.310035731	0.772575	0.9820139
0.31182807	0.762887	1.0192025
0.313620409	0.695318	0.8229209
0.315412748	0.695318	0.8312324
0.317204035	0.695318	0.8942008
0.318996374	0.695318	0.8977319
0.320788713	0.697813	0.9066718
0.322581053	0.701135	0.9725429
0.324372339	0.704457	0.9725429
0.326164678	0.706335	0.9826124
0.327957018	0.695318	1.0626377

0.329749357	0.695318	1.0573636
0.331541696	0.697837	0.9858592
0.333332983	0.726793	0.9171304
0.335125322	0.772575	0.8613513
0.336917661	0.77745	0.7834132
0.33871	0.817957	0.7135173
0.340502339	0.841621	0.7063654
0.342293626	0.772575	0.6732989
0.344085965	0.772575	0.6810718
0.345878304	0.772575	0.7481099
0.347670643	0.772575	0.7557107
0.349462982	0.772575	0.8250231
0.351254269	0.772575	0.8406212
0.353046608	0.772575	0.8433144
0.354838947	0.772575	0.8894054
0.356631286	0.772575	0.8148787
0.358422573	0.772575	0.8185519
0.360214912	0.772575	0.8229209
0.362007251	0.772575	0.8312623
0.363799591	0.772575	0.8977319
0.36559193	0.772575	0.8977319
0.367383216	0.772575	0.8977319
0.369175556	0.772575	0.8912084
0.370967895	0.772575	0.8244396
0.372760234	0.772575	0.848409
0.374552573	0.772575	0.9039861
0.37634386	0.772575	0.9787073
0.378136199	0.772575	1.0473539
0.379928538	0.772575	1.0446457
0.381720877	0.772575	1.0103523
0.383512164	0.772575	0.9959512
0.385304503	0.772575	0.8687576
0.387096842	0.772575	0.8977319
0.388889181	0.772575	0.8995797
0.39068152	0.772575	0.9233172
0.392472807	0.772575	0.973867
0.394265146	0.772575	0.9878268
0.396057485	0.772575	0.9889564
0.397849825	0.767314	1.0365586
0.399642164	0.7001	0.8920986
0.40143345	0.77008	0.890565

0.403225789	0.772575	0.8229209
0.405018129	0.772575	0.8229209
0.406810468	0.772575	0.8229209
0.408602807	0.772575	0.8229209
0.410394094	0.771733	0.8265717
0.412186433	0.752651	0.9031632
0.413978772	0.716085	1.2400969
0.415771111	0.722397	1.139708
0.417562398	0.772575	1.0504585
0.419354737	0.772575	1.0159931
0.421147076	0.772575	0.9769941
0.422939415	0.774623	0.8957494
0.424731754	0.809126	0.8623388
0.426523041	0.804174	0.8577155
0.42831538	0.772575	0.7058342
0.430107719	0.772575	0.7773386
0.431900058	0.772575	0.8444216
0.433692398	0.772575	0.822068
0.435483684	0.772575	0.806829
0.437276023	0.772575	0.8188961
0.439068363	0.772575	1.0337308
0.440860702	0.775357	1.1722807
0.442651988	0.843683	1.041152
0.444444328	0.772575	0.9669994
0.446236667	0.775782	0.8319207
0.448029006	0.772575	0.9091256
0.449821345	0.772575	1.0505034
0.451612632	0.772575	1.1434935
0.453404971	0.772058	1.0161577
0.45519731	0.756135	0.8830764
0.456989649	0.872423	0.9683011
0.458781988	0.849833	1.0751536
0.460573275	0.849833	1.1491567
0.462365614	0.849833	1.0757746
0.464157953	0.847987	0.931337
0.465950292	0.772575	0.8615308
0.467741579	0.772575	0.8654584
0.469533918	0.774144	0.8940886
0.471326257	0.849833	0.7220682
0.473118596	0.849833	0.749449
0.474910936	0.849833	0.8241702

0.476702222	0.849833	0.89747
0.478494561	0.849833	0.8821113
0.480286901	0.849833	0.7490899
0.48207924	0.849833	0.8255168
0.483871579	0.849879	1.043329
0.485662866	0.850652	1.0458277
0.487455205	0.849833	0.9767472
0.489247544	0.849833	0.9089535
0.491039883	0.849369	0.9069187
0.49283117	0.772575	0.960416
0.494623509	0.772575	0.9420275
0.496415848	0.772575	0.954087
0.498208187	0.772668	0.9725055
0.500000526	0.849833	0.9476084
0.501791813	0.849833	0.9259207
0.503584152	0.849833	0.8978067
0.505376491	0.849833	0.8977319
0.50716883	0.849833	0.9345613
0.508961169	0.849833	0.9315165
0.510752456	0.849833	0.9722287
0.512544795	0.849833	1.0196065
0.514337134	0.926349	1.2980904
0.516129474	0.927091	0.9881784
0.517921813	0.927091	0.8249707
0.519713099	0.927091	0.9253297
0.521505439	0.850938	1.1414736
0.523297778	0.849833	1.1382567
0.525090117	0.849833	1.1223294
0.526881404	0.849833	1.1908937
0.528673743	1.001397	1.0502416
0.530466082	0.928659	1.1206462
0.532258421	0.851494	1.1221648
0.53405076	0.925337	1.0490521
0.535842047	1.002502	1.0332221
0.537634386	1.079666	1.0853354
0.539426725	1.00638	1.173545
0.541219064	0.929215	1.2690712
0.543011403	0.927091	1.3178854
0.54480269	0.927091	1.273111
0.546595029	0.927091	1.2390495
0.548387368	0.927091	1.1623832

0.550179708	0.927091	1.1233244
0.551970994	0.970393	1.0918814
0.553763333	1.003305	1.0218807
0.555555672	1.004348	0.998405
0.557348012	1.004348	1.0456931
0.559140351	1.004348	1.1733056
0.560931637	1.004348	1.2681286
0.562723977	1.004348	1.2602285
0.564516316	1.069538	1.1197485
0.566308655	1.081351	0.9074049
0.568100994	1.081606	0.8286215
0.569892281	1.082363	0.8252625
0.57168462	0.99242	0.8234969
0.573476959	0.981549	0.8871835
0.575269298	0.982206	0.8872733
0.577061637	0.989499	0.9420499
0.578852924	1.003429	0.9547603
0.580645263	1.057803	0.99049
0.582437602	1.057517	0.9692661
0.584229941	1.054195	1.0024224
0.586021228	0.934971	0.8909091
0.587813567	0.93477	0.9046519
0.589605906	0.96473	0.9341798
0.591398246	0.963641	0.9739194
0.593190585	0.887859	1.0229879
0.594981871	0.924093	1.0782358
0.596774211	0.974496	1.0940135
0.59856655	1.009802	1.1279253
0.600358889	0.807851	0.9499051
0.602151228	0.8457	1.0393566
0.603942515	0.921737	1.1050032
0.605734854	0.989638	1.1035369
0.607527193	1.063249	1.0458202
0.609319532	1.078044	0.9113849
0.611110819	1.010073	0.9669994
0.612903158	1.004348	0.9755203
0.614695497	0.861646	0.7717053
0.616487836	0.849833	0.8957643
0.618280175	0.920995	1.0365736
0.620071462	0.982878	1.11618
0.621863801	1.055392	1.0534285

0.62365614	1.129235	1.0473539
0.625448479	1.132279	1.1159106
0.627240819	1.128957	1.1906319
0.629032105	0.873559	0.8550971
0.630824444	0.920354	0.8229209
0.632616784	0.927091	0.8911186
0.634409123	0.997426	0.927761
0.636200409	1.004348	0.9274917
0.637992749	1.074498	0.9001707
0.639785088	1.081606	0.8298933
0.641577427	1.15157	0.8229209
0.643369766	0.94924	0.7552618
0.645161053	0.927091	0.7481099
0.646953392	0.996777	0.8155894
0.648745731	1.004348	0.8837946
0.65053807	1.073849	0.8973279
0.652330409	1.151014	0.9649421
0.654121696	1.158608	1.0375013
0.655914035	1.158863	1.0467703
0.657706374	0.959639	0.8465163
0.659498713	0.939552	0.91134
0.661291053	0.942874	0.9010161
0.663082339	0.929169	0.9479226
0.664874678	0.927091	1.0560768
0.666667017	0.881308	1.0501219
0.668459357	0.878905	0.9309554
0.670250643	0.882235	0.9932356
0.672042982	0.853928	0.8034551
0.673835322	0.849833	0.7518729
0.675627661	0.849833	0.7770917
0.67742	0.849833	0.8957045
0.679211287	0.849833	0.9419227
0.681003626	0.849833	0.7934977
0.682795965	0.849833	0.703328
0.684588304	0.849833	0.7220383
0.686380643	0.782179	0.8498828
0.68817193	0.772575	0.8850589
0.689964269	0.772575	0.8313745
0.691756608	0.776925	0.7660945
0.693548947	0.840075	0.8150807
0.695340234	0.848172	0.8229209

0.697132573	0.84485	0.8837048
0.698924912	0.841528	0.8966621
0.700717251	0.724514	0.7778847
0.702509591	0.764162	0.814774
0.704300877	0.823527	0.8875426
0.706093216	0.780224	0.8977319
0.707885556	0.772575	0.9413841
0.709677895	0.730416	0.945192
0.711470234	0.766132	0.9419751
0.71326152	0.808917	0.9387582
0.71505386	0.810911	0.9989362
0.716846199	0.814109	0.9487679
0.718638538	0.817431	0.8772636
0.720429825	0.820761	0.7817449
0.722222164	0.780209	0.7305592
0.724014503	0.772575	0.7263923
0.725806842	0.772575	0.7453269
0.727599181	0.720427	0.8115721
0.729390468	0.762663	0.8760666
0.731182807	0.772575	0.8255991
0.732975146	0.772575	0.8757225
0.734767485	0.772575	0.9580445
0.736559824	0.772575	1.0335213
0.738351111	0.772575	1.0352868
0.74014345	0.772575	0.9121255
0.741935789	0.772575	0.8420725
0.743728129	0.772575	0.8365963
0.745520468	0.772575	0.8256889
0.747311754	0.772575	0.8229209
0.749104094	0.772575	0.8229209
0.750896433	0.772575	0.8229209
0.752688772	0.798132	0.8229209
0.754480059	0.806638	0.8229209
0.756272398	0.843019	0.8229209
0.758064737	0.785864	0.764314
0.759857076	0.772575	0.7233175
0.761649415	0.772575	0.7430602
0.763440702	0.814349	0.7481099
0.765233041	0.845723	0.7481099
0.76702538	0.849833	0.7639773
0.768817719	0.849833	0.7642017

0.770610058	0.849833	0.7609774
0.772401345	0.786605	0.6886352
0.774193684	0.772575	0.6732989
0.775986023	0.772575	0.6732989
0.777778362	0.835525	0.6732989
0.779569649	0.849833	0.6732989
0.781361988	0.849833	0.7288461
0.783154327	0.849833	0.7462845
0.784946667	0.849833	0.7481099
0.786739006	0.863268	0.7611195
0.788530292	0.853665	0.7674186
0.790322632	0.849833	0.7706355
0.792114971	0.849833	0.7531222
0.79390731	0.849833	0.7481099
0.795699649	0.87651	0.7481099
0.797490936	0.85708	0.7481099
0.799283275	0.817918	0.7172055
0.801075614	0.868383	0.8329456
0.802867953	0.930297	0.8320179
0.80465924	0.949518	0.8017643
0.806451579	0.890725	0.7586283
0.808243918	0.825721	0.7481099
0.810036257	0.935975	0.7481099
0.811828596	0.926094	0.7481099
0.813619883	0.81971	0.7481099
0.815412222	0.952848	0.9253521
0.817204561	0.94255	0.9135544
0.818996901	0.866266	0.8381973
0.82078924	0.8493	0.7660047
0.822580526	0.97112	0.6950165
0.824372865	1.01151	0.7338434
0.826165205	0.946598	0.806657
0.827957544	0.854391	0.8694309
0.829749883	0.966183	0.9081007
0.83154117	0.944164	0.8611717
0.833333509	0.907058	0.8284644
0.835125848	0.920593	0.8229209
0.836918187	0.986996	0.8472494
0.838709474	1.004348	0.8575135
0.840501813	1.004348	0.8029015
0.842294152	0.944721	0.7574688

0.844086491	0.951419	0.8057592
0.84587883	0.955336	0.8229209
0.847670117	0.952014	0.8414591
0.849462456	0.991384	0.843838
0.851254795	1.004348	0.8406212
0.853047134	1.004348	0.8373968
0.854839474	0.995471	0.7770692
0.85663076	0.996043	0.6991311
0.858423099	1.003158	0.7313896
0.860215439	1.004348	0.7481099
0.862007778	1.004348	0.7481099
0.863799064	1.004348	0.7481099
0.865591404	1.004348	0.8046894
0.867383743	1.004348	0.8229209
0.869176082	1.004348	0.8229209
0.870968421	1.004348	0.8229209
0.872759708	1.194757	1.0073001
0.874552047	1.068449	1.0533761
0.876344386	0.946474	1.0473539
0.878136725	1.042652	0.9914027
0.879929064	1.139294	0.9166815
0.881720351	1.043672	0.8977319
0.88351269	0.946845	0.8420501
0.885305029	0.984501	0.8229209
0.887097368	1.061665	0.9894352
0.888889707	1.081606	0.9919414
0.890680994	1.024474	0.8618899
0.892473333	0.947301	0.8229209
0.894265672	0.927091	0.8780715
0.896058012	0.983952	0.8977319
0.897849298	1.004348	0.8427608
0.899641637	1.061024	0.7172953
0.901433977	1.079782	0.8931011
0.903226316	1.023454	0.9149983
0.905018655	0.996043	0.8398656
0.906809942	0.989399	0.7736728
0.908602281	0.942248	0.704136
0.91039462	0.89149	0.6869744
0.912186959	0.910024	0.7024453
0.913978246	0.947942	0.7426412
0.915770585	1.019529	0.8817373

0.917562924	0.985822	0.884625
0.919355263	0.9808	0.8355116
0.921147602	0.94836	0.8229209
0.922938889	0.927794	0.7951959
0.924731228	0.956271	0.8411523
0.926523567	0.978845	0.8655557
0.928315906	1.025718	0.8687725
0.930108245	1.00098	0.8553515
0.931899532	1.012058	0.8826799
0.933691871	1.024288	0.9371872
0.93548421	1.063999	0.9867121
0.93727655	1.081606	1.052628
0.939068889	1.129196	1.0903777
0.940860175	1.152219	1.1028561
0.942652515	1.207659	1.0643135
0.944444854	0.96429	0.8367759
0.946237193	1.012653	0.8541769
0.94802848	1.244148	0.9501968
0.949820819	1.36049	0.9725429
0.951613158	1.278643	0.9202575
0.953405497	1.182218	0.8977319
0.955197836	1.266491	0.9498377
0.956989123	1.404643	1.0609171
0.958781462	1.245253	0.9585008
0.960573801	1.233123	0.8977319
0.96236614	1.40669	0.9494861
0.964158479	1.602708	1.0242073
0.965949766	1.81957	1.0989286
0.967742105	2.024302	1.1736498
0.969534444	2.160144	1.248371
0.971326784	2.243606	1.2717868
0.97311807	2.284467	1.2205712
0.974910409	2.522343	1.2107186
0.976702748	2.79677	1.2533833
0.978495088	2.829658	1.2811008
0.980287427	2.750353	1.3259949
0.982078713	2.771398	1.3973646
0.983871053	2.73443	1.4241319
0.985663392	2.652043	1.4222168
0.987455731	2.524135	1.3220374
0.98924807	2.526198	1.3858287

0.991039357	2.338841	1.4333486
0.992831696	2.185925	1.4308874
0.994624035	1.885919	1.2080778
0.996416374	1.659654	1.0462841
0.998208713	1.494269	0.9950311
1	1.424969	1.0639769

Table A 5:Measurement data of Actin and Myosin intensity from cell 1

Cell 2

Norm Distance	Dapi	Actin	Myosin
0	0.667382	1.080608	1.2499287
0.003030681	0.623028	1.135852	1.2890614
0.006061361	0.600644	1.19511	1.329175
0.009090262	0.600644	1.261967	1.3607281
0.012120942	0.600644	1.315016	1.3718746
0.015151623	0.625871	1.462286	1.5069836
0.018182304	0.615032	1.649797	1.6225504
0.021212984	0.600644	1.825886	1.7357643
0.024241885	0.557231	2.076279	1.9172976
0.027272565	0.533906	2.30058	2.0439422
0.030303246	0.490759	2.430968	2.0501294
0.033333927	0.467167	2.547773	2.1702027
0.036362827	0.427932	2.551132	2.3658595
0.039393508	0.527966	2.822414	2.7600813
0.042424188	0.600644	2.672692	2.9480967
0.045454869	0.558172	2.33319	3.0789736
0.04848555	0.533906	2.13888	3.0295244
0.05151445	0.491707	1.920406	2.670395
0.054545131	0.425102	1.870316	2.4431234
0.057575812	0.400429	1.929616	2.3434842
0.060606492	0.387762	1.767907	2.0252916
0.063637173	0.433278	1.870033	2.0623871
0.066666073	0.467167	1.943248	2.1983536
0.069696754	0.467167	1.860291	2.1551395
0.072727435	0.467167	1.725946	2.0626752
0.075758115	0.467167	1.583323	1.9228949
0.078787016	0.467167	1.458197	1.7556428
0.081817696	0.467167	1.362222	1.6063417
0.084848377	0.467167	1.314301	1.4727554
0.087879058	0.507751	1.220397	1.5585936
0.090909738	0.533906	1.11335	1.5958605
0.093938639	0.533906	1.080608	1.4903428

0.096969319	0.493729	1.030567	1.3531211
0.1	0.467167	0.997484	1.2163932
0.103030681	0.467167	0.947776	1.0835546
0.106061361	0.428172	0.867337	0.9959398
0.109090262	0.417194	0.837787	0.9733176
0.112120942	0.488277	0.829292	0.9165014
0.115151623	0.561542	0.816623	0.8676078
0.118182304	0.62491	0.823556	0.8296755
0.121211204	0.67762	0.831237	0.7861527
0.124241885	0.664799	0.846822	0.7493796
0.127272565	0.695892	0.861967	0.7366555
0.130303246	0.827694	0.886148	0.7433091
0.133333927	1.014421	0.908816	0.7710964
0.136362827	1.23493	0.816806	0.7874766
0.139393508	1.436266	0.780714	0.7757333
0.142424188	1.645183	0.841685	0.7505457
0.145454869	1.831977	0.890728	0.7324987
0.14848555	1.884406	0.880903	0.753461
0.15151445	1.972768	0.851386	0.7911464
0.154545131	2.222135	0.922889	0.8409866
0.157575812	2.423037	1.025289	0.8717646
0.160606492	2.34528	0.94298	0.866085
0.163637173	2.515489	0.8393	0.8742888
0.166666073	2.699186	0.831237	0.8917185
0.169696754	2.62536	0.831237	0.9296851
0.172727435	2.422323	0.831237	0.9944719
0.175758115	2.341483	0.831237	1.024413
0.178787016	2.389634	0.876747	1.0591763
0.181817696	2.623565	0.91436	1.0808725
0.184848377	2.574105	0.746816	0.9020075
0.187879058	2.345007	0.610078	0.7671385
0.190909738	2.270907	0.658946	0.818138
0.193938639	2.17997	0.726434	0.8738292
0.196969319	2.118297	0.792617	0.8917185
0.2	2.081044	0.851926	0.8746455
0.203030681	2.093424	0.891692	0.8265887
0.206061361	2.11823	0.930628	0.7748828
0.209090262	2.042663	0.795493	0.7183615
0.212120942	2.143284	0.664989	0.7121401
0.215151623	2.346074	0.70848	0.7471984
0.218182304	2.478256	0.748113	0.7839989

0.221211204	2.509897	0.791271	0.8189268
0.224241885	2.4319	0.831237	0.8586014
0.227272565	2.470414	0.874062	0.8917185
0.230303246	2.534249	0.912847	0.9269139
0.233333927	2.333761	0.860671	0.925254
0.236362827	2.203295	0.737382	0.8917185
0.239393508	2.23003	0.657134	0.8569346
0.242424188	2.18996	0.676568	0.8231247
0.245454869	2.168985	0.790165	0.8141321
0.24848555	2.138005	0.878875	0.7781821
0.25151445	2.080877	0.88161	0.754531
0.254545131	2.035642	0.865085	0.754531
0.257575812	2.038244	0.782917	0.7020637
0.260606492	2.101779	0.7068	0.6686517
0.263635393	2.18308	0.729136	0.7010416
0.266666073	2.281258	0.748113	0.7469103
0.269696754	2.356906	0.788586	0.8002968
0.272727435	2.382353	0.831237	0.856379
0.275758115	2.353362	0.841452	0.9001486
0.278787016	2.315475	0.848368	0.9126464
0.281817696	2.267744	0.752194	0.859795
0.284848377	2.23964	0.660243	0.8771355
0.287879058	2.256966	0.664989	1.0193097
0.290909738	2.173556	0.704282	1.0638064
0.293938639	2.103868	0.748113	0.9282309
0.296969319	2.110362	0.787073	0.7878813
0.3	2.131171	0.831237	0.7822703
0.303030681	2.222095	0.831237	0.8743986
0.306061361	2.228815	0.763183	0.8566259
0.309090262	2.207366	0.715778	0.754531
0.312120942	2.058139	0.773757	0.754531
0.315151623	1.947854	0.776308	0.754531
0.318182304	2.002146	0.748113	0.754531
0.321211204	1.954375	0.748113	0.754531
0.324241885	2.010875	0.748113	0.754531
0.327272565	2.140754	0.785394	0.754531
0.330303246	2.064653	0.779958	0.754531
0.333333927	1.970011	0.732718	0.754531
0.336362827	1.943009	0.758587	0.754531
0.339393508	1.912683	0.795718	0.7314629
0.342424188	1.910327	0.794795	0.6931739

0.345454869	1.920859	0.748113	0.6859373
0.34848555	1.960962	0.748113	0.6859373
0.35151445	2.030997	0.749634	0.6859373
0.354545131	2.011569	0.783881	0.6861156
0.357575812	1.915666	0.831237	0.7174561
0.360606492	1.860848	0.831237	0.754531
0.363635393	1.827979	0.831237	0.7792248
0.366666073	1.828626	0.831237	0.786235
0.369696754	1.856176	0.831237	0.7473698
0.372727435	1.916401	0.831237	0.7139921
0.375758115	1.968056	0.831237	0.6760735
0.378787016	2.015627	0.810373	0.6813004
0.381817696	2.061196	0.769733	0.7162832
0.384848377	2.0403	0.748113	0.71961
0.387879058	1.992716	0.76374	0.7358324
0.390909738	1.974643	0.768462	0.7660068
0.393938639	2.004842	0.748113	0.797114
0.396969319	2.074684	0.748113	0.8231247
0.4	2.124944	0.748113	0.8304437
0.403030681	2.144799	0.773973	0.9021173
0.406061361	2.141956	0.817131	0.9287522
0.409090262	2.085061	0.821162	0.8148112
0.412120942	2.028167	0.825194	0.8719017
0.415151623	1.9719	0.829225	0.933204
0.418182304	1.942242	0.831237	0.8385035
0.421211204	1.970105	0.831237	0.7526035
0.424241885	1.999042	0.831237	0.7956804
0.427272565	1.927346	0.831237	0.8773275
0.430303246	1.856403	0.831237	0.8656666
0.433333927	1.922754	0.831237	0.8231247
0.436362827	1.965713	0.831237	0.7973472
0.439393508	1.96881	0.831237	0.7288975
0.442424188	1.951498	0.831237	0.6859373
0.445454869	1.93456	0.831237	0.6859373
0.44848555	1.886956	0.831237	0.6735561
0.45151445	1.902105	0.831237	0.705754
0.454545131	1.964272	0.831237	0.7711581
0.457575812	1.945292	0.831237	0.7222645
0.460606492	1.979228	0.831237	0.6964527
0.463635393	2.048522	0.801512	0.6443626
0.466666073	2.076599	0.748113	0.6085018

0.469696754	2.005309	0.748113	0.6173436
0.472727435	1.925697	0.748113	0.6198267
0.475758115	1.965433	0.748113	0.6197786
0.478787016	2.088839	0.748113	0.6173436
0.481817696	1.920779	0.751637	0.6202519
0.484848377	1.739971	0.78162	0.6449937
0.487879058	1.627064	0.831237	0.6859373
0.490909738	1.535592	0.831237	0.6859373
0.493938639	1.423399	0.852649	0.6859373
0.496969319	1.363154	0.890687	0.6859373
0.5	1.386673	0.868177	0.7926417
0.503030681	1.44276	0.831237	1.011394
0.506059581	1.439523	0.831237	1.0160378
0.509090262	1.436286	0.831237	0.9482534
0.512120942	1.444495	0.831237	0.814674
0.515151623	1.46824	0.831237	0.7126683
0.518182304	1.46824	0.831237	0.6942166
0.521211204	1.46824	0.831237	0.7521783
0.524241885	1.537641	0.857603	0.836185
0.527272565	1.653105	0.908325	0.8064839
0.530303246	1.486994	0.877952	0.7630984
0.533333927	1.267926	0.831237	0.7331915
0.536362827	1.253176	0.807721	0.6859373
0.539393508	1.136211	0.750208	0.6859373
0.542424188	1.226187	0.747805	0.6853611
0.545454869	1.133321	0.71941	0.6859373
0.54848377	1.109369	0.745511	0.7456276
0.55151445	1.067811	0.936637	0.8636293
0.554545131	1.067811	0.926405	0.8189268
0.557575812	1.053135	0.908118	0.7905839
0.560606492	0.995821	0.881792	0.7344399
0.563635393	0.876092	0.840239	0.6789202
0.566666073	0.695559	0.793183	0.6466125
0.569696754	0.562356	0.785394	0.6173436
0.572727435	0.467167	0.825011	0.627173
0.575758115	0.467167	0.91436	0.6591034
0.578787016	0.448427	0.900495	0.7051984
0.581817696	0.393775	0.852674	0.754531
0.584848377	0.36704	0.831237	0.7676461
0.587879058	0.315358	0.831237	0.791311
0.590909738	0.248753	0.813373	0.7505594

0.593938639	0.200215	0.761712	0.7277795
0.596969319	0.251943	0.841876	0.7206732
0.6	0.379367	1.032213	0.8014766
0.603030681	0.333691	0.892366	0.7363811
0.606059581	0.312648	0.831237	0.6669368
0.609090262	0.263062	0.851195	0.6227487
0.612120942	0.254086	0.903779	0.6260755
0.615151623	0.223673	0.882175	0.6294023
0.618182304	0.230147	0.798411	0.6327223
0.621211204	0.239684	0.740865	0.6643989
0.624241885	0.245516	0.831237	0.7227035
0.627272565	0.24228	0.831237	0.6922411
0.630303246	0.239043	0.831237	0.7004792
0.633333927	0.22711	0.831237	0.6628692
0.636362827	0.200215	0.841004	0.692927
0.639393508	0.200215	0.878775	0.7195002
0.642424188	0.200215	0.91436	0.690341
0.645454869	0.189797	0.901742	0.6056826
0.64848377	0.152891	0.839175	0.5687037
0.65151445	0.1614	0.803889	0.5774494
0.654545131	0.200215	0.792077	0.6300746
0.657575812	0.200215	0.847454	0.6759569
0.660606492	0.200215	0.906297	0.6792837
0.663635393	0.214457	0.928067	0.6679726
0.666666073	0.266953	0.997484	0.6173436
0.669696754	0.252257	0.97918	0.5591212
0.672727435	0.200215	0.91436	0.3914027
0.675758115	0.200215	0.91436	0.5402785
0.678787016	0.200215	0.91436	0.6977766
0.681817696	0.200215	0.91436	0.7233552
0.684848377	0.200215	0.919439	0.6659834
0.687879058	0.200215	0.942572	0.6769309
0.690909738	0.200215	0.957086	0.73658
0.693938639	0.178925	0.954002	0.7177099
0.696969319	0.10604	0.788411	0.553812
0.7	0.133476	0.792443	0.5917375
0.703030681	0.133476	0.803357	0.6309251
0.706059581	0.146557	0.831237	0.6859373
0.709090262	0.204372	0.831237	0.672637
0.712120942	0.227731	0.831237	0.6173436
0.715151623	0.266953	0.831237	0.6144215

0.718182304	0.23967	0.799999	0.5946665
0.721211204	0.126562	0.680442	0.5487498
0.724241885	0.133476	0.748113	0.5613574
0.727272565	0.133476	0.763225	0.6173436
0.730303246	0.14647	0.831237	0.6173436
0.733333927	0.200215	0.846016	0.6173436
0.736362827	0.210592	0.91436	0.6280099
0.739393508	0.25793	0.926438	0.6747154
0.742424188	0.235005	0.940062	0.6503303
0.745454869	0.095456	0.762219	0.5603902
0.74848377	0.161833	0.845176	0.6252867
0.75151445	0.200215	0.928134	0.6654758
0.754545131	0.189296	0.997484	0.6813827
0.757575812	0.133476	0.991374	0.6547614
0.760606492	0.144128	0.949081	0.6623822
0.763635393	0.210733	0.90126	0.7323547
0.766666073	0.246191	0.831237	0.77526
0.769696754	0.133476	0.831237	0.6074661
0.772727435	0.133476	0.831237	0.6890857
0.775758115	0.140911	0.831237	0.7033944
0.778787016	0.188489	0.831237	0.6979892
0.781817696	0.200215	0.831237	0.6843665
0.784848377	0.201256	0.831237	0.6795306
0.787879058	0.213122	0.831237	0.6962264
0.790907958	0.248233	0.819649	0.755018
0.793938639	0.133476	0.762136	0.7451062
0.796969319	0.133476	0.831237	0.6851485
0.8	0.133476	0.840846	0.6767937
0.803030681	0.142239	0.899248	0.6841127
0.806059581	0.200215	0.897694	0.754531
0.809090262	0.200215	0.903779	0.7520959
0.812120942	0.200215	0.831237	0.7234924
0.815151623	0.191992	0.824844	0.6548849
0.818182304	0.133476	0.783374	0.6256571
0.821211204	0.133476	0.787405	0.6859373
0.824241885	0.133476	0.7961	0.6939765
0.827272565	0.141165	0.831237	0.762433
0.830303246	0.200215	0.840638	0.8308827
0.833332147	0.200215	0.91436	0.8942564
0.836362827	0.200215	0.91436	0.9166111
0.839393508	0.200215	0.912257	0.9568414

0.842424188	0.200215	0.898741	0.9241907
0.845454869	0.200215	0.90397	0.8326867
0.84848377	0.200215	0.91436	0.8406985
0.85151445	0.200215	0.92224	0.958371
0.854545131	0.200215	1.005547	1.0226708
0.857575812	0.200215	1.088496	0.9640506
0.860606492	0.200215	1.170664	0.9801289
0.863635393	0.195069	1.227845	1.1016564
0.866666073	0.146824	1.157821	1.0365267
0.869696754	0.150061	1.099468	0.971397
0.872727435	0.153298	1.073559	0.9062672
0.875758115	0.158243	0.992979	0.8448552
0.878787016	0.173926	0.944459	0.8197637
0.881817696	0.17069	0.917261	0.7872708
0.884848377	0.167453	0.955166	0.8218763
0.887879058	0.16461	0.959197	0.8391894
0.890907958	0.172712	0.963229	0.9785581
0.893938639	0.175949	0.96726	0.9042506
0.896969319	0.179179	0.976994	0.8278371
0.9	0.18034	1.058438	0.8975078
0.903030681	0.148039	1.063642	0.9831814
0.906059581	0.144802	1.080608	1.0932057
0.909090262	0.141565	1.080608	1.0242416
0.912120942	0.141672	1.08025	0.9630697
0.915151623	0.1986	1.078596	1.0942689
0.918182304	0.200215	1.082619	1.0974997
0.921211204	0.200215	1.090699	1.0974997
0.924241885	0.196844	1.163731	1.0974997
0.927272565	0.133476	1.160381	1.0974997
0.930303246	0.133476	1.097897	1.0974997
0.933332147	0.133476	1.076917	1.0974997
0.936362827	0.136306	1.002122	1.101485
0.939393508	0.200215	1.110831	1.1870694
0.942424188	0.200215	1.114863	1.2535298
0.945454869	0.200215	1.118894	1.3323577
0.94848377	0.197925	1.124331	1.4055472
0.95151445	0.133476	1.166416	1.4049505
0.954545131	0.133476	1.249374	1.5028269
0.957575812	0.133476	1.331516	1.7150284
0.960606492	0.135232	1.392138	1.8137417
0.963635393	0.199814	1.540057	2.1979077

0.966666073	0.186867	1.632549	2.3041388
0.969696754	0.188956	1.794299	2.2762143
0.972727435	0.133476	1.970945	2.3736311
0.975758115	0.133476	2.071708	2.6932024
0.978787016	0.133476	2.243341	2.8828641
0.981817696	0.129873	2.255885	3.0328786
0.984848377	0.068086	2.345093	3.284501
0.987879058	0.200215	2.600399	3.7325895
0.990907958	0.200215	2.641603	3.7168678
0.993938639	0.200008	2.20035	3.7042054
0.996969319	0.15245	2.160833	3.7333578
1	0.133476	1.967263	3.6126054

Table A 6: Measurement data of Actin and Myosin intensity from cell 2

Cell 3

Norm Distance	Actin	Myosin
0	1.385905	2.0332479
0.001400735	1.362715	2.0885333
0.002801471	1.498724	2.1202357
0.004201383	1.683904	2.0112525
0.005602119	1.835517	1.8441601
0.007002854	1.837765	1.6567811
0.008403589	1.925391	1.6945792
0.009804325	2.11108	1.9389888
0.011204238	2.118361	1.9784835
0.012604973	2.120966	2.060733
0.014005708	2.122391	2.114031
0.015406444	2.127864	2.245652
0.016806356	2.134168	2.3259019
0.018207092	2.147117	2.3209938
0.019607827	2.154872	2.3663661
0.021008562	2.139735	2.4349336
0.022409298	2.182457	2.3986382
0.02380921	2.389266	2.3622458
0.025209946	2.55465	2.395657
0.026610681	2.597627	2.438133
0.028011416	2.693196	2.4896373
0.029412152	2.888863	2.5710628
0.030812065	3.085727	2.6650552
0.0322128	3.044583	2.640018

0.033613535	2.912164	2.5661426
0.035014271	2.643235	2.4980356
0.036414183	2.54793	2.4071213
0.037814919	2.406924	2.3045851
0.039215654	2.272425	2.2055028
0.040616389	2.194863	2.1442428
0.042017125	1.991143	2.0231772
0.043417037	1.720746	1.9150544
0.044817773	1.907555	1.8196077
0.046218508	2.033848	1.7625408
0.047619243	2.077394	1.9235375
0.049019979	2.032669	2.2041697
0.050419892	2.035775	2.2652721
0.051820627	2.06302	2.1451518
0.053221362	2.048417	1.8858968
0.054622098	1.931857	1.5200945
0.05602201	2.225172	1.6444564
0.057422746	2.540276	1.720598
0.058823481	2.635386	1.7167443
0.060224216	2.604619	1.7224522
0.061624952	2.551485	1.8755111
0.063024864	2.541982	2.1677894
0.0644256	2.517315	2.1680803
0.065826335	2.498487	1.7666611
0.06722707	2.576915	1.8159963
0.068627806	2.643235	1.9746298
0.070027719	2.664151	2.1028333
0.071428454	2.616541	2.2654539
0.072829189	2.484461	2.4055216
0.074229925	2.387017	2.4862562
0.07563066	2.218757	2.3806298
0.077030573	1.951347	2.0743181
0.078431308	1.875719	2.0820377
0.079832043	1.820752	2.1345115
0.081232779	1.729834	2.1209386
0.082632692	1.65446	2.1073657
0.084033427	1.582981	2.0937807
0.085434162	1.505164	2.0802077
0.086834897	1.350081	1.9319236
0.088235633	1.127566	1.5706779
0.089635546	1.187921	1.5947819

0.091036281	1.190102	1.6737593
0.092437016	1.196059	1.6361187
0.093837752	1.187921	1.5221304
0.095238487	1.165028	1.3705742
0.0966384	1.10307	1.1792809
0.098039135	1.041247	1.0165997
0.09943987	0.875532	0.8744476
0.100840606	0.878697	1.1235349
0.102240519	0.895523	1.3583222
0.103641254	0.933367	1.4053548
0.105041989	0.945254	1.2784117
0.106442724	0.97536	1.1358354
0.10784346	0.972186	1.0879908
0.109243373	0.915522	1.0081893
0.110644108	0.763664	0.8393155
0.112044843	0.763664	0.8793435
0.113445579	0.78553	0.8699152
0.114846314	0.848515	0.936677
0.116246227	0.848515	0.9412094
0.117646962	0.848515	0.9208985
0.119047697	0.851935	0.8531914
0.120448433	0.813268	0.7979666
0.121848346	0.698404	0.6364852
0.123249081	0.760694	0.7575629
0.124649816	0.763664	0.8483076
0.126050551	0.786599	0.8483076
0.127451287	0.848515	0.8483076
0.1288512	0.867352	0.8752111
0.130251935	0.921479	0.9823887
0.13165267	0.884034	1.0149394
0.133053406	0.798181	0.8483076
0.134454141	0.848515	0.8483076
0.135854054	0.863152	0.8483076
0.137254789	0.905637	0.8680368
0.138655524	0.902472	0.9253703
0.14005626	0.887114	0.9325082
0.141456995	0.848515	0.9694944
0.142856908	0.828312	0.9255278
0.144257643	0.763664	0.8033352
0.145658379	0.763664	0.8483076
0.147059114	0.763664	0.8483076

0.148459027	0.763664	0.8483076
0.149859762	0.770341	0.8483076
0.151260497	0.789094	0.8483076
0.152661233	0.785929	0.8556757
0.154061968	0.773948	0.869285
0.155461881	0.751394	0.8483076
0.156862616	0.780159	0.8483076
0.158263351	0.841116	0.8483076
0.159664087	0.848515	0.8483076
0.161064822	0.848515	0.8483076
0.162464735	0.829424	0.8483076
0.16386547	0.763664	0.8483076
0.165266206	0.746125	0.8503072
0.166666941	0.688239	0.8617714
0.168066854	0.691413	0.8623168
0.169467589	0.694578	0.8483076
0.170868324	0.708052	0.8483076
0.17226906	0.74156	0.8218283
0.173669795	0.738386	0.7271208
0.175069708	0.735221	0.7271208
0.176470443	0.73887	0.7368642
0.177871178	0.763664	0.7767953
0.179271914	0.763664	0.7813155
0.180672649	0.763664	0.7991421
0.182072562	0.763664	0.8483076
0.183473297	0.763664	0.8483076
0.184874033	0.763664	0.8483076
0.186274768	0.763664	0.8483076
0.187675503	0.745998	0.8400184
0.189075416	0.678812	0.8130059
0.190476151	0.678812	0.8175261
0.191876887	0.678812	0.8220585
0.193277622	0.696164	0.8106912
0.194677535	0.763664	0.7443172
0.19607827	0.763664	0.7397969
0.197479005	0.763664	0.7352645
0.198879741	0.763155	0.7536122
0.200280476	0.763664	0.8490347
0.201680389	0.763664	0.8483076
0.203081124	0.746872	0.8483076
0.20448186	0.678812	0.8483076

0.205882595	0.678812	0.844575
0.20728333	0.675596	0.8247731
0.208683243	0.659161	0.8021597
0.210083978	0.672397	0.7271208
0.211484714	0.737674	0.7271208
0.212885449	0.734509	0.7271208
0.214285362	0.731335	0.7414087
0.215686097	0.72554	0.8072253
0.217086832	0.717471	0.8483076
0.218487568	0.720644	0.8483076
0.219888303	0.723809	0.8483076
0.221288216	0.74061	0.8257911
0.222688951	0.790977	0.7495282
0.224089687	0.763664	0.8483076
0.225490422	0.763664	0.8633832
0.226891157	0.748212	0.9352106
0.22829107	0.678812	0.9231768
0.229691805	0.663522	0.8483076
0.231092541	0.593961	0.8265788
0.232493276	0.624227	0.7487284
0.233893189	0.763664	0.8462353
0.235293924	0.763664	0.8411818
0.236694659	0.763664	0.8248943
0.238095395	0.748849	0.7287083
0.23949613	0.678812	0.7271208
0.240896043	0.677488	0.7252303
0.242296778	0.66796	0.6934672
0.243697514	0.696181	0.6507731
0.245098249	0.837018	0.8522704
0.246498984	0.780583	0.7512854
0.247898897	0.763664	0.7271208
0.249299632	0.7592	0.7473711
0.250700368	0.724657	0.8483076
0.252101103	0.678812	0.8405153
0.253501016	0.672864	0.7766862
0.254901751	0.645873	0.709064
0.256302486	0.678812	0.8893778
0.257703222	0.692516	0.7818609
0.259103957	0.763664	0.7271208
0.26050387	0.763664	0.7464743
0.261904605	0.763664	0.8483076

0.263305341	0.763664	0.8351467
0.264706076	0.763664	0.7413724
0.266106811	0.763664	0.6724655
0.267506724	0.763664	0.8687639
0.268907459	0.763664	0.8483076
0.270308195	0.763664	0.8483076
0.27170893	0.776578	0.829863
0.273109665	0.848515	0.7271208
0.274509578	0.848515	0.7268784
0.275910313	0.848515	0.7271208
0.277311049	0.848515	0.745117
0.278711784	0.848515	0.8483076
0.280111697	0.836076	0.8305416
0.281512432	0.763664	0.7271208
0.282913168	0.763664	0.7271208
0.284313903	0.763664	0.7271208
0.285714638	0.751538	0.7098032
0.287114551	0.678812	0.605934
0.288515286	0.690776	0.6401087
0.289916022	0.763664	0.8483076
0.291316757	0.763664	0.8483076
0.292717492	0.763664	0.8315596
0.294117405	0.763664	0.7271208
0.29551814	0.763664	0.7271208
0.296918876	0.763664	0.7175349
0.298319611	0.763664	0.6455984
0.299719524	0.763664	0.6651459
0.301120259	0.763664	1.0266461
0.302520995	0.763664	0.8323473
0.30392173	0.763664	0.7271208
0.305322465	0.774677	0.7428508
0.306722378	0.848515	0.8483076
0.308123113	0.848515	0.8328078
0.309523849	0.848515	0.6975633
0.310924584	0.837824	0.5655788
0.312325319	0.774279	1.0755207
0.313725232	0.845741	0.9470142
0.315125967	0.842576	0.8269787
0.316526703	0.840522	0.7417238
0.317927438	0.841201	0.7643251
0.319328173	0.7862	0.8052499

0.320728086	0.73467	0.9014844
0.322128822	0.741314	0.9171417
0.323529557	0.713754	0.9481049
0.324930292	0.710699	0.925237
0.326330205	0.73237	0.8712482
0.32773094	0.73316	0.796476
0.329131676	0.767949	0.7731839
0.330532411	0.804469	0.7290598
0.331933146	0.807634	0.794331
0.333333059	0.809755	0.7914589
0.334733794	0.798207	0.6552691
0.33613453	0.795033	0.6590865
0.337535265	0.798003	0.7314835
0.338936	0.848515	0.7720447
0.340335913	0.848515	0.8483076
0.341736649	0.855498	0.8582813
0.343137384	0.917839	0.9473172
0.344538119	0.882159	0.9196503
0.345938032	0.54445	0.6321831
0.347338767	0.614028	0.6345947
0.348739503	0.689936	0.7311927
0.350140238	0.780905	0.7271208
0.351540973	0.933367	0.7391183
0.352940886	0.932713	0.8483076
0.354341621	0.923541	0.8483076
0.355742357	0.905306	0.8366494
0.357143092	0.763664	0.7271208
0.358543827	0.763664	0.7271208
0.35994374	0.763664	0.7271208
0.361344476	0.771504	0.7271208
0.362745211	0.848515	0.7271208
0.364145946	0.848515	0.7271208
0.365545859	0.856118	0.7271208
0.366946594	0.906664	0.7163715
0.36834733	0.63928	0.605934
0.369748065	0.686177	0.616453
0.3711488	0.770952	0.7271208
0.372548713	0.855728	0.7374217
0.373949449	0.933367	0.8483076
0.375350184	0.926316	0.8515675
0.376750919	0.848515	0.8901534

0.378151654	0.834727	0.9375132
0.379551567	0.678812	0.592046
0.380952303	0.685549	0.736743
0.382353038	0.763664	0.8401032
0.383753773	0.77024	0.737349
0.385153686	0.848515	0.7108454
0.386554421	0.85493	0.6150957
0.387955157	0.93234	0.7361734
0.389355892	0.910703	0.8219373
0.390756627	0.684989	0.5041007
0.39215654	0.763664	0.6209854
0.393557276	0.769688	0.6327163
0.394958011	0.848515	0.7339194
0.396358746	0.842652	0.8216586
0.397759481	0.763664	0.8543063
0.399159394	0.757962	0.9318174
0.40056013	0.688103	0.9140151
0.401960865	0.815796	0.7271208
0.4033616	0.812623	0.7271208
0.404762336	0.809458	0.7348162
0.406162248	0.806285	0.8483076
0.407562984	0.80312	0.8483076
0.408963719	0.799946	0.8514584
0.410364454	0.796781	0.900018
0.411764367	0.790086	0.9623686
0.413165103	0.738437	0.8483076
0.414565838	0.763664	0.8483076
0.415966573	0.763664	0.8483076
0.417367308	0.768339	0.8483076
0.418767221	0.848515	0.8483076
0.420167957	0.848515	0.8483076
0.421568692	0.848515	0.8483076
0.422969427	0.839801	0.8479683
0.424370163	0.683089	0.8463686
0.425770075	0.769518	0.8601839
0.427170811	0.848515	1.0840038
0.428571546	0.848515	1.0959043
0.429972281	0.848515	1.1901392
0.431372194	0.85174	1.0645412
0.43277293	0.919578	0.9443724
0.434173665	0.990921	0.9358287

0.4355744	0.848515	0.8483076
0.436975136	0.848515	0.8466837
0.438375048	0.850755	0.8050803
0.439775784	0.899935	0.80056
0.441176519	0.89487	0.7960276
0.442577254	0.848515	0.7915073
0.44397799	0.848515	0.7869749
0.445377902	0.845427	0.7828304
0.446778638	0.763664	0.7975061
0.448179373	0.763664	0.8020263
0.449580108	0.763664	0.8038805
0.450980844	0.764512	0.7283327
0.452380757	0.786557	0.759817
0.453781492	0.785394	0.7552967
0.455182227	0.848515	0.7507643
0.456582963	0.845673	0.7456866
0.457982875	0.753728	0.7271208
0.459383611	0.763664	0.7271208
0.460784346	0.763664	0.7271208
0.462185081	0.763664	0.7271208
0.463585817	0.763664	0.7271208
0.464985729	0.763664	0.7271208
0.466386465	0.763664	0.7271208
0.4677872	0.763664	0.7271208
0.469187935	0.763664	0.7271208
0.470588671	0.763664	0.7271208
0.471988584	0.763664	0.7271208
0.473389319	0.763664	0.7271208
0.474790054	0.763664	0.7271208
0.47619079	0.763664	0.7271208
0.477590702	0.763664	0.7271208
0.478991438	0.763664	0.7271208
0.480392173	0.763664	0.7271208
0.481792908	0.763698	0.7271208
0.483193644	0.772454	0.7271208
0.484593556	0.778793	0.7271208
0.485994292	0.784936	0.7271208
0.487395027	0.763664	0.7271208
0.488795762	0.763409	0.7271208
0.490196498	0.723444	0.7269148
0.491596411	0.763664	0.6999628

0.492997146	0.763664	0.7044952
0.494397881	0.763664	0.7087004
0.495798617	0.763426	0.6195069
0.497198529	0.678812	0.6149866
0.498599265	0.678812	0.6104543
0.5	0.678812	0.605934
0.501400735	0.678812	0.605934
0.502801471	0.678812	0.7268905
0.504201383	0.678812	0.6198099
0.505602119	0.678812	0.6240393
0.507002854	0.678812	0.6060431
0.508403589	0.678812	0.605934
0.509804325	0.678812	0.605934
0.511204238	0.678812	0.605934
0.512604973	0.678812	0.5655424
0.514005708	0.678812	0.7255696
0.515406444	0.678812	0.7271208
0.516807179	0.678812	0.7271208
0.518207092	0.678812	0.7271208
0.519607827	0.678812	0.7271208
0.521008562	0.678812	0.7271208
0.522409298	0.678812	0.7271208
0.52380921	0.678812	0.7271208
0.525209946	0.678812	0.8072253
0.526610681	0.678812	0.7286477
0.528011416	0.678812	0.7271208
0.529412152	0.678812	0.7271208
0.530812065	0.678812	0.7271208
0.5322128	0.678812	0.6085395
0.533613535	0.678812	0.605934
0.535014271	0.678812	0.605934
0.536415006	0.596023	0.8390004
0.537814919	0.677404	0.7311684
0.539215654	0.761551	0.7272662
0.540616389	0.83936	0.7271208
0.542017125	0.838299	0.7271208
0.543417037	0.765734	0.6094363
0.544817773	0.697412	0.605934
0.546218508	0.635419	0.605934
0.547619243	0.699745	0.8406122
0.549019979	0.679661	0.7670882

0.550419892	0.650557	0.7285266
0.551820627	0.595776	0.6101149
0.553221362	0.593961	0.605934
0.554622098	0.638389	0.605934
0.556022833	0.677251	0.605934
0.557422746	0.722163	0.7224793
0.558823481	0.727059	0.6106845
0.560224216	0.730232	0.605934
0.561624952	0.733397	0.605934
0.563024864	0.736571	0.605934
0.5644256	0.739736	0.605934
0.565826335	0.742909	0.605934
0.56722707	0.746074	0.605934
0.568627806	0.749247	0.605934
0.570027719	0.763138	0.7214614
0.571428454	0.682851	0.7271208
0.572829189	0.602751	0.7271208
0.574229925	0.674697	0.7271208
0.57563066	0.680093	0.7271208
0.577030573	0.75954	0.7271208
0.578431308	0.68325	0.7271208
0.579832043	0.588123	0.7271208
0.581232779	0.753711	0.6125023
0.582633514	0.763664	0.605934
0.584033427	0.683564	0.605934
0.585434162	0.678812	0.605934
0.586834897	0.678812	0.605934
0.588235633	0.678812	0.605934
0.589635546	0.599035	0.605934
0.591036281	0.593961	0.605934
0.592437016	0.832826	0.8333774
0.593837752	0.808932	0.8483076
0.595238487	0.766574	0.796064
0.5966384	0.763664	0.7316289
0.598039135	0.684361	0.7271208
0.59943987	0.678812	0.6139687
0.600840606	0.599663	0.605934
0.602241341	0.593961	0.5239026
0.603641254	0.812267	0.7123481
0.605041989	0.768424	0.7271208
0.606442724	0.763664	0.7271208

0.60784346	0.763664	0.6146473
0.609243373	0.684989	0.605934
0.610644108	0.604109	0.605934
0.612044843	0.594037	0.4951571
0.613445579	0.598237	0.490855
0.614846314	0.824935	0.5908099
0.616246227	0.840039	0.5938274
0.617646962	0.701943	0.6046252
0.619047697	0.629149	0.605934
0.620448433	0.629929	0.6295533
0.621849168	0.636268	0.6361459
0.623249081	0.642606	0.6725504
0.624649816	0.648944	0.684463
0.626050551	0.698387	0.8259729
0.627451287	0.696003	0.7578659
0.6288512	0.723486	0.6801488
0.630251935	0.68269	0.6114722
0.63165267	0.718344	0.5518483
0.633053406	0.690377	0.5511697
0.634454141	0.738531	0.5556899
0.635854054	0.752489	0.6017894
0.637254789	0.687934	0.5706686
0.638655524	0.670972	0.5580652
0.64005626	0.69759	0.6297593
0.641456995	0.698141	0.6335403
0.642856908	0.742502	0.7177773
0.644257643	0.750673	0.7271208
0.645658379	0.812708	0.8238763
0.647059114	0.82855	0.8388065
0.648459849	0.480921	0.4289891
0.649859762	0.578017	0.4740464
0.651260497	0.67311	0.488407
0.652661233	0.684837	0.6022014
0.654061968	0.679754	0.7160201
0.655461881	0.678812	0.8357526
0.656862616	0.754788	0.9568182
0.658263351	0.839563	0.9694944
0.659664087	0.564772	0.4559653
0.661064822	0.609887	0.6156653
0.662464735	0.697827	0.8264213
0.66386547	0.757817	0.8882265

0.665266206	0.839165	0.8537489
0.666666941	0.848515	0.7405846
0.668067676	0.809475	0.8347347
0.669467589	0.768644	0.9558003
0.670868324	0.546597	0.5997171
0.67226906	0.525036	0.6002867
0.673669795	0.559044	0.7130874
0.675069708	0.640782	0.8341651
0.676470443	0.675876	0.9552428
0.677871178	0.698014	0.9694944
0.679271914	0.697429	0.8627894
0.680672649	0.694264	0.8483076
0.682072562	0.754856	0.6199432
0.683473297	0.763664	0.6043464
0.684874033	0.763664	0.605934
0.686274768	0.763664	0.7120694
0.687675503	0.763664	0.8326503
0.689075416	0.763664	0.8476653
0.690476151	0.763664	0.9457054
0.691876887	0.763664	0.9553519
0.693277622	0.627214	0.7722144
0.694678357	0.669911	0.7503159
0.69607827	0.752574	0.7548483
0.697479005	0.783273	0.7593686
0.698879741	0.840675	0.7319925
0.700280476	0.848515	0.7271208
0.701680389	0.802848	0.7271208
0.703081124	0.768441	0.7271208
0.70448186	0.650285	0.7271208
0.705882595	0.635555	0.7271208
0.70728333	0.63872	0.7271208
0.708683243	0.714942	0.7271208
0.710083978	0.758937	0.7271208
0.711484714	0.763664	0.7271208
0.712885449	0.787185	0.7271208
0.714285362	0.83986	0.7271208
0.715686097	0.685168	0.6233607
0.717086832	0.676224	0.6877108
0.718487568	0.678812	0.7240548
0.719888303	0.741356	0.8305416
0.721288216	0.762425	0.8585358

0.722688951	0.763664	0.8557727
0.724089687	0.765412	0.8487439
0.725490422	0.83482	0.8483076
0.726891157	0.775848	0.6477798
0.72829107	0.763664	0.7103001
0.729691805	0.763664	0.7271208
0.731092541	0.763664	0.7271208
0.732493276	0.763664	0.7271208
0.733894011	0.763664	0.805153
0.735293924	0.763664	0.8150418
0.736694659	0.763664	0.8423452
0.738095395	0.717207	0.6800034
0.73949613	0.755357	0.6527848
0.740896043	0.763664	0.715911
0.742296778	0.763664	0.7271208
0.743697514	0.763664	0.7271208
0.745098249	0.796603	0.7271208
0.746498984	0.79987	0.7271208
0.747898897	0.796705	0.7271208
0.749299632	0.768627	0.7570297
0.750700368	0.763664	0.8038078
0.752101103	0.763664	0.741845
0.753501838	0.763664	0.7271208
0.754901751	0.763664	0.7271208
0.756302486	0.763664	0.7437234
0.757703222	0.833938	0.7426206
0.759103957	0.848515	0.7381003
0.76050387	0.778402	0.8230523
0.761904605	0.763664	0.8479683
0.763305341	0.763664	0.8483076
0.764706076	0.763664	0.8483076
0.766106811	0.763664	0.8483076
0.767506724	0.763664	0.8483076
0.768907459	0.763664	0.8483076
0.770308195	0.763664	0.8483076
0.77170893	0.833149	0.8726783
0.773109665	0.848515	0.8825913
0.774509578	0.779191	0.8554091
0.775910313	0.763664	0.8483076
0.777311049	0.763664	0.8483076
0.778711784	0.763664	0.8483076

0.780112519	0.763664	0.8483076
0.781512432	0.763664	0.8483076
0.782913168	0.732294	0.8035048
0.784313903	0.72817	0.8386975
0.785714638	0.757503	0.8483076
0.787114551	0.763664	0.8483076
0.788515286	0.763664	0.8483076
0.789916022	0.763664	0.8483076
0.791316757	0.779497	0.8483076
0.792717492	0.780142	0.8672491
0.794117405	0.766277	0.8520401
0.79551814	0.763664	0.8483076
0.796918876	0.763664	0.8483076
0.798319611	0.763664	0.8483076
0.799720346	0.763664	0.8483076
0.801120259	0.763664	0.8483076
0.802520995	0.759107	0.8483076
0.80392173	0.754788	0.8483076
0.805322465	0.828796	0.9448329
0.806723201	0.848515	0.9694944
0.808123113	0.795695	0.9694944
0.809523849	0.76811	0.9694944
0.810924584	0.763664	0.9694944
0.812325319	0.763664	0.9694944
0.813725232	0.806208	0.8736599
0.815125967	0.841328	0.8483076
0.816526703	0.781567	0.943924
0.817927438	0.763664	0.9694944
0.819328173	0.763664	0.9694944
0.820728086	0.763664	0.9694944
0.822128822	0.763664	0.9694944
0.823529557	0.763664	0.9694944
0.824930292	0.830136	0.9694944
0.826330205	0.848515	0.9029144
0.82773094	0.914827	1.0446181
0.829131676	0.867132	0.9960828
0.830532411	0.848515	0.9694944
0.831933146	0.79225	0.9694944
0.833333059	0.76576	0.9694944
0.834733794	0.763664	0.8753565
0.83613453	0.763664	0.8483076

0.837535265	0.76374	0.8483076
0.838936	0.766913	1.0359169
0.840335913	0.765123	1.0906812
0.841736649	0.763664	1.0801137
0.843137384	0.753829	0.9930531
0.844538119	0.760007	0.9694944
0.845938855	0.763664	0.8762533
0.847338767	0.828864	0.8483076
0.848739503	0.848515	0.8483076
0.850140238	0.935488	1.0340991
0.851540973	0.900173	1.0906812
0.852940886	0.791851	1.0906812
0.854341621	0.763664	1.0906812
0.855742357	0.763664	1.0906812
0.857143092	0.763664	1.0906812
0.858543827	0.66286	1.0906812
0.85994374	0.563541	1.0906812
0.861344476	0.774194	1.0906812
0.862745211	0.848515	0.9987974
0.864145946	0.848515	0.9042838
0.865546682	0.848515	0.947402
0.866946594	0.784418	0.9694944
0.86834733	0.763664	1.0447029
0.869748065	0.763664	0.995186
0.8711488	0.763664	0.8782892
0.872548713	0.950829	1.1156214
0.873949449	0.890228	1.1200447
0.875350184	0.784894	1.0001062
0.876750919	0.763664	0.9694944
0.878151654	0.827124	0.8788588
0.879551567	0.848515	0.8483076
0.880952303	0.848515	0.9387129
0.882353038	0.785292	0.9694944
0.883753773	0.889948	1.0807317
0.885154509	0.933367	1.0991037
0.886554421	0.933367	1.0906812
0.887955157	0.870458	1.0906812
0.889355892	0.848515	1.0009545
0.890756627	0.822152	0.9318416
0.892157363	0.775696	0.8654919
0.893557276	0.763664	0.8483076

0.894958011	0.792904	1.1161425
0.896358746	0.800184	1.1226987
0.897759481	0.834863	1.0016331
0.899159394	0.848515	0.8805554
0.90056013	0.848515	0.7594777
0.901960865	0.893173	0.7271208
0.9033616	0.927809	0.7271208
0.904762336	0.933367	0.8156114
0.906162248	0.933367	1.0984856
0.907562984	0.933367	1.0310088
0.908963719	0.933367	0.8813431
0.910364454	0.933367	0.8483076
0.91176519	0.933367	0.9362286
0.913165103	0.933367	0.9710577
0.914565838	0.929981	0.8933042
0.915966573	0.919858	0.7117422
0.917367308	0.850102	0.8744839
0.918767221	0.820149	0.9492441
0.920167957	0.826301	0.9447117
0.921568692	0.842745	0.9401914
0.922969427	0.865528	0.935659
0.924370163	0.875371	0.9311388
0.925770075	0.917805	0.9266064
0.927170811	0.933367	0.9220861
0.928571546	0.820811	0.8433632
0.929972281	0.797647	0.8806645
0.931373017	0.896685	0.9519587
0.93277293	0.933367	0.9694944
0.934173665	0.898518	0.883379
0.9355744	0.881158	0.8483076
0.936975136	0.95648	0.9043565
0.938375048	1.033356	1.0502896
0.939775784	0.985907	0.8245792
0.941176519	0.953332	0.822313
0.942577254	0.950159	0.9408216
0.94397799	0.937397	0.9694944
0.945377902	0.933367	0.8947948
0.946778638	0.933367	0.9364952
0.948179373	0.930482	1.0503502
0.949580108	0.932416	1.1722884
0.950980844	0.992703	0.9598237

0.952380757	1.018218	0.9352712
0.953781492	0.965008	0.9694944
0.955182227	0.99603	0.9694944
0.956582963	1.018218	0.9694944
0.957982875	1.077165	1.0536829
0.959383611	1.161931	1.0906812
0.960784346	1.229804	1.0906812
0.962185081	1.185019	1.0906812
0.963585817	1.260563	1.0906812
0.964985729	1.400381	1.0906812
0.966386465	1.508312	1.174191
0.9677872	1.617771	1.3786574
0.969187935	1.800074	1.5375211
0.970588671	2.131631	1.7417573
0.971988584	2.406296	1.9008513
0.973389319	2.408655	1.731214
0.974790054	2.577229	1.9300573
0.97619079	3.008988	2.3697472
0.977591525	3.310465	2.6781071
0.978991438	3.555839	2.6960306
0.980392173	3.760416	2.7484802
0.981792908	4.348216	2.9643381
0.983193644	4.767705	3.2173156
0.984593556	4.842502	3.353784
0.985994292	5.46409	3.8831886
0.987395027	6.628719	4.6939404
0.988795762	7.210394	5.450558
0.990196498	6.626199	5.9376805
0.991596411	5.479143	5.5157444
0.992997146	4.222152	4.1372567
0.994397881	3.076572	2.9003758
0.995798617	2.001919	1.9906992
0.997199352	1.38515	1.7070009
0.998599265	1.207777	1.5348066
1	1.206775	1.211868

Table A 7 Measurement data of Actin and Myosin intensity from cell 3

Validation of Pressure inside channel using Computational Fluid Dynamics:

To calculate the magnitude of force that was applied on the cell in both creep and dislodge experiment, it is essential to calculate the effective pressure inside the channel. In both creep and dislodge experimental setups, when a negative pressure was applied, the corresponding effective pressure in the micro channel could be significantly different due to the difference is geometric size between the channel and the rest of the pressure apparatus (tubing, syringe, needle, reservoir) which differs in dimension by several orders of magnitude. The relatively smaller channel dimension, which is in the order of microns, can generate significant amount of hydraulic resistance and it can be hypothesized that a portion of the applied negative pressure will be lost and the effective pressure inside the channel would be lower than the applied pressure level.

A computational model of the pressure setup was generated using actual dimensions of the syringe, tubing, needle, the reservoir and the channel (**Fig A1-a**). The geometry was built using Solidworks to represent the continuous fluid domain in the experimental setup. Using Finite Element Analysis (**FEA**) in COMSOL, a steady-state analysis was conducted on the continuous fluid domain governed by the Navier stokes equation. A static pressure ***p*** was applied was applied at the end of the syringe domain and at the opposite end, the top surface of the reservoir was set to zero (since the pressure gauge is zero referenced against atmospheric pressure). No slip boundary condition was applied at the remaining edges of the fluid domain.

A parametric analysis was carried out varying the negative pressure value of ***p*** from 1 kpa, 5 kPa-35 kPa with every 5 kPa interval. The corresponding result shows that for every pressure level the pressure drop is predominant across the channel than the rest of the fluid domain.

However, the presence of a cell inside the channel could alter the scenario significantly and since 5µm x 5µm channels are small enough for the cell to block almost the entire cross section during migration, it can be hypothesized that there will not be any flow of fluid in the channels. Since there is no flow of fluid, no pressure drop is expected across the length of the channel. To validate this theory, we modified the CFD model considering the presence of a cell boundary blocking the fluid flow (**A1-b**). The presence of a

cell in the channel was mimicked by a no-slip boundary condition at the midsection of the channel. The geometry was reduced to a closed fluid domain extending only 250 µm from the central reservoir. A no-slip boundary condition was applied at all the boundary surfaces except the pressure inlet.

To establish a relationship for any given applied pressure at these segmented locations, effective pressure has been expressed as parameter normalized by corresponding applied pressure and effective pressure ratio (EPR) has been introduced.

$$Effective\ Pressure\ Ratio\ (\ EPR) = \frac{Effective\ Pressure\ at\ the\ midpoint}{Applied\ Pressure}$$

Although **Fig A3** demonstrates that in an open channel a significant amount of is lost along the length of the channel, however when a cell is present either at the midpoint of the channel or the entrance, no pressure drop occurs inside the channel and the effective pressure ratio remains unity.

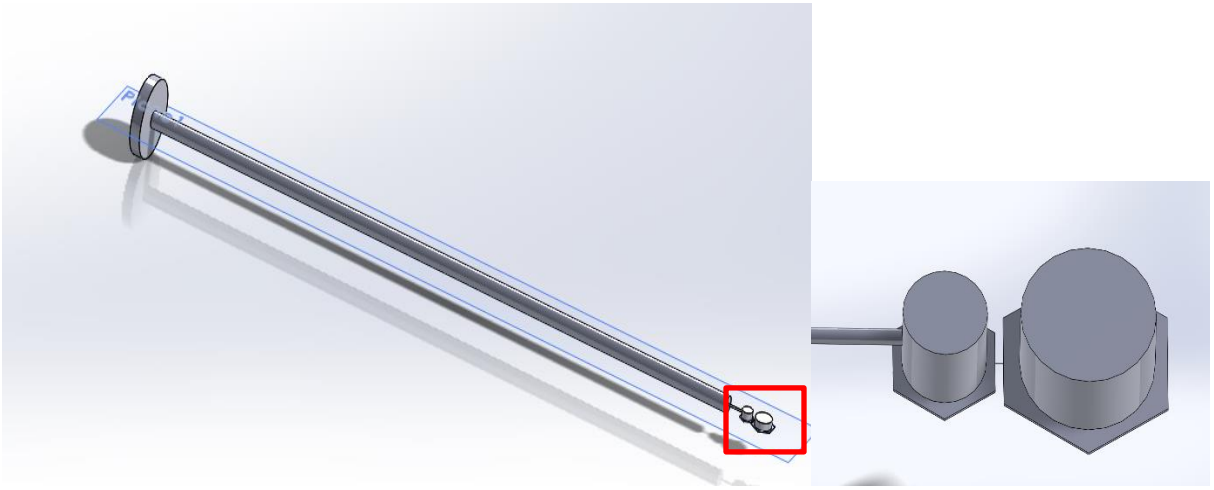

(a)

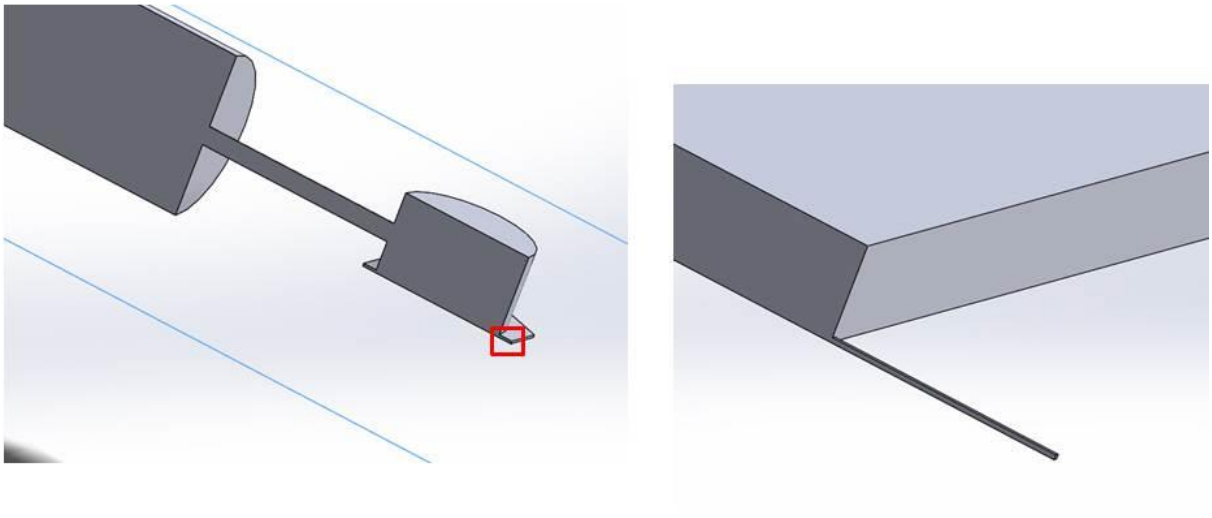

(b)

Figure A 1: Geometry of the fluid domain of the experimental setup with an open channel (a) (Considering no presence of a cell in the channel) and the fluid domain upto halfway the length of the channel (considering the presence of a migrating cell in the middle of the channel)

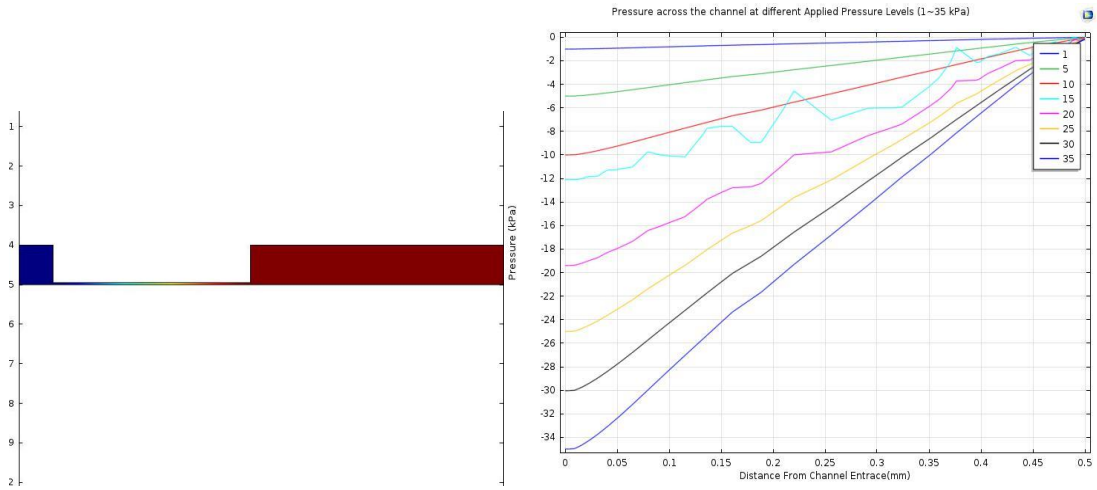

(a)

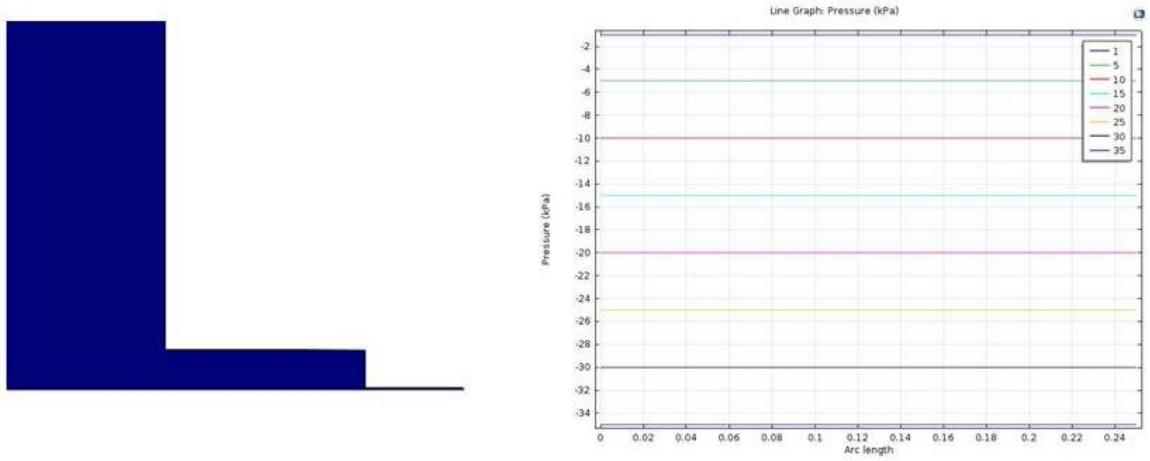

(b)

*Figure A 2*Pressure drop across the channel for difference pressure levels (a) in the absence of any cell and (b) when the fluid domain is reduced due to presence of a cell.

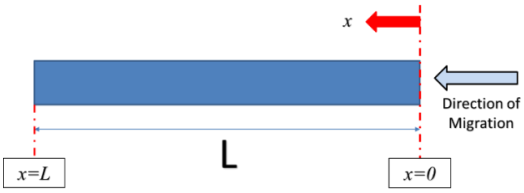

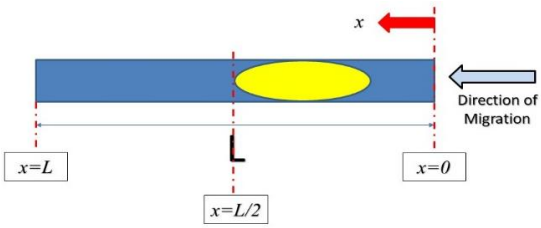

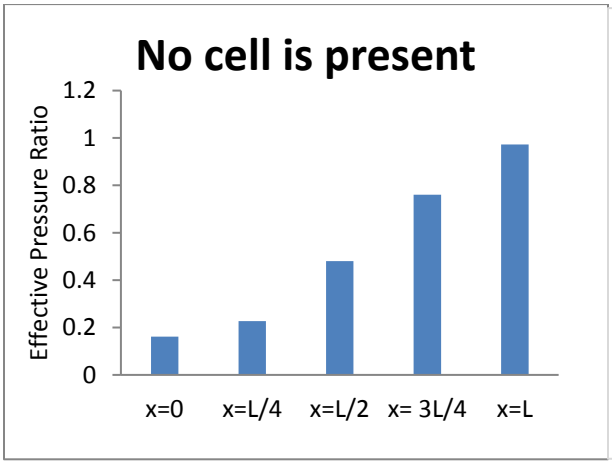

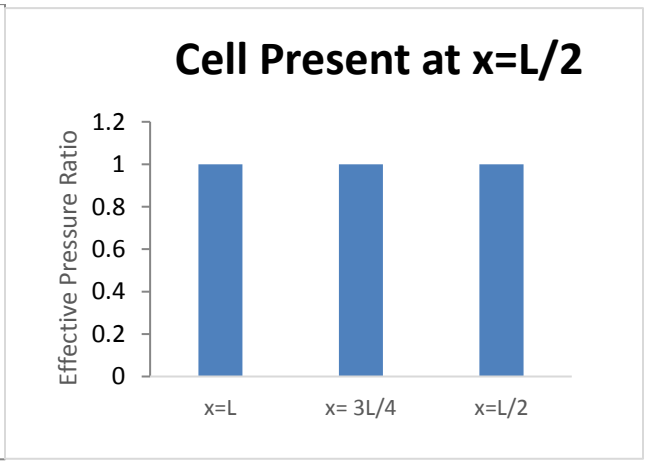

*Figure A 3*Effective Pressure Ratio at different locations of the channel (Presence of a migrating cell is not considered)

Summary of Adhesion strength measurement on 2D substrate

Cell Type	Method	Detachment Force	Adhesion Strength	Reference	Remarks
Fibroblast	Hydrodynamic shear force	-	80-110 Pa	[19]	Single cell adhesion strength estimated from results obtained from distribution of cell population
T24- Human epithelial bladder cancer cell	Hydrodynamic shear force	10-1400 nN	400-7000 Pa	[90]	Indirect measurement of single cell adhesion strength
L929-Mouse Fibroblast	Traction Force Microscopy		300 Pa	[91]	Bead displacement monitored over time during trypsinization
WT NR6 Fibroblast	Hydrodynamic Shear Force		10-1000 Pa	[20]	Shear Stress obtained from numerical analysis

Ovarian cell	Hydrodynamic Shear Forces		5-30 Pa	[21]	Compared the role of different ECM proteins on the strength of adhesion
Fibroblast	Microfluidic Shear Force assay		10- 40 Pa	[92]	Compared adhesion strength on fibrinogen coated glass surface treated with Ethelyn glycol
Human fibrosarcoma cells	Hydrodynamic shear force – Rotating Disk		10-15 Pa	[93]	Detachment strength for different fibronectin matrices were compared
L929 Fibroblast	AFM	350-600 nN	530-750 Pa	[27]	Stage displaced while keeping the AFM cantilever stationary
Human Breast cancer cell	Hydrodynamic Shear Force		0.5-10 Pa	[94]	Detachment of cells from collagen IV coated glass surfaces were measured
Human Bone Marrow cell	Hydrodynamic Force – Rotating Disk		10-20 Pa	[95]	Cells were seeded on surfaces of different roughness

Human Fibroblasts	Parallel plate flow chamber		35 Pa	[96]	Cell Adhesion strength on glass surfaces were measured
Osteoblast	Hydrodynamic force – Rotating Disc		6-8 Pa	[97]	Adhesion strength studied on glass coated with fibronectin
Fibroblast	Hydrodynamic-parallel plate flow chamber		5-10 Pa	[98]	Compared cell spreading and adhesion strength between glass and silane surface
Fibroblast	Hydrodynamic-Jet Impingement		30-140 Pa	[99]	Tested the effect of exposure time on cell adhesion
Aortic endothelial cell	Hydrodynamic-Parallel plate flow chamber		6-10 Pa	[100]	Studied the effect of fibronectin amount on cell adhesion
Platelets	Parallel plate flow chamber		3-4 Pa	[101]	Conducted platelet study for validation of flow chamber

Erythroleukemia cell	Rotating disk flow chamber		2-8 Pa	[102]	Quantified adhesion strength for different fibronectin coating levels
Endothelial cell	Rotating disk flow chamber		4.5-9 Pa	[103]	Adhesion strength measured polystyrene surfaces
Fibroblasts	Rotating disk flow chamber		1.8-2 Pa	[104]	Cell adhesion studied on different copolymer surfaces
Fibroblast	Parallel plate flow chamber		50-8.5 Pa	[105]	Adhesion strength quantified on fibronectin coated surfaces
Leukocytes	Parallel plate flow chamber		2-3 Pa	[106]	Adhesion strength between leukocytes and endothelial cells studied
Fibroblast	Micro-pillars		50 Pa	[107]	Adhesion strengthening with FN concentration

Endothelial cells	Variable height flow chamber		5 Pa	[108]	Cell receptor-ligand affinity was studied on glass coated with FN
RBC	Micropipette aspiration	0.5 – 2.4 nN		[109]	Effect of hydrophobicity on cell adhesion studied

Table A 8 Summary of cell-substrate adhesion studies

Cell Type	Method	Detachment Force	Reference	Remarks
Chinese Hamster Ovarian cell	AFM	2 -8 nN	[110]	Adhesion strength in laminin coated substrate higher than collagen coated substrate
HeLa	AFM	20-60 nN	[111]	Cell attached to bead-modified cantilever tip, Detachment of single bond measured
Ovarian Cell	AFM	1.4 nN	[110]	Substrate Coated in Laminin, Collagen

Vascular SMC(K562)	AFM	1.5 nN	[112]	Substrate Coated in Fibronectin,
Endothelial Cell	AFM	0.08 nN	[113]	The attachment force increased after histamine treatment

Table A 9 Summary of receptor-ECM adhesion studies

Additional images from bleb generation model

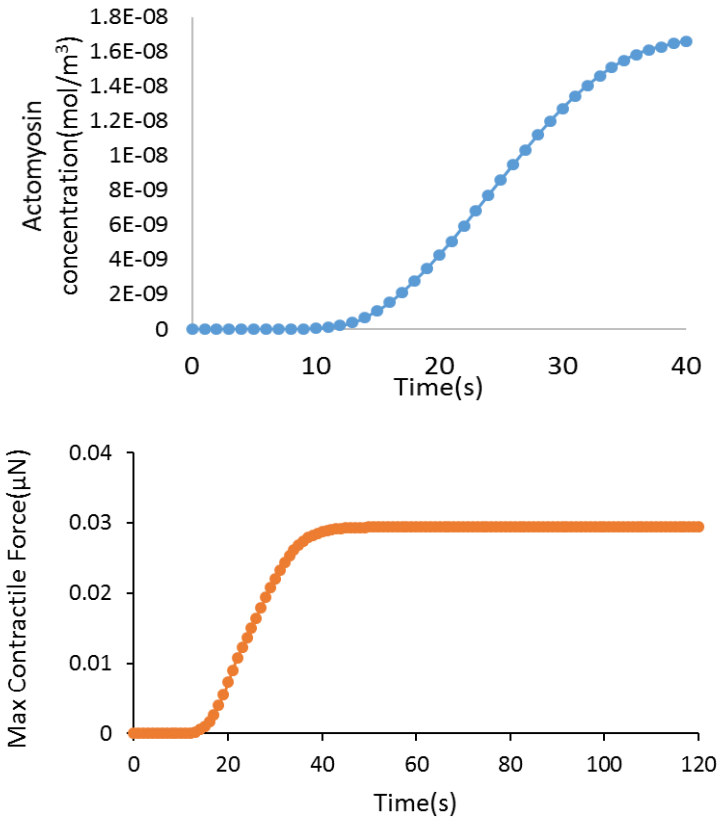

Figure A 4 Rate of reaction in the acto-myosin complex and the resulting change in Actomyosin concentration.

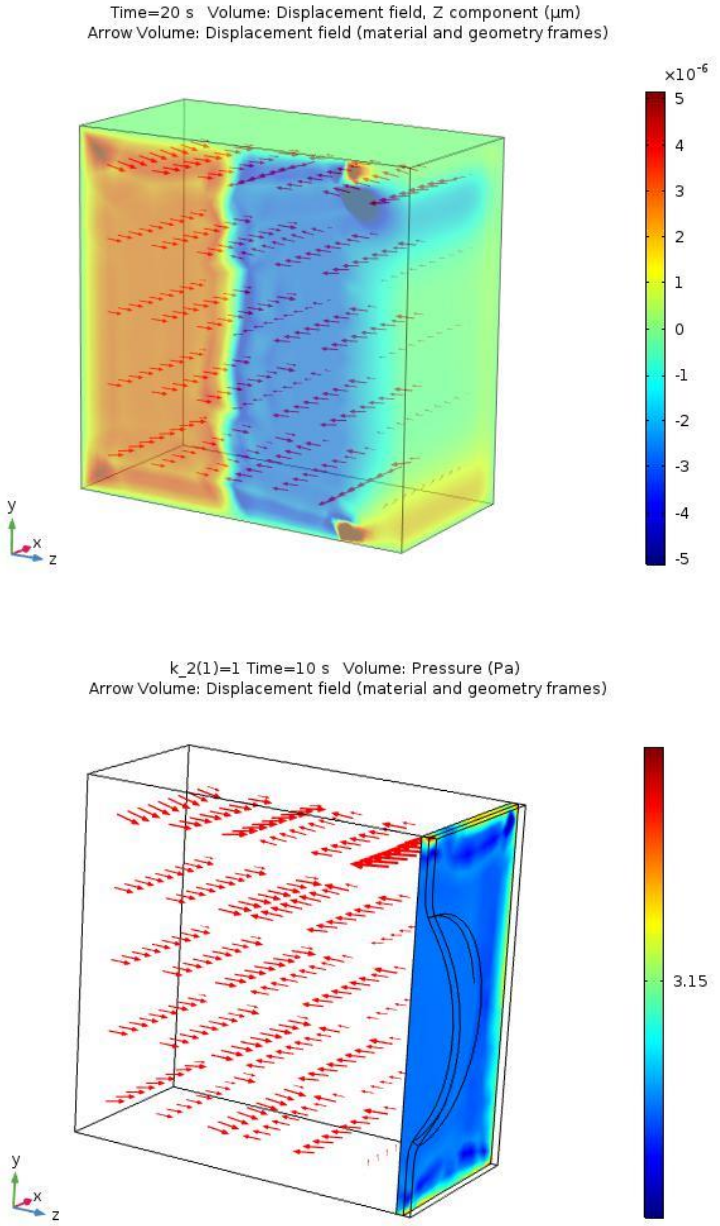

Figure A 5 Displacement and Pressure field in the poroelastic domain

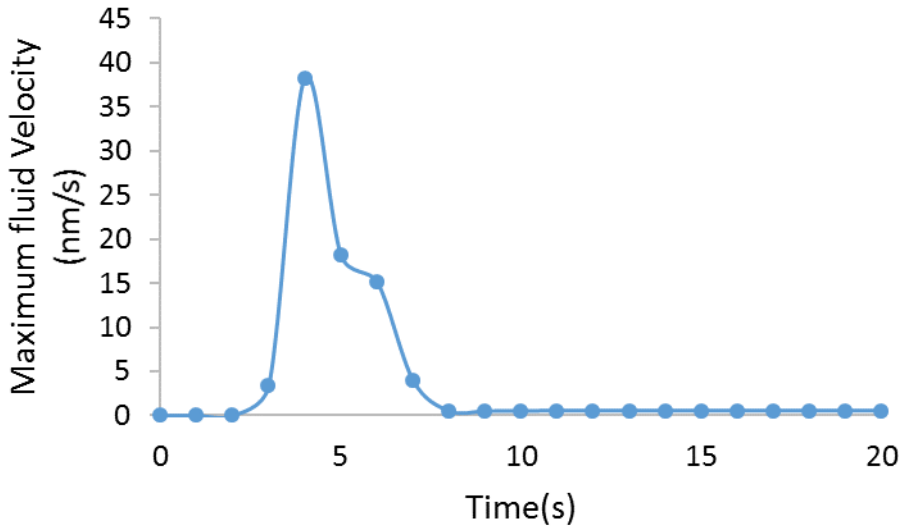

Figure A 6Maximum fluid velocity adjacent to the membrane

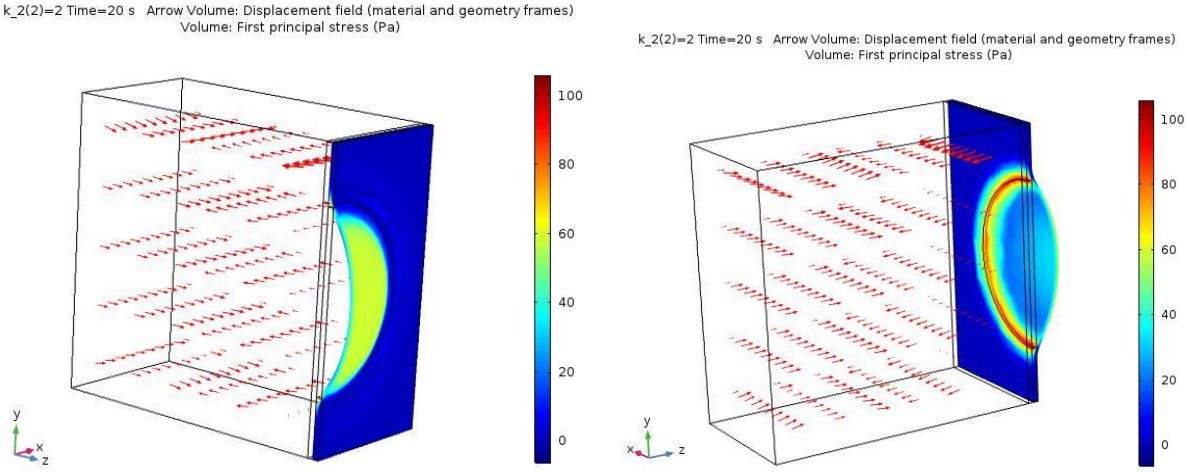

Figure A 71st principal stress exerted on the elastic membrane at the end of the expansion phase.

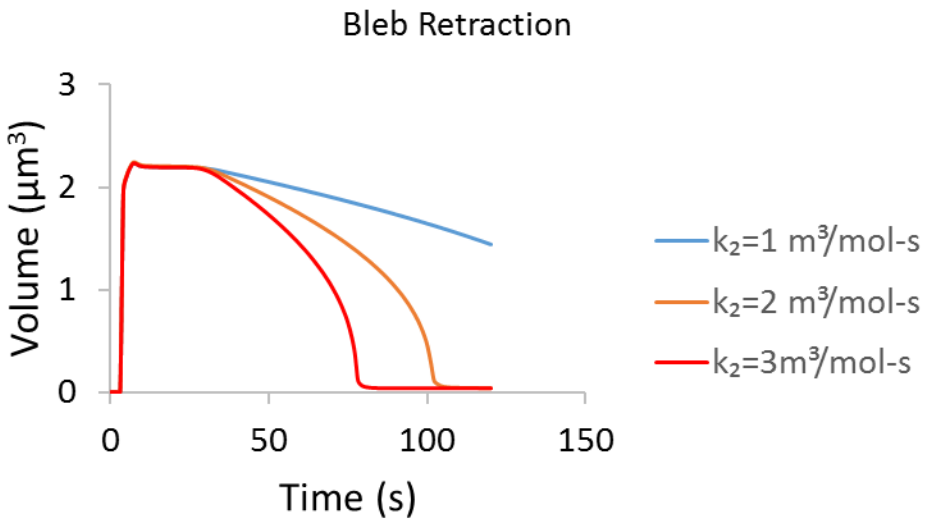

Figure A 8Change of Bleb volume for different reaction rates of actin attachment to Myosin

References

1. Yuan, X., et al., *Isolation of cancer stem cells from adult glioblastoma multiforme.* Oncogene, 2004. **23**(58): p. 9392-9400.
2. Giese, A. and M. Westphal, *Glioma invasion in the central nervous system.* Neurosurgery, 1996. **39**(2): p. 235-252.
3. G Gritsenko, P., O. Ilina, and P. Friedl, *Interstitial guidance of cancer invasion.* The Journal of pathology, 2012. **226**(2): p. 185-199.
4. Bernstein, J.J. and C.A. Woodard, *Glioblastoma cells do not intravasate into blood vessels.* Neurosurgery, 1995. **36**(1): p. 124-132.
5. Pathak, A. and S. Kumar, *Independent regulation of tumor cell migration by matrix stiffness and confinement.* Proceedings of the National Academy of Sciences of the United States of America, 2012. **109**(26): p. 10334-10339.
6. Irimia, D. and M. Toner, *Spontaneous migration of cancer cells under conditions of mechanical confinement.* Integrative Biology, 2009. **1**(8-9): p. 506-512.
7. Tavano, F., et al., *Custom-Built Optical Tweezers for Locally Probing the Viscoelastic Properties of Cancer Cells.* International Journal of Optomechatronics, 2011. **5**(3): p. 234-248.
8. Ketene, A.N., et al., *The effects of cancer progression on the viscoelasticity of ovarian cell cytoskeleton structures.* Nanomedicine: Nanotechnology, Biology and Medicine, 2012. **8**(1): p. 93-102.
9. Zhao, M., et al., *Rate-and depth-dependent nanomechanical behavior of individual living Chinese hamster ovary cells probed by atomic force microscopy.* Journal of Materials Research, 2006. **21**(08): p. 1906-1912.
10. Igawa, S., et al., *Nitric oxide generated by iNOS reduces deformability of Lewis lung carcinoma cells.* Cancer science, 2004. **95**(4): p. 342-347.
11. Ochalek, T., et al., *Correlation between cell deformability and metastatic potential in B16-F1 melanoma cell variants.* Cancer research, 1988. **48**(18): p. 5124-5128.
12. Moraes, C., et al., *An Undergraduate lab (on-a-chip): probing single cell mechanics on a microfluidic platform.* Cellular and Molecular Bioengineering, 2010. **3**(3): p. 319-330.
13. Bui, L., et al., *Role of key genetic mutations on increasing migration of brain cancer cells through confinement.* Biomedical Microdevices, 2017. **19**(3): p. 56.
14. Vallittu, P. and K. Ekstrand, *In vitro cytotoxicity of fibre–polymethyl methacrylate composite used in dentures.* Journal of oral rehabilitation, 1999. **26**(8): p. 666-671.
15. Gingras, M.-c., et al., *Comparison of cell adhesion molecule expression between glioblastoma multiforme and autologous normal brain tissue.* Journal of neuroimmunology, 1995. **57**(1): p. 143-153.
16. Wirtz, D., K. Konstantopoulos, and P.C. Searson, *The physics of cancer: the role of physical interactions and mechanical forces in metastasis.* Nature Reviews Cancer, 2011. **11**(7): p. 512-522.
17. Bergert, M., et al., *Cell mechanics control rapid transitions between blebs and lamellipodia during migration.* Proceedings of the National Academy of Sciences, 2012. **109**(36): p. 14434-14439.
18. Bergert, M., et al., *Force transmission during adhesion-independent migration.* Nature cell biology, 2015. **17**(4): p. 524-529.

19. Christ, K.V., et al., *Measurement of single-cell adhesion strength using a microfluidic assay.* Biomedical microdevices, 2010. **12**(3): p. 443-455.
20. Lu, H., et al., *Microfluidic shear devices for quantitative analysis of cell adhesion.* Analytical chemistry, 2004. **76**(18): p. 5257-5264.
21. Zhang, X., P. Jones, and S.J. Haswell, *Attachment and detachment of living cells on modified microchannel surfaces in a microfluidic-based lab-on-a-chip system.* Chemical engineering journal, 2008. **135**: p. S82-S88.
22. Taubenberger, A.V., D.W. Hutmacher, and D.J. Muller, *Single-cell force spectroscopy, an emerging tool to quantify cell adhesion to biomaterials.* Tissue Engineering Part B: Reviews, 2013. **20**(1): p. 40-55.
23. Sung, K.-L.P., et al., *Adhesion strength of human ligament fibroblasts.* Journal of biomechanical engineering, 1994. **116**(3): p. 237-242.
24. Andersson, M., et al., *Using optical tweezers for measuring the interaction forces between human bone cells and implant surfaces: System design and force calibration.* Review of Scientific Instruments, 2007. **78**(7): p. 074302.
25. Neuman, K.C. and A. Nagy, *Single-molecule force spectroscopy: optical tweezers, magnetic tweezers and atomic force microscopy.* Nature methods, 2008. **5**(6): p. 491-505.
26. Kollmannsberger, P. and B. Fabry, *BaHigh-force magnetic tweezers with force feedback for biological applications.* Review of Scientific Instruments, 2007. **78**(11): p. 114301.
27. Yamamoto, A., et al., *A new technique for direct measurement of the shear force necessary to detach a cell from a material.* Biomaterials, 1998. **19**(7): p. 871-879.
28. Müller, D.J., et al., *Force probing surfaces of living cells to molecular resolution.* Nature chemical biology, 2009. **5**(6): p. 383.
29. Helenius, J., et al., *Single-cell force spectroscopy.* Journal of cell science, 2008. **121**(11): p. 1785-1791.
30. Bui, L., et al., *Brain Tumor Genetic Modification Yields Increased Resistance to Paclitaxel in Physical Confinement.* Scientific reports, 2016. **6**: p. 26134.
31. Brazma, A., et al., *A quick introduction to elements of biology-cells, molecules, genes, functional genomics, microarrays.* European ioinformatics Institute, on-line tutorial di www. ebi. ac. uk/microarray/biology intro. html, 2001.
32. Dunn, A.C., et al., *Friction coefficient measurement of hydrogel materials on living epithelial cells.* Tribology Letters, 2008. **30**(1): p. 13.
33. Charras, G.T., et al., *Non-equilibration of hydrostatic pressure in blebbing cells.* Nature, 2005. **435**(7040): p. 365-369.
34. Fackler, O.T. and R. Grosse, *Cell motility through plasma membrane blebbing.* The Journal of cell biology, 2008. **181**(6): p. 879-884.
35. Charras, G.T., et al., *Life and times of a cellular bleb.* Biophysical journal, 2008. **94**(5): p. 1836-1853.
36. Friedl, P. and K. Wolf, *Tumour-cell invasion and migration: diversity and escape mechanisms.* Nature reviews. Cancer, 2003. **3**(5): p. 362.
37. Diz-Muñoz, A., et al., *Control of directed cell migration in vivo by membrane-to-cortex attachment.* PLoS biology, 2010. **8**(11): p. e1000544.
38. Maugis, B., et al., *Dynamic instability of the intracellular pressure drives bleb-based motility.* J Cell Sci, 2010. **123**(22): p. 3884-3892.

39. Yoshida, K. and T. Soldati, *Dissection of amoeboid movement into two mechanically distinct modes.* Journal of cell science, 2006. **119**(18): p. 3833-3844.
40. Yip, A.K., K.-H. Chiam, and P. Matsudaira, *Traction stress analysis and modeling reveal that amoeboid migration in confined spaces is accompanied by expansive forces and requires the structural integrity of the membrane–cortex interactions.* Integrative Biology, 2015. **7**(10): p. 1196-1211.
41. Charras, G. and E. Paluch, *Blebs lead the way: how to migrate without lamellipodia.* Nature reviews Molecular cell biology, 2008. **9**(9): p. 730-736.
42. Paluch, E.K. and E. Raz, *The role and regulation of blebs in cell migration.* Current opinion in cell biology, 2013. **25**(5): p. 582-590.
43. Lim, F.Y., K.-H. Chiam, and L. Mahadevan, *The size, shape, and dynamics of cellular blebs.* EPL (Europhysics Letters), 2012. **100**(2): p. 28004.
44. Woolley, T.E., et al., *Three mechanical models for blebbing and multi-blebbing.* The IMA Journal of Applied Mathematics, 2014. **79**(4): p. 636-660.
45. Tinevez, J.-Y., et al., *Role of cortical tension in bleb growth.* Proceedings of the National Academy of Sciences, 2009. **106**(44): p. 18581-18586.
46. Strychalski, W. and R.D. Guy, *Intracellular pressure dynamics in blebbing cells.* Biophysical journal, 2016. **110**(5): p. 1168-1179.
47. Young, J. and S. Mitran, *A numerical model of cellular blebbing: A volume-conserving, fluid–structure interaction model of the entire cell.* Journal of biomechanics, 2010. **43**(2): p. 210-220.
48. Spangler, E.J., et al., *Computer simulation of cytoskeleton-induced blebbing in lipid membranes.* Physical Review E, 2011. **84**(5): p. 051906.
49. Tozluoglu, M., et al., *Matrix geometry determines optimal cancer cell migration strategy and modulates response to interventions.* Nature cell biology, 2013. **15**(7): p. 751.
50. Jacobs, C.R., H. Huang, and R.Y. Kwon, *Introduction to cell mechanics and mechanobiology*. 2012: Garland Science.
51. Eisenberg, E., T.L. Hill, and Y.-d. Chen, *Cross-bridge model of muscle contraction. Quantitative analysis.* Biophysical Journal, 1980. **29**(2): p. 195-227.
52. Pollard, T.D., L. Blanchoin, and R.D. Mullins, *Molecular mechanisms controlling actin filament dynamics in nonmuscle cells.* Annual review of biophysics and biomolecular structure, 2000. **29**(1): p. 545-576.
53. Enrique, M., et al., *The kinetic mechanism of myosin V.* Proceedings of the National Academy of Sciences, 1999. **96**(24): p. 13726-13731.
54. Pantaloni, D., C. Le Clainche, and M.-F. Carlier, *Mechanism of actin-based motility.* Science, 2001. **292**(5521): p. 1502-1506.
55. De La Cruz, E.M. and E.M. Ostap, *Relating biochemistry and function in the myosin superfamily.* Current opinion in cell biology, 2004. **16**(1): p. 61-67.
56. Taber, L., et al., *A poroelastic model for cell crawling including mechanical coupling between cytoskeletal contraction and actin polymerization.* Journal of mechanics of materials and structures, 2011. **6**(1): p. 569-589.
57. Cross, S.E., et al., *AFM-based analysis of human metastatic cancer cells.* Nanotechnology, 2008. **19**(38): p. 384003.

58. Huxley, A.F. and R.M. Simmons, *Proposed mechanism of force generation in striated muscle.* Nature, 1971. **233**(5321): p. 533-538.
59. Lämmermann, T., et al., *Rapid leukocyte migration by integrin-independent flowing and squeezing.* Nature, 2008. **453**(7191): p. 51-55.
60. Lekka, M., et al., *Elasticity of normal and cancerous human bladder cells studied by scanning force microscopy.* European Biophysics Journal, 1999. **28**(4): p. 312-316.
61. Lekka, M., et al., *Local elastic properties of cells studied by SFM.* Applied Surface Science, 1999. **141**(3): p. 345-349.
62. Ward, K.A., et al., *Viscoelastic properties of transformed cells: role in tumor cell progression and metastasis formation.* Biorheology, 1991. **28**(3-4): p. 301-313.
63. Rebelo, L.M., et al., *Comparison of the viscoelastic properties of cells from different kidney cancer phenotypes measured with atomic force microscopy.* Nanotechnology, 2013. **24**(5): p. 055102.
64. Li, Q.S., et al., *AFM indentation study of breast cancer cells.* Biochemical and biophysical research communications, 2008. **374**(4): p. 609-613.
65. Hou, H.W., et al., *Deformability study of breast cancer cells using microfluidics.* Biomedical Microdevices, 2009. **11**(3): p. 557-564.
66. Korb, T., et al., *Integrity of actin fibers and microtubules influences metastatic tumor cell adhesion.* Experimental cell research, 2004. **299**(1): p. 236-247.
67. Lam, W.A., M.J. Rosenbluth, and D.A. Fletcher, *Chemotherapy exposure increases leukemia cell stiffness.* Blood, 2007. **109**(8): p. 3505-3508.
68. Beil, M., et al., *Sphingosylphosphorylcholine regulates keratin network architecture and visco-elastic properties of human cancer cells.* Nature cell biology, 2003. **5**(9): p. 803-811.
69. Li, J., et al., *PTEN, a putative protein tyrosine phosphatase gene mutated in human brain, breast, and prostate cancer.* Science, 1997. **275**(5308): p. 1943-1947.
70. Coughlin, M.F., et al., *Cytoskeletal stiffness, friction, and fluidity of cancer cell lines with different metastatic potential.* Clinical & experimental metastasis, 2013. **30**(3): p. 237-250.
71. Xu, W., et al., *Cell stiffness is a biomarker of the metastatic potential of ovarian cancer cells.* PloS one, 2012. **7**(10): p. e46609.
72. Swaminathan, V., et al., *Mechanical stiffness grades metastatic potential in patient tumor cells and in cancer cell lines.* Cancer research, 2011. **71**(15): p. 5075-5080.
73. Yanai, M., et al., *Intracellular elasticity and viscosity in the body, leading, and trailing regions of locomoting neutrophils.* American Journal of Physiology-Cell Physiology, 1999. **277**(3): p. C432-C440.
74. Sheetz, M.P., et al. *Cell migration as a five-step cycle*. in *Biochemical Society symposium*. 1999.
75. Lämmermann, T. and M. Sixt, *Mechanical modes of 'amoeboid'cell migration.* Current opinion in cell biology, 2009. **21**(5): p. 636-644.
76. Balzer, E.M., et al., *Physical confinement alters tumor cell adhesion and migration phenotypes.* The FASEB Journal, 2012. **26**(10): p. 4045-4056.

77. Liu, Y.-J., et al., *Confinement and low adhesion induce fast amoeboid migration of slow mesenchymal cells.* Cell, 2015. **160**(4): p. 659-672.
78. Bouillard, K., A. Nordez, and F. Hug, *Estimation of individual muscle force using elastography.* PloS one, 2011. **6**(12): p. e29261.
79. Gennisson, J.-L., et al., *Viscoelastic and anisotropic mechanical properties of in vivo muscle tissue assessed by supersonic shear imaging.* Ultrasound in medicine and biology, 2010. **36**(5): p. 789-801.
80. Yoshitake, Y., et al., *Muscle shear modulus measured with ultrasound shear-wave elastography across a wide range of contraction intensity.* Muscle & nerve, 2014. **50**(1): p. 103-113.
81. Shinohara, M., et al., *Real-time visualization of muscle stiffness distribution with ultrasound shear wave imaging during muscle contraction.* Muscle & nerve, 2010. **42**(3): p. 438-441.
82. Kollmannsberger, P., C.T. Mierke, and B. Fabry, *Nonlinear viscoelasticity of adherent cells is controlled by cytoskeletal tension.* Soft Matter, 2011. **7**(7): p. 3127-3132.
83. An, S.S., et al., *Stiffness changes in cultured airway smooth muscle cells.* American Journal of Physiology-Cell Physiology, 2002. **283**(3): p. C792-C801.
84. Berrier, A.L. and K.M. Yamada, *Cell–matrix adhesion.* Journal of cellular physiology, 2007. **213**(3): p. 565-573.
85. Friedl, P., *To adhere or not to adhere?* Nature Reviews Molecular Cell Biology, 2010. **11**(1): p. 3-3.
86. Renkawitz, J. and M. Sixt, *Mechanisms of force generation and force transmission during interstitial leukocyte migration.* EMBO reports, 2010. **11**(10): p. 744-750.
87. Bendas, G. and L. Borsig, *Cancer cell adhesion and metastasis: selectins, integrins, and the inhibitory potential of heparins.* International journal of cell biology, 2012. **2012**.
88. Charras, G. and E. Sahai, *Physical influences of the extracellular environment on cell migration.* Nature reviews. Molecular cell biology, 2014. **15**(12): p. 813.
89. Mackenzie Jr, J.M., et al., *Muscle development in Caenorhabditis elegans: mutants exhibiting retarded sarcomere construction.* Cell, 1978. **15**(3): p. 751-762.
90. Couzon, C., A. Duperray, and C. Verdier, *Critical stresses for cancer cell detachment in microchannels.* European Biophysics Journal, 2009. **38**(8): p. 1035-1047.
91. Das, T., T.K. Maiti, and S. Chakraborty, *Traction force microscopy on-chip: shear deformation of fibroblast cells.* Lab on a chip, 2008. **8**(8): p. 1308-1318.
92. Christophis, C., M. Grunze, and A. Rosenhahn, *Quantification of the adhesion strength of fibroblast cells on ethylene glycol terminated self-assembled monolayers by a microfluidic shear force assay.* Physical Chemistry Chemical Physics, 2010. **12**(17): p. 4498-4504.
93. Engler, A.J., et al., *A novel mode of cell detachment from fibrillar fibronectin matrix under shear.* Journal of cell science, 2009. **122**(10): p. 1647-1653.

94. Rupprecht, P., et al., *A tapered channel microfluidic device for comprehensive cell adhesion analysis, using measurements of detachment kinetics and shear stress-dependent motion.* Biomicrofluidics, 2012. **6**(1): p. 014107.
95. Deligianni, D.D., et al., *Effect of surface roughness of hydroxyapatite on human bone marrow cell adhesion, proliferation, differentiation and detachment strength.* Biomaterials, 2000. **22**(1): p. 87-96.
96. Van Kooten, T., et al., *Development and use of a parallel-plate flow chamber for studying cellular adhesion to solid surfaces.* Journal of Biomedical Materials Research Part A, 1992. **26**(6): p. 725-738.
97. García, A.J., P. Ducheyne, and D. Boettiger, *Quantification of cell adhesion using a spinning disc device and application to surface-reactive materials.* Biomaterials, 1997. **18**(16): p. 1091-1098.
98. Truskey, G.A. and T.L. Proulx, *Relationship between 3T3 cell spreading and the strength of adhesion on glass and silane surfaces.* Biomaterials, 1993. **14**(4): p. 243-254.
99. Bundy, K., et al., *Measurement of fibroblast and bacterial detachment from biomaterials using jet impingement.* Cell Biology International, 2001. **25**(4): p. 289-307.
100. Burmeister, J.S., et al., *Effect of fibronectin amount and conformation on the strength of endothelial cell adhesion to HEMA/EMA copolymers.* Journal of Biomedical Materials Research Part A, 1996. **30**(1): p. 13-22.
101. Usami, S., et al., *Design and construction of a linear shear stress flow chamber.* Annals of biomedical engineering, 1993. **21**(1): p. 77-83.
102. García, A.J., F. Huber, and D. Boettiger, *Force required to break α5β1integrin-fibronectin bonds in intact adherent cells is sensitive to integrin activation state.* Journal of Biological Chemistry, 1998. **273**(18): p. 10988-10993.
103. Pratt, K.J., et al., *Kinetics of endothelial cell—surface attachment forces.* Journal of vascular surgery, 1988. **7**(4): p. 591-599.
104. Horbett, T., et al., *Cell adhesion to a series of hydrophili–hydrophobic copolymers studies with a spinning disc apparatus.* Journal of Biomedical Materials Research Part A, 1988. **22**(5): p. 383-404.
105. Truskey, G.A. and J.S. Pirone, *The effect of fluid shear stress upon cell adhesion to fibronectin-treated surfaces.* Journal of Biomedical Materials Research Part A, 1990. **24**(10): p. 1333-1353.
106. Lawrence, M., L. McIntire, and S. Eskin, *Effect of flow on polymorphonuclear leukocyte/endothelial cell adhesion.* Blood, 1987. **70**(5): p. 1284-1290.
107. Gallant, N.D., K.E. Michael, and A.J. García, *Cell adhesion strengthening: contributions of adhesive area, integrin binding, and focal adhesion assembly.* Molecular biology of the cell, 2005. **16**(9): p. 4329-4340.
108. Xiao, Y. and G.A. Truskey, *Effect of receptor-ligand affinity on the strength of endothelial cell adhesion.* Biophysical journal, 1996. **71**(5): p. 2869-2884.
109. Francis, G., et al., *Direct measurement of cell detachment force on single cells using a new electromechanical method.* Journal of cell science, 1987. **87**(4): p. 519-523.

110. Dao, L., et al., *Revealing non-genetic adhesive variations in clonal populations by comparative single-cell force spectroscopy.* Experimental cell research, 2012. **318**(17): p. 2155-2167.
111. Friedrichs, J., J. Helenius, and D.J. Müller, *Stimulated single-cell force spectroscopy to quantify cell adhesion receptor crosstalk.* Proteomics, 2010. **10**(7): p. 1455-1462.
112. Li, F., et al., *Force measurements of the α5β1 integrin–fibronectin interaction.* Biophysical journal, 2003. **84**(2): p. 1252-1262.
113. Trache, A., et al., *Histamine effects on endothelial cell fibronectin interaction studied by atomic force microscopy.* Biophysical journal, 2005. **89**(4): p. 2888-2898.

Biographical Information

Ishan Kamal Khan completed his Bachelors in Mechanical Engineering from Bangladesh University of Engineering and technology(BUET) in 2009. During the fall of 2010 and spring of 2011 he attended Louisiana Tech University. In fall of 2011, he entered the biomedical engineering PhD program at the University of Texas at Arlington focused in biomechanics track. The focus of his research has been mechanical property changes of migrating cells and computational modeling of intracellular actomyosin contraction. He earned his PhD degree in the spring of 2018.